ANALYSIS OF A ROTARY ULTRASONIC MOTOR FOR APPLICATION IN FORCE-FEEL SYSTEMS

by

Devon Patrick Murphy

Thesis submitted to the Faculty of the

Virginia Polytechnic Institute and State University

in partial fulfillment of the requirements for the degree of

Master of Science

in

Mechanical Engineering

Approved:

Daniel Inman, Chairman

Thomas Michael Seigler

Mary Kasarda

25 August 2008

Blacksburg, Virginia

ABSTRACT

ANALYSIS OF A ROTARY ULTRASONIC MOTOR FOR APPLICATION IN FORCE-FEEL SYSTEMS

Devon Patrick Murphy

A qualitative analysis of a rotary traveling wave-type ultrasonic motor (USM) used to supply feedback forces in force-feel systems is carried out. Prior to simulation, the subsystems and contact mechanics needed to define the motor's equations of motion are discussed along with the pitfalls of modeling a USM. A mathematical model is assembled and simulated in MATLAB Simulink. Accompanying the dynamic model, a new reduced model is presented from which predictions of USM performance can be made without a complicated dynamic model. Outputs from the reduced model are compared with those of the dynamic model to show the differences in the transient solution, agreement in the steady state solution, and above all that it is an efficient tool for approximating a motor's steady state response as a function of varying the motor parameters. In addition, the reduced model provides the means of exploring the USMs response to additive loading, loads acting in the direction of motor motion, where only resistive loads, those opposite to the motor rotation, had been considered previously. Fundamental differences between force-feel systems comprising standard DC brushless motors as the feedback actuators and the proposed system using the USM are explained by referencing the USM contact mechanics. Outputs from USM model simulations are explored, and methods by which the motor can be implemented in the force-feel system are derived and proven through simulation. The results show that USMs, while capable of providing feedback forces in feel systems, are far from ideal for the task. The speed and position of the motor can be controlled through varying stator excitation parameters, but the transient motor output torque cannot; it is solely a function of the motor load, whether additive or resistive.

Acknowledgements

I would like to thank my advisor, Dr. Daniel Inman, for his guidance, encouragement and open-mindedness through all of the twists and turns of the project. I would also like to thank Dr. Michael Seigler for his ever-calm approach to life, education and the problems that arise when the two subjects mingle. Thank you also to Dr. Mary Kasarda for so generously agreeing at such late notice to serve on my committee. I would especially like to thank Dr. Bob Stirling, Dennis Messenger and Hisako Yamashiro of Stirling Dynamics Inc. for providing both funding and support throughout this project.

I would also like to extend my sincere appreciation to all of my colleagues in CIMSS for making my time here unforgettable. To have been a part of such a culturally diverse, well-rounded group of people is an honor. Thank you for being the family that has made the lab like a second home.

And finally, to my Father and Mother, Mark and Carolyn, my little and baby sisters, Erin and Catherine, and my friends Kelly Shelton, David Ficke and Daniel Mirenda…

…for your belief in me, your never ending support, and your ability to remind me of who I am and what I'm capable of in the times when I'm convinced that all is lost…

THANK YOU

I am here only because of you.

Table of Contents

List of Figures

List of Tables

1 Introduction

This chapter introduces the material needed to understand the full scope of this thesis. First, a brief introduction to force-feel systems is presented along with discussion of the motivation behind experimenting with ultrasonic motors as replacements for DC motors in force-feel systems. Presented in the next section are the objectives of the research. The chapter is concluded with a section outlining the thesis and another discussing the specific contributions described within.

1.1 Motivation

In recent years, electromechanical devices have been introduced into machines requiring control surface actuation in response to an operator input. The term *control surface* refers to the piece of a machine that is being controlled by the operator's input; mechanisms such as ailerons and flaps in aircraft, for example. These electromechanical actuators (EMAs) severed the complex physical connections between the operators and the control surfaces. As a result, system design complexity was reduced, the force and deflection range of the control surface was increased, pre-processing of actuator inputs to reduce noise inputs (inputs from shaky body movements resulting from the operating environment) became possible, and a new requirement of the system design became necessary; the force-feel system.

Prior to the integration of EMAs, operators and control surfaces were connected through complex mechanical systems using machines like pulleys and linkages. These systems allowed the forces acting on the control surfaces to be transmitted back to the operator as feedback giving the operator a "feel" for the system. With the introduction of EMAs, the complex mechanical systems were replaced with by-wire systems, a reference to the fact that only signals from a motion sensor at the operator interface traveled "by-wire" between the input and the actuator at the control surface. Feedback forces were lost. To account for the lost forces, force-feel systems were introduced, a task accomplished by connecting additional EMAs to the operator inputs.

These devices were used to output the feedback that was lost with the elimination of the mechanical linkages, reinstating to some degree, system feel.

The DC motor was the EMA of choice for most of the feel-systems, as it was readily available, and its principle of operation allowed for the control of the speed and output torque. As the demands for motors capable of higher torque and lower speeds increased, gearboxes were introduced into the feel-systems, once again increasing the overall system complexity.

The development of smart material technology has given rise to a new division of EMAs known as smart material actuators. These new systems use materials such as piezoelectrics and shape memory alloys to actuate linear or rotary motion. Mechanisms including friction, high frequency-low displacement steps, or resistive heating of materials are used to induce movement.

One popular smart actuator is the traveling wave rotary ultrasonic motor, hereafter referred to as a USM. These motors are significantly different from standard DC motors in that their rotation is induced by friction rather than magnetism. Numerous mathematical models of the USM have been proposed ranging in complexity from simple electric circuit models that predict steady state motor operation to complex dynamic models that predict both transient and steady state responses. Various finite element models have also been presented to predict USM performance under varying design parameters.

Despite ample literature about USM modeling, there is little documentation of research where predictive models are applied to determine the suitability of ultrasonic motors for new applications or as upgrades from DC motors. Therein lays the motivation and objective of this project; assemble and simulate an ultrasonic motor model to determine potential applications of USMs by first focusing on their ability to replace DC motors in force-feel systems. Force-feel systems were chosen as the application for this research based on their designs requiring actuators whose displacement *and* torque can be controlled. Furthermore, several unique properties of the USM are highly compatible for such a system. These properties are given below followed by their motivating influence towards this project.

- **High torque density**: USMs have torque densities three to ten times higher than standard DC motors [1]. Therefore, smaller USMs can take the place of DC motors and still exhibit higher torque outputs. Smaller, higher torque motors will allow for a decrease in system volume and weight, both important factors when incorporating systems into aircraft where weight and space are critical design considerations.
- **High torque-low speed capability**: As previously mentioned, gearing has been introduced into DC motor actuated feel-systems in order to achieve high torque-low speed motor outputs. The USMs ability to output the motor specific maximum torque at speeds approaching zero angular velocity may eliminate the need for gearing which would result in reduced system complexities, lower failure rates and reduced repair costs.
- **High motor programmability and control**: USMs have been widely used as the actuator in auto-focusing camera lenses, a testament to their programmability and control capabilities. These properties are critical to the success of feel-systems to allow for motion and torque control during various feedback applications.

In summary, USMs offer an attractive alternative to DC motors based on the bulleted properties above, but little has been done to determine useful applications of the motors based on their principles of operation. As an attempted remedy, this research has been conducted on USMs in force-feel systems to analyze motion and torque capabilities of the motor and aid future designers by lending a generalized answer to the question: Is the ultrasonic motor a viable solution for this design problem?

1.2 Objectives

The main objectives of this project have been to:

1. Establish a background in force-feel systems, including their history, design progressions and their capabilities with special consideration given to those systems incorporating ultrasonic motors.

2. Assemble a mathematical model of a traveling wave ultrasonic motor from existing publications in MATLAB Simulink to capture the nonlinear properties of the motor within its operational envelope.

3. Identify the feasibility of using a rotary USM in a force-feel system by evaluating potential force feedback scenarios in the Simulink environment.

While the scientific community is saturated with information describing the many models of ultrasonic motors, there is little documentation about their functionality once incorporated into systems. The overall objective of this research was to first assemble a model of an ultrasonic motor and then to apply the model to a force-feel system to determine whether improvements in performance, design complexity and functionality could be made by replacing DC motors with USMs.

1.3 Outline

The contents of this thesis are organized into six chapters and two appendices:

Chapter 2 contains a literature review covering information relative to this project. Force-feel systems, their place in the research area of haptic feedback and several requirements of feel-system design are presented. A section describing previous efforts to integrate ultrasonic motors into feel-systems follows. The chapter is concluded with a section detailing the finite element, equivalent circuit and the complex dynamic USM models available in literature. The potential of each model to be used in the research of this thesis is presented.

Chapter 3 details the contact mechanics and subsystems needed to assemble the complex dynamic model of the ultrasonic motor. The process of calculating the half-contact length and stick-points using dynamic systems is specified along with a discussion of a motor's torque output during transient and steady state operation. The equations of motion for each subsystem are also presented along with the formulas needed to calculate feedback forces caused by the stator/rotor interaction. The chapter is concluded with a section detailing subsystem and motor outputs under resistive loading.

Chapter 4 presents the derivation and validation of the reduced dynamic model. The process of obtaining the formulas used to calculate the half-contact and stick-points as functions of only the traveling wave amplitude is given, and the method of integrating the reduced model into Simulink is described. After validating the reduced model against the complex model for cases of resistive loading, it is used to approximate the motor response under additive loading.

Chapter 5 details the fundamental difference between the DC and ultrasonic motors when used in force feel systems. By this point in the research, it was clear that the USMs would only work in very specific cases of force feedback; those where the external loads acting on the motor are controlled. The chapter focuses on two such cases, constant force and linear spring force, for resistive and additive motor loading, and the motor outputs for each are presented.

Chapter 6 contains the conclusions of the research and suggestions for future work.

Appendices A and B contain the model breakdown of the complex and reduced dynamic models and the codes needed to run both models, respectively. The models and codes are detailed in such a way that any reader should be able to copy the block diagram, input the correct simulation parameters, run the .m-file code and as a result, have a functioning model of an ultrasonic motor.

1.4 Contributions

In the study of an ultrasonic motor, its potential applications to a force-feel system and its performance therein, two significant contributions have been made.

1. A new reduced dynamic model of a USM was derived and assembled. The model allows predictions of the USM's steady state performance to be made without fully assembling a complex dynamic model.

2. After simulating the two models used in this thesis, it has been established that ultrasonic motors should be used as positioning devices and not as controllable source of torque as originally desired for their integration in force-feel systems.

Assembling a dynamic model is a difficult task despite a large field of research covering the subject. Dynamic, equivalent circuit and FEM models of USMs have all been explored to either model a specific motor or predict the output of a new design. In all cases, there is no quick implementation of the model. In response to this, a simple model of the USM stator coupled with two MATLAB functions has been derived which allows accurate prediction of steady state motor outputs without assembling a full dynamic model. The new model allows focus to remain on motor design and integration, rather than on piecing together a complicated and often fickle complex dynamic model from literature. Additionally, the reduced model allows for the exploration of motor responses under a previously unpublished loading scenario. Until now, only resistive motor loading, loads that resist the motion of the motor, have been considered; a limitation of the dynamic model. The reduced model, however, is capable of solving for the steady state motor response under additive loading, motor loads acting in the direction of the motors rotation, in addition to resistive loading.

While trying to determine how the USM could replace the DC motor in a force feel system, the comparison of output capability between the two motors revealed that they are not fully interchangeable. Position and speed control of both motors is possible based on their separate principles of operation (DCM: magnetism, USM: friction), but control of the transient output torque for both motors is not. The output torque of both motors will match their torque load in steady state, but while a DC motors transient output torque is a function of current and easily controlled, the USMs transient output torque is a nonlinear function of the traveling wave amplitude and the external load acting on the motor and cannot be.

2 Background

The information in this section provides an introduction to the subject areas central to this thesis. To begin, force-feel systems, their beginnings and their progression into modern applications are discussed. Next, a review of research examining rotary ultrasonic motors in force-feel systems is presented, and an abbreviated history of the various USM modeling efforts follows. The chapter is concluded with a summary and a short discussion of how the work of this thesis aims to determine whether USMs are fit to be the sole actuator to provide controlled torque and displacement in a force-feel system.

2.1 Force-Feel Systems

Force-feel systems fall under the umbrella of haptic feedback systems, or systems capable of providing force feedback and tactile feedback. Force feedback is the simulation of hardness, weight and inertia, and tactile feedback is the simulation of contact geometries, smoothness, slippage and temperature [2]. Haptic feedback is especially important in virtual reality simulations to provide a user a feel for the virtual environment, but it has been equally important for increasing the control of by-wire systems. Without actuators providing feedback forces to the user, the virtual reality interface remains solely an input device to the computer just as a control stick lacking a feel-system is just an input to the aircraft [3]. The feel-systems considered in this thesis require only force feedback, so tactile feedback is given no further consideration.

Originally used on a robotic tele-operation system for nuclear environments in 1954, advancements in force feedback research extended its use to systems including electromechanical arms for virtual molecular docking, active control sticks for both flight simulators and fly-by-wire aircraft and feedback gloves for the handling of virtual reality objects. By the late 1990s, inexpensive haptic joysticks were even available for computer games [2].

Regardless of application, one of the most important goals of feel-system design is its transparency, a term describing the lack of forces exerted by the system on the operator’s hand

when no forces exist in the virtual reality environment or on the surfaces that the input device controls. A systems backdrivability is the quantification of its transparency and is maximized in cases of low actuator inertia and static friction [3]. The result is minimal resistance to operator inputs. Good backdrivability increases the range of feedback forces that can be output by the feel-system by allowing small forces, originally masked by friction or gear forces, to be felt.

Prior to determining an actuators backdrivability, the actuator's speed and torque capabilities, including ranges and maximum continuous outputs, must be obtained. These are manufacturer specifications and easily acquired. Speed and torque controllability must also be proven; a task typically involving both modeling and experimental validation. With respect to ultrasonic motors, speed and position control are clearly possible, as they are the most widely used actuator in present day auto-focusing camera lenses. Whether the output torque of a USM can be controlled remains a point of speculation requiring a full analysis of its operating characteristics through motor modeling for confirmation.

2.2 USMs in Force-Feel Systems

Design and modeling have been major research areas since the USMs introduction in the 1980s. With respect to design, increasing the motor's load carrying capability is generally of most concern, as the torque range of commercially available USMs is only a fraction of that covered by DC motors. In terms of modeling, considerable research has gone into developing schemes that predict motor outputs as a function of its inputs. It would seem that given the large body of knowledge covering those subjects that further research would tend towards the application of USMs as engineering solutions, but it is not the case. Clearly, accurate position and speed control laws have been developed for USMs, as they are being used in innovative designs as positioning actuators. However, few publications exist that examine the USM as a source of controllable torque. Some of the more recent pertaining to force-feel systems include:

> 2000: Researchers at the University of Paderborn suggested the USM be applied in an active control stick feel-system citing its high torque density and high torque capability at low rotational speeds as beneficial to a fly-by-wire aircraft control systems. A torque

control algorithm was formulated in order to control the motor torque which generated restorative feedback forces to the control stick to return it from a forward or backward sweep [4].

2006: Researchers at the Polytech'Lille/USTL in France expanded on the active control stick application by exploring a torque control method in which the motor torque was considered a function of the ideal and actual rotor speeds [5].

2007: Researchers at the National University of Singapore developed a haptic knob composed of a USM and an active powder brake coupled by a differential gear. The USM acted as velocity source while the brake acted as a clutch allowing torque control of the system [6].

Of the research conducted on USMs in force-feel, only [6] recognized the limited torque capabilities of ultrasonic motors with respect to output range and controllability. None of the literature cited includes an analysis of the stator/rotor contact mechanics, derived in [7], and thus they fail to clarify two important facts. First, the speed of a rotor is a function of the electrical excitation and the load torque on the motor. The output torque of the motor, however, is not a function of the speed. Second, based on the difference in driving mechanism of DC motors and USMs, magnetism and friction, respectively, there are significant differences in the method by which the motors must be applied in force-feel systems. These points are discussed in greater detail in Chapters 4 and 5 , respectively.

2.3 USM modeling

Since the introduction of ultrasonic motors, mathematical modeling to approximate the transient and steady state motor dynamics has been the subject of numerous publications. The overall goal of the modeling is to predict and understand the USMs response to external inputs. In the following sections, overviews of the finite element, equivalent electric circuit and complex dynamic USM models are presented along with their potential application to the analysis of this thesis.

2.3.1 Finite Element Models

The finite element method (FEM) remains a popular means of modeling ultrasonic motors and their components for design purposes. As the popularity of USMs as engineering solutions increases, higher motor torque and speed outputs are desired. FEM allows motor designers to experiment and predict the response of new motor designs as a function of the materials used to manufacture the stator and rotor, the rotor contact surface and the piezoelectric patches that induce the traveling wave.

FEM is typically reserved for USM stator design to determine the natural frequency of the stator that produces the traveling wave as demonstrated in [8]. The natural frequency solved by modeling a free stator is not the motors natural frequency, but it gives the designer a general idea of what frequency range the motor driver and piezoelectrics must output to induce the motor movement.

USM modeling by FEM has been extended to analyze the contact mechanics of the stator/rotor interface in an effort to approximate output torque capabilities. The method is demonstrated in [9], showing that in addition to calculating the natural frequencies of the stator, the stick/slip interaction of the contact area and motor losses due to friction can be approximated.

By combining the methods similar to those of [8] and [9], full finite element models of USMs have been created, as in [10]. Complete USM models are composed of three structures representing the piezoelectric patches, the stator and the rotor, and assumptions regarding the deformability of the structures are made prior to simulation. Furthermore, a contact algorithm is needed to approximate the rotor's motion under stator forcing. Simulation results showed that rotor speeds could be predicted as a function of both the piezoelectric excitation voltage and frequency and the external load compressing the stator/rotor combination.

Though full FEM models of USMs exist, they remain computationally expensive, and the algorithms needed to define the stator/rotor contact mechanics are still evolving. While helpful in motor design, FEM is complicated and not as easily employed to simulate and monitor the variables that determine a motors outputs that are important to force-feel systems.

2.3.2 Equivalent Circuit Models

Elements used to model a mechanical system such as masses, springs and dampers have electrical equivalents which allow most mechanical systems to be modeled by an electrical equivalent; both producing the same response when analyzed. The choice of whether to use a mechanical or electrical model is usually a personal preference.

The equivalent circuit model (ECM) of an ultrasonic motor is largely simplified model, not equivalent in accuracy to a full mechanical model, but it is helpful in understanding motor outputs as a function of voltage and excitation frequency inputs. The ECM is used to approximate the steady state velocity of the rotor, which is represented a "motional" current scaled by a conversion factor. First, a maximum motional current value is calculated and assigned to the ECM. The maximum current represents the motor speed before the losses associated with friction, motor load and temperature. Next, the max current value is reduced using DC current sources representing, again, factors like friction, motor load and temperature. The magnitude of the final motional current running through the circuit after the DC current sources represents the rotors velocity. The ECM derived in [11] is shown in Figure 2.1 without the current source accounting for rotor speed reductions caused by frictional heating of the motor. The capacitor with value C_f can be used to tune the circuit to the correct natural frequency of the motor which varies from that of the free stator.

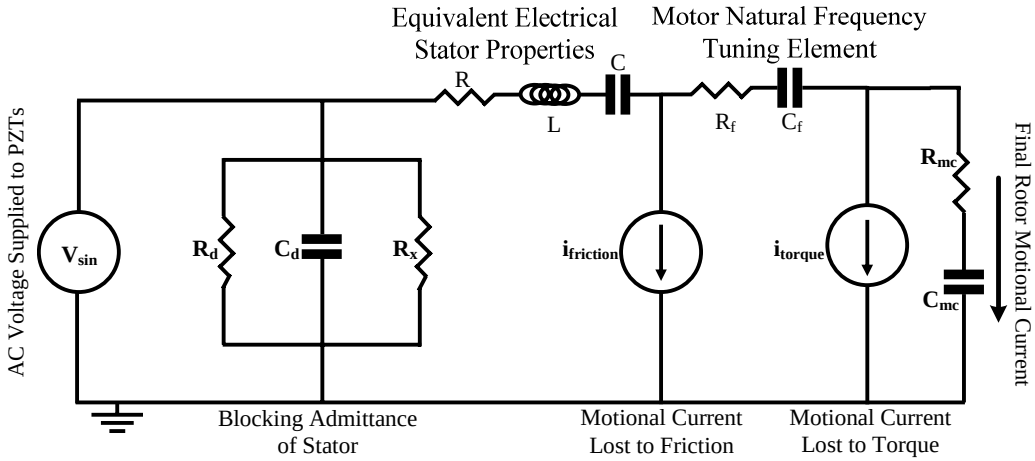

Figure 2.1. Equivalent Circuit Model of the USM; adapted from [11].

The motional current in the ECM of Figure 2.1 can be solved for by first neglecting the circuit components that have no affect on the circuit in steady state. The reduced ECM of Figure 2.1 is presented in Figure 2.2. Next, the currents leaving the nodes above both current sources can be summed, and from the two equations, $i_{motional}$ solved for such that

$$i_{motional} = \left| \frac{\frac{V_s}{Z_{eq}} - i_f - i_t\left(\frac{Z_{Cf}}{Z_{eq}} - 1\right)}{\left(\frac{Z_{Cf}}{Z_{eq}} + 1\right)} \right|. \tag{1}$$

Using (1), the rotor speed of the motor can be plotted as a function of the input voltage and the DC current losses in the ECM.

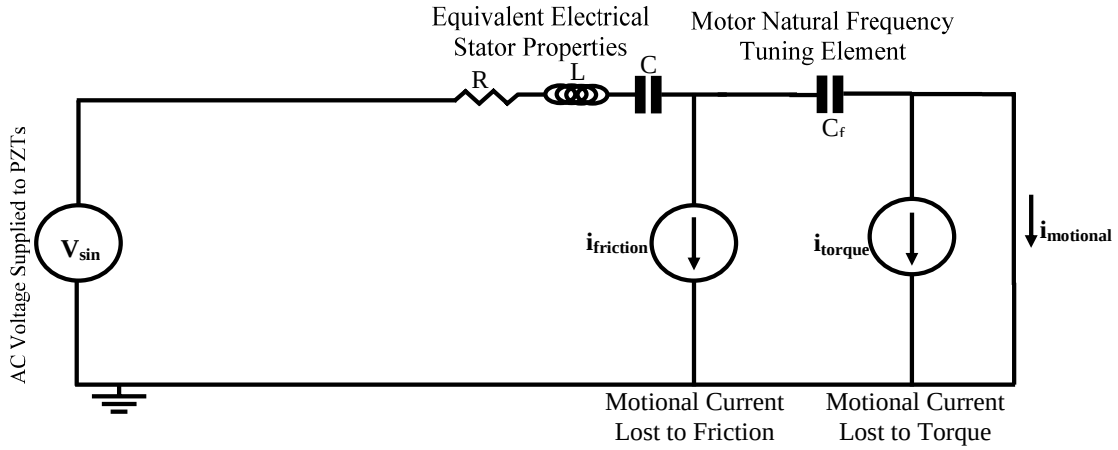

Figure 2.2. Reduced ECM of Figure 2.1 needed to solve for rotor motional current.

Unfortunately, ECMs are not accurate over large torque or frequency ranges, as the values used for the current sources are only valid in ranges deemed *linear* by observation of experimental data gathered from the motor prior to the models assembly. As equivalent circuit models cannot be used to monitor the contact mechanics at the stator/rotor interface, it is not used for any analysis in this thesis. A more robust model, one accounting for all the non-linear dynamics of the USM, is used instead.

2.3.3 Complex Dynamic Models

The finite element and equivalent circuit models of sections 2.3.1 and 2.3.2 are useful when applied in ultrasonic motor design and acquiring rough motor speed approximations. Finite element models, while capable of quantifying interaction forces at the stator/rotor interface and approximating the resulting rotor speeds, are computationally expensive and are not useful for controls analysis. Equivalent circuit models are a mix between dynamic modeling and a curve fitting, do not involve any analysis of the stator/rotor contact mechanics and are only valid in small frequency and load ranges. Neither model is useful in analyzing the complex stator/rotor coupling due to feedback forces, the contact mechanics that allow the motor to function or the dynamic effects of an external load on the rotor.

Many complex dynamic models of the ultrasonic motor have been published as in [11-13]. Each varies in complexity depending on what electrical inputs it can receive and the depth to which the contact mechanics are modeled. For instance, if a phase difference other than +/- 90 degrees between electrical signal inputs is allowed, the contact mechanics formulas used to determine motor output torque and stator/rotor coupling feedback forces increase in complexity, as shown in [13]. Cross coupling of the sine and cosine vibration modes can also be accounted for, as in [13], but it is often disregarded based on its negligible effect on the model outputs. In [11], the motor natural frequency shifts due to frictional heating were integrated into the model allowing for a better overlap of simulation outputs and experimental data.

Regardless of intricacies used to fine-tune the models to match their physical counterparts, complex dynamic models consist of three coupled dynamic subsystems that, once solved, account for motion of the stator under the effect of electrical forcing and the rotor motion in the vertical and angular directions as a function of the contact mechanics derived in [7]. Therefore, though not as helpful in stator design, dynamic models allow the accurate monitoring of motor speeds as functions of stator electrical inputs and external motor loads without the computational expense of FEM or the approximations of the ECM, making them the model of choice for this thesis.

2.4 Summary

Feel-systems are an ever-evolving technology requiring constant improvement to reflect advances in controls and actuator technology in response to increased performance demands and the need for minimum size, weight and maximum durability. A new actuator is deemed qualified for use in a feel-system first if it is versatile enough to have its speed and torque controlled by an external signal and then if it falls within the size, weight, and min, max, and sustainable speed and torque requirements. The force feedback category in the field of haptics is no longer a futuristic concept. Its applications range from high-end virtual reality simulators, to aircraft control sticks, to the most recent gaming system controllers.

Ultrasonic motors have been the subject of many modeling efforts to achieve higher accuracy during model validation, to aid in the development of control algorithms and to understand their capabilities. With respect to modeling, [7] has become the standard reference defining the contact mechanics of a USM. References [11-13] have presented dynamic models consisting of the motor subsystems coupled by feedback forces. The model in [11] represents the commercially available Shinsei USR60 ultrasonic motor, and is validated as such. However, even with all these models available for assembly, no definitive statements have been made about the limitations of USMs as actuators. It seems that the ultrasonic motor, disregarding its limited torque range, is equivalent to DC motor in terms of how its outputs can be controlled.

The research documented in this thesis aims to qualify the ultrasonic motor for use as the sole actuator in a force-feel system. By first assembling a dynamic model from available literature, simulations will be run to assess USM torque controllability, and the question of DC and ultrasonic motor equivalence will be firmly defined.

3 Complex Dynamic Model (CDM) of the USM

The following chapter details the assembly and simulation of a complete USM model in MATLAB Simulink. The complex dynamic model is composed of several subsystems needed to determine specific displacements and angular velocities of the USM components. These subsystems are given below along with a description of the displacement that must be calculated from subsystem analysis.

1. **USM Stator:** amplitude of vertical stator point displacements as a function of the PZT and stator/rotor interaction forces. These displacements are needed to determine the USM traveling wave amplitude.

2. **USM Rotor (Vertical):** amplitude of rotor displacement in vertical direction away from stator surface. This displacement is related to the contact length of the traveling wave, a value used to calculate the motor output torque and angular motion of the rotor.

3. **USM Rotor (Angular):** The angular speed of the USM rotor is analyzed instead of the angular displacements to determine values known as stick-points, also necessary in determining the motors output torque.

A visual representation of the components of a Shinsei USR60 USM is given in Figure 3.1. Of the additional components shown, only the mass of the disc spring is accounted for in the model, and it is a component of the rotor's effective mass. The disc spring provided the preload between the rotor and the stator.

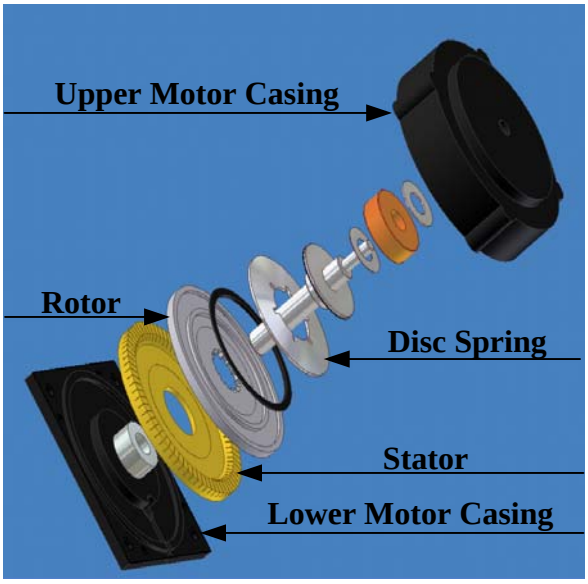

Figure 3.1. Exploded view of the ultrasonic USR60 USM showing the components modeled.

In the following section, the USM contact mechanics are discussed. Next, the equations of motion for subsystems 1-3 are presented. A section outlining the difficulties of USM modeling follows. Finally, the outputs from the CDM are presented.

3.1 CDM: Contact Mechanics

The contact mechanics of USMs refers to the friction interaction between the stator and rotor surfaces that induce motor movement. Three values central to understanding the operation of the USM are presented in separate sections. These are the half-contact length, the rotor stick-points and the motor's output torque.

3.1.1 Half-Contact Length, x_o

The actuation of the USM is achieved by exciting the stator at its natural frequency using two sets of piezoceramics attached with epoxy to its base. Based on the design of the stator, a traveling wave is induced when the piezoceramics are excited by two ultrasonic sinusoids, 90 degrees out of phase from one another. Dynamic frictional forces caused by the stator/rotor interaction drive the rotor into motion. The undeformed and deformed stators are represented in Figure 3.2.

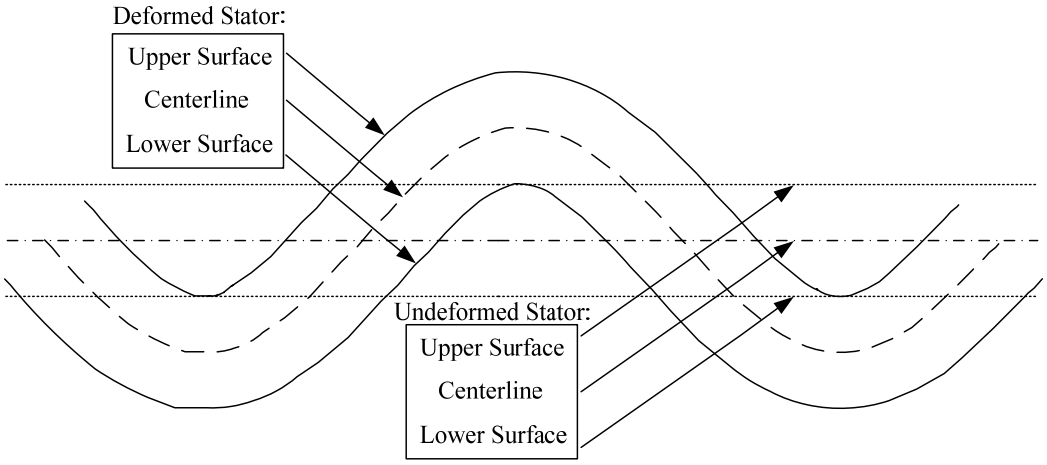

Figure 3.2. Drawing of undeformed and deformed stators.

For simplification, the stator surface is treated as undeformable, unlike the thin layer of contact material on the bottom surface of the rotor that deforms on contact. The rigid-stator/deformable-rotor combination is represented in Figure 3.3 along with dimensions critical to the modeling of the USM, the first of which is the half-contact length, x_o. The half-contact length is defined as half of the horizontal length of the traveling wave crest of the stator submerged within the rotor from its point of entry to its exit.

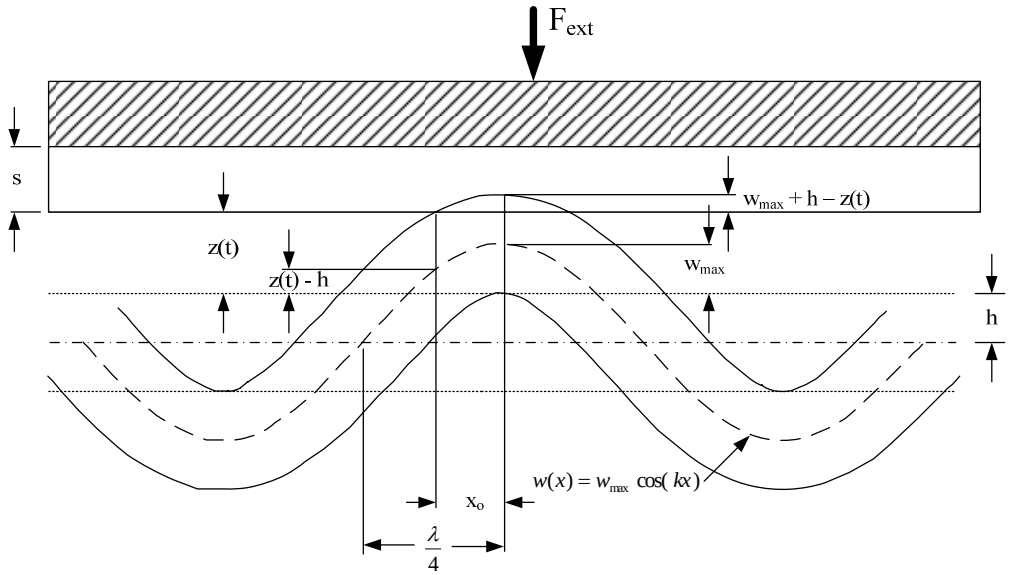

Figure 3.3. Drawing of stator pressing into rotor contact material.

As the traveling wave of the stator develops, the wave crest presses into the rotor contact material creating a normal force, F_N, calculated as shown in [7] to be

$$F_N = \frac{2nc_N w_{\max}}{k}\left(\sin(kx_o) - kx_o\cos(kx_o)\right) \tag{2}$$

where n is the number of wave crests, c_N is the contact material stiffness, w_{max} is the traveling wave amplitude and k is the wave number. The contact material is treated as a linear spring with a stiffness also calculated in [7] to be

$$c_N = \frac{Eb}{s} \tag{3}$$

where E is the modulus of the contact material, b is the width of the material in the radial direction and s is the material thickness in the vertical direction as shown in Figure 3.3.

As w_{max} increases from zero, F_N increases towards F_{ext}, the preload between the rotor and the stator. At a critical value of w_{max}, with the contact length set at its maximum of $\lambda/4$, F_N becomes larger than F_{ext}, and the rotor accelerates away from the stator surface to a height $z(t)$. By monitoring the rotor height, the half-contact length can be calculated as in [11] to be

$$x_o = \frac{1}{k}a\cos\left(\frac{z(t)-h}{w_{\max}}\right) \tag{4}$$

where $z(t)$ is the vertical distance between the rotor's lowest surface and the top surface of the undeformed stator and h is the half-thickness of the stator.

3.1.2 Stick-points, x_s

As the cosine wave travels around the stator, the surface points of the stator travel in an elliptical orbit where the surface point displacements are described by the equations

$$\zeta = \frac{2\pi h w_{\max}}{\lambda}\sin(kx - \omega t) \tag{5}$$

$$\zeta = w_{\max} \cos(kx - \omega t). \tag{6}$$

where λ is the wavelength and k is the wave number of the traveling wave, calculated respectively as

$$\lambda = \frac{2\pi R_o}{n} \tag{7}$$

$$k = \frac{2\pi}{\lambda}. \tag{8}$$

The velocity of each surface point is perpendicular to its displacement as seen in

Figure **3.4** (a).

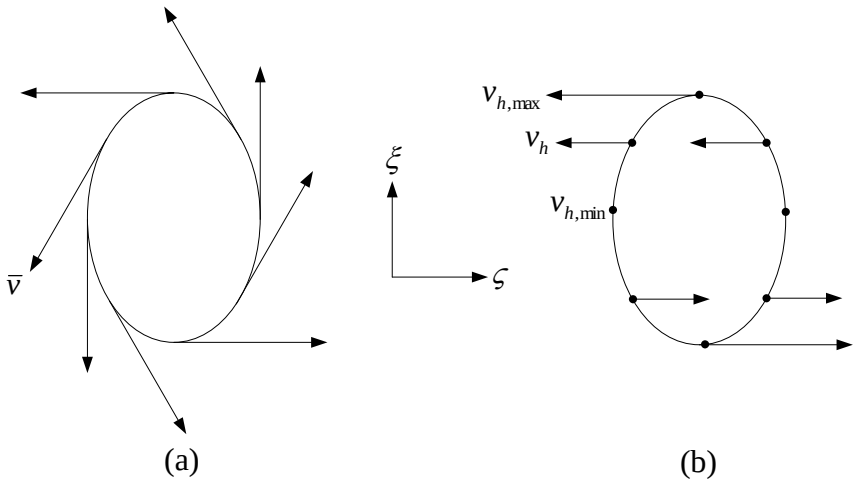

Figure 3.4. (a) Surface point velocity vectors. (b) Horizontal velocity vector components.

For purposes of simulation, the horizontal velocity components like those of

Figure **3.4** (b) are the critical values needed to determine the stick-points of the stator-rotor surface. By differentiating equation (5), the horizontal velocity components can be calculated as

$$v_{h,rotor} = \frac{\partial \zeta}{\partial t} = -\frac{2\pi\omega h w_{\max}}{\lambda}\cos(kx - \omega t) = v_{h,\max}\cos(kx - \omega t) \tag{9}$$

where ω is the excitation frequency of the piezoelectrics in rad/s.

Stick-points, x_s, are defined as the location where the horizontal velocity component of the stator surface point matches the horizontal velocity of the rotor, and their magnitude represents the length from the traveling wave crest to that location. If the rotor is traveling with an angular velocity of $\dot{\theta}$, the horizontal velocity of the rotor is calculated as

$$v_{h,rotor} = R_o\dot{\theta} \tag{10}$$

where R_o is the effective radius of the traveling wave. Therefore, by equating equations (9) and (10) with time, t, set to zero, the stick-point can be calculated as in [13] to be

$$x_s = \frac{1}{k}a\cos\left(\frac{R_o\dot{\theta}}{v_{h,\max}}\right). \tag{11}$$

During simulation, the angular velocity of the rotor must be monitored along with the maximum horizontal surface-point velocity such that the stick-points can be found. For the ideal traveling wave motor, where the phases of the two standing waves are separated by ninety degrees, the stick-points are symmetric about the wave crest, and only one stick-point calculation is needed for each time step.

3.1.3 Torque generation (Steady State)

The output torque of a USM is a function of the preload between the rotor and the stator, the external load on the motor, the coefficient of friction between the stator and rotor contact surfaces, and the location of the stick-point within the half-contact length. The motors output torque, M_{USM}, was derived in [7] using a linear spring contact model to be

$$M_{USM} = \frac{2n\mu c_N w_{\max} R_o}{k}\left(2\phi(x_s) - \phi(x_o)\right) \tag{12}$$

where

$$\phi(x) = \sin(kx) - kx_o \cos(kx_o). \tag{13}$$

Equation (12) was derived with the knowledge that the wave crest submerged into the rotor produces both driving and braking torques depending on which side of the stick-point is being analyzed. To reiterate, in steady state, the stick-point length is less than or equal to the half-contact length, and the horizontal stator surface-point velocity at the stick-point is equal to the rotor horizontal velocity. Furthermore,

$$v_{h,\min} \le v_{h,rotor} \le v_{h,\max} \tag{14}$$

where $v_{h,max}$ is shown in (9), and $v_{h,min}$ is the surface-point velocity at the edge of the contact area calculated as

$$v_{h,\min} = v_{h,\max} \cos(kx_o). \tag{15}$$

$v_{h,min}$ ranges from zero to $v_{h,max}$, corresponding to the cases when the contact length is equal to $\lambda/4$ or when the contact length approaches single-point contact on account of increasing wave amplitudes, respectively.

To determine the location of the driving and braking zones on the submerged wave crest, the horizontal surface-point velocities on either side of the stick-point are compared with velocity of the rotor. The surface-point horizontal velocities on the wave crest side of the stick-point are higher in magnitude than that of the rotor causing a driving effect between the stator and rotor surfaces. The stator forces the rotor forward in that region. Conversely, the surface point horizontal velocities between x_s and x_o are lower in magnitude than the rotor causing a braking effect between the stator and rotor surfaces. An illustration of the preceding statements can be seen in Figure 3.5. The figure illustrates that there are driving and braking zones on either side of the wave crest. However, based on the symmetric property of the traveling wave, the torque output by the motor is determined in [7] by considering only one side of the wave crest and multiplying the result by two.

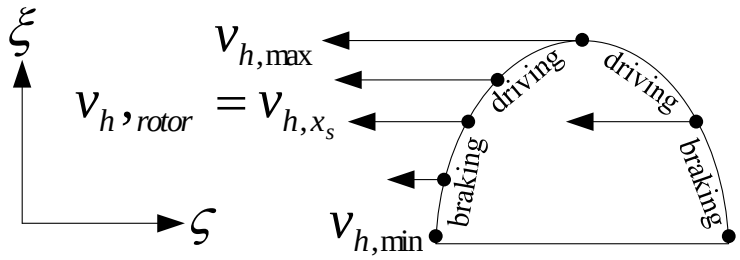

Figure 3.5. Drawing of surface point velocities dictating the driving and braking zones of the USM.

In steady state, w_{max} is fully developed, $z(t)$ is constant, and x_o is constant and has adjusted such that

$$F_N = F_{ext}. \tag{16}$$

The steady state stick-point value will also be constant, and the following formula

$$M_{USM} = \frac{2n\mu c_N w_{\max} R_o}{k}\left(2\varphi(x_s) - \varphi(x_o)\right) = -M_{load} \tag{17}$$

which can also be also be expressed as

$$M_{USM} = (F_{driving} - F_{braking})R_o = -M_{load} \tag{18}$$

is satisfied. The maximum torque the rotor can carry in steady state is

$$M_{USM,\max} = \mu F_{ext} R_o = \mu F_N R_o = -M_{load,\max} \tag{19}$$

which occurs when the stick-point and the half-contact length are equal

$$x_o = x_s, \tag{20}$$

and only a driving region exists, or when the stick-point is located on the top of the traveling wave crest and only a braking region occurs. The negative sign of equations (17)-(19) accounts for the fact that the output torque of the motor always opposes the motor load. For all other

loads placed on the motor less than $M_{load,max}$, the stick-points magnitude is between zero and x_o in steady state.

3.1.4 Torque generation (Transient)

The transient period of USM operation is defined as the period in time that the traveling wave amplitude is developing and has not yet reached its steady state value. During the transient, the contact length will fluctuate such that equation (2) is satisfied, and the stick-point of the wave crest will shift to satisfy equation (17). The transient periods of the simulations in this thesis range from seven to ten milliseconds.

When the motor is running in steady state without a load inducing slip between the stator and rotor surfaces, the stick-point lengths will be equal or less in magnitude to the half-contact lengths. The same is not necessarily true for the transient period of operation. As the motor increases speed from zero to its steady state value, it is possible for the stick-point to fall outside of the contact length. In such a case, the horizontal velocity components of the stator points are of a higher magnitude than the horizontal velocity of the rotor for all points of the traveling wave located inside the rotor contact material, and only a driving zone, as illustrated in Figure 3.5, exists. In the motor model, if the stick-point is calculated to be larger than the contact length, it is set equal to the half-contact length. In equation form, the previous statement is as follows,

$$x_s = \begin{cases} x_s, & x_s \le x_o \\ x_o, & x_s > x_o \end{cases} \tag{21}$$

In the time frame where (21) must be applied, the motor torque calculated in (17) is maximized.

3.2 CDM: Subsystems

The type of motor used for all analysis in this thesis is the ideal traveling wave ultrasonic motor. The term *ideal* suggests that there is no cross coupling between the stator modes thereby resulting in a perfect traveling wave. Additionally, it is assumed that phase difference between the electrical signals exciting the motor's piezoelectrics are ninety degrees out of phase at all

times. While a non-ideal model might allow a more accurate validation between a math model and the physical motor it describes, the reduced complexity of simulation associated with retaining the symmetric quality of the ideal traveling wave outweighs the need for an exact solution.

In the complete models of a USM such as those published by [11, 13, 14], the transient and steady state operation points of the motor are solved numerically by simulating three subsystems. These are the stator, the rotor (vertical) and the rotor (angular), and all are coupled by complex feedback forces. Brief descriptions of the subsystems and the feedback forces follow.

3.2.1 Stator

The stator is represented by two spring-mass-damper systems as shown in Figure 3.6.

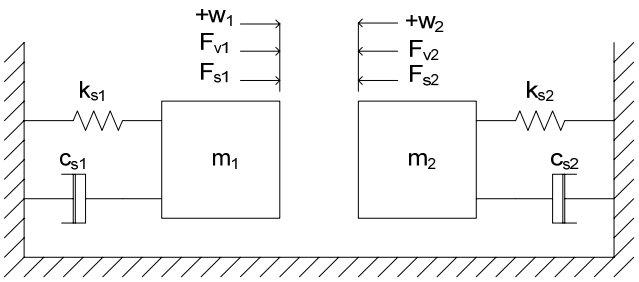

Figure 3.6. Spring-Mass-Damper representation of the USM stator; adapted from [13].

Each system is forced by an individual set of piezoceramics each excited by an ultrasonic sinusoidal electrical signal. The equations of motion for the systems are

$$m_{eff}\ddot{w}_1 + c_{s1}\dot{w}_1 + k_{s1}w_1 = F_{V1} + F_{S1} \tag{22}$$

$$m_{eff}\ddot{w}_2 + c_{s2}\dot{w}_2 + k_{s2}w_2 = F_{V2} + F_{S2} \tag{23}$$

where m_{eff}, c_s, and k_s, are the effective mass, damping and spring coefficient of the stator, and F_V and F_S are the piezo-forces and feedback forces experienced by the stator, respectively [13]. The

outputs of (22) and (23) are the out-of-plane (vertical) displacements of the stator used to calculate the traveling wave amplitude as

$$w_{\max} = \sqrt{w_1^2 + w_2^2}\ . \tag{24}$$

The traveling wave amplitude is the most important simulated parameter in any USM model, as it serves as the variable input to the vertical and angular rotor subsystems further allowing for the calculation of the contact length and stick-points, the values that ultimately determine the steady state angular velocity of the rotor.

The piezo-force inputs to (22) and (23), F_{V1} and F_{V2}, are sinusoidal electrical inputs multiplied by a piezoelectric force factor, η (N/V), such that

$$F_{V1} = \eta V \sin(2\pi\ f\ t) \tag{25}$$

and

$$F_{V2} = \eta V \cos(2\pi\ f\ t) \tag{26}$$

where f is the resonant frequency of the coupled stator/rotor systems in kHz [11]. It warrants mention that the natural frequency of the stator/rotor combination is different from the natural frequency of the free stator, a point discussed in Section 3.3, Modeling Difficulties.

The feedback forces, F_{S1} and F_{S2}, are composed of normal and tangential components, and as functions of the half-contact length and the stick-points, they serve as the coupling terms between the stator subsystem and the rotor subsystems. The normal force components are calculated as shown in [13] to be

$$F_{FB,N1} = -nc_n w_1 \left(kx_o - \frac{1}{2}\sin(2kx_o) \right) \tag{27}$$

$$F_{FB,N2} = -nc_n w_2 \left(kx_o - \frac{1}{2}\sin(2kx_o) \right). \tag{28}$$

The tangential feedback forces for the ideal motor operating within its load carrying range are

$$F_{FB,T1} = 2n\mu hc_N w_2\left(\frac{1}{2}kx_o + \frac{1}{4}\sin(2kx_o) - \sin(kx_o)\cos(kx_o)\right) \tag{29}$$

$$F_{FB,T2} = -2n\mu hc_N w_1\left(\frac{1}{2}kx_o + \frac{1}{4}\sin(2kx_o) - \sin(kx_o)\cos(kx_o)\right) \tag{30}$$

where μ is the dynamic coulomb friction coefficient [13]. In a non-ideal model, additional terms would be added to equations (29) and (30) accounting for unequal stick-point lengths on either side of the traveling wave crest. However, following the ideal wave assumption, the stick-point lengths to the right and left of the wave crest are of equal length and the additional terms cancel each other in the feedback calculation.

The total feedback force experienced by each system of the stator is determined by combining equations (27)-(30) such that

$$F_{S1} = F_{FB,N1} - dir(R)F_{FB,T1} \tag{31}$$

$$F_{S2} = F_{FB,N2} - dir(R)F_{FB,T2} \tag{32}$$

where *dir(R)* represents the positive or negative direction of the rotor [13].

3.2.2 Rotor (Vertical)

The rotor of the USM has two degrees of freedom, each represented by a subsystem. The first subsystem discussed, the vertical system, represents the out of plane motion of the rotor as it is forced out of it's neutral position, z_o equal to zero when the motor is off, to a finite steady state position, z_{ss}. The system from which the EOM for the vertical rotor system is derived is shown in Figure 3.7

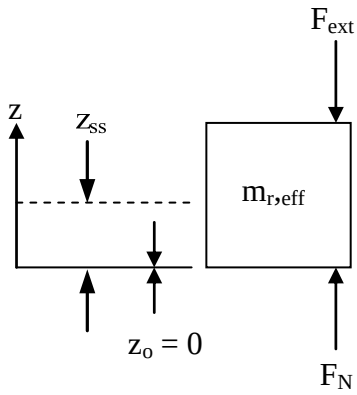

Figure 3.7. Diagram of the rotor (Vertical) subsystem from which the EOM is derived.

The equation describing this vertical motion is

$$m_{R,eff}\,\ddot{z} = F_N - F_{ext} \tag{33}$$

where $m_{R,eff}$ is the effective mass of the rotor, F_{ext} is the constant external force pressing the rotor into the stator and F_N is the normal force created by the traveling wave, calculated using (2).

3.2.3 Rotor (Angular)

The second rotor subsystem describes its angular motion. The system is represented by Figure 3.8.

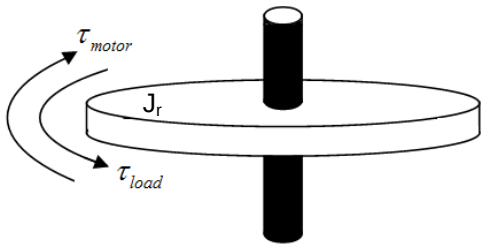

Figure 3.8. Rotor (Angular) system used to derive angular equation of motion

The equation of motion for the rotational degree of freedom for the rotor is given by

$$J_r\,\dot{w}_{rot} = M_{USM} - M_{load} \tag{34}$$

where J_r is the inertia of the rotor, M_{USM} is the output torque of the motor, and M_{load} is the external load torque carried by the motor [13].

Equations (2)-(34) have been modeled in the MATLAB Simulink environment using motor properties taken from [11], those specific to the Shinsei USR60 USM. The equations describing the contact mechanics and equations of motion for the USM have been assembled referencing sources [7, 11, 13, 14]. Therefore, while the physical properties of the motor model match the USR60, the model outputs do not overlay with the simulation outputs of [11]. All analysis using the USM model in this thesis is therefore treated as qualitative instead of quantitative; consistent with the point of the thesis, which is to prove capability and functionality instead of specific performance characteristics. The exact MATLAB Simulink complex dynamic model used for all simulations hereafter is detailed in Appendix A along with a breakdown of the subsystems and functions that represent all equations discussed in sections 3.2 and 3.3.

3.3 CDM: Modeling Difficulties

Equations (2)-(34) summarize the ideal model for a USM, and it would seem that after wading through an in-depth derivation of the formulas (see [7, 11, 13, 14]), that implementing them in the Simulink environment would be straightforward. This is not the case. The main difficulty with simulating the full USM model is caused by the coupling between each subsystem. An accurate solution for the stator vibration is not possible unless the feedback forces are calculated correctly. The normal and tangential feedback forces cannot be calculated without the correct forcing input to the rotor's vertical system, a function of both the traveling wave amplitude (a stator output) and the half-contact length (a rotor vertical system output). In addition, if the traveling wave amplitude and half-contact length are incorrect, the angular subsystem of the rotor will fail. In short, calculation errors in any motor subsystem will lock up the entire USM model. The USM subsystems and their couplings are represented in Figure 3.9.

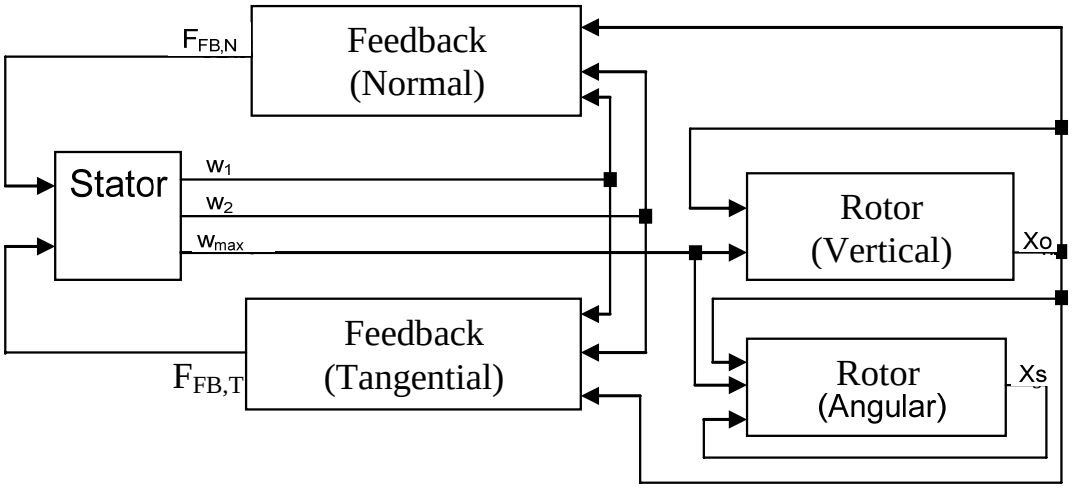

Figure 3.9. Schematic of USM subsystems and their coupling lines.

An attractive simplification for the debugging process is to remove the feedback-force lines and simulate an in-line system like that of Figure 3.10. In doing so, the stator subsystem that was originally nonlinear can now be modeled as a linear system with an explicit solution.

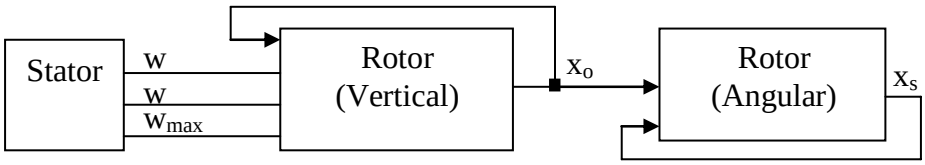

Figure 3.10. Schematic of the reduced USM subsystems for the in-line model.

The problem with simulating the reduced model of Figure 3.10 can be seen by comparing plots of the steady-state traveling wave amplitude versus the electrical input frequency to the stator for separate simulations that either include or neglect feedback-forces. The results of three such simulations are shown in Figure 3.11. Represented by Plot A is the response of a stator experiencing no feedback-forces; a free stator. Represented by Plots B and C are the responses of a stator affected by feedback-forces where the external load pressing the rotor into the stator is altered between simulations.

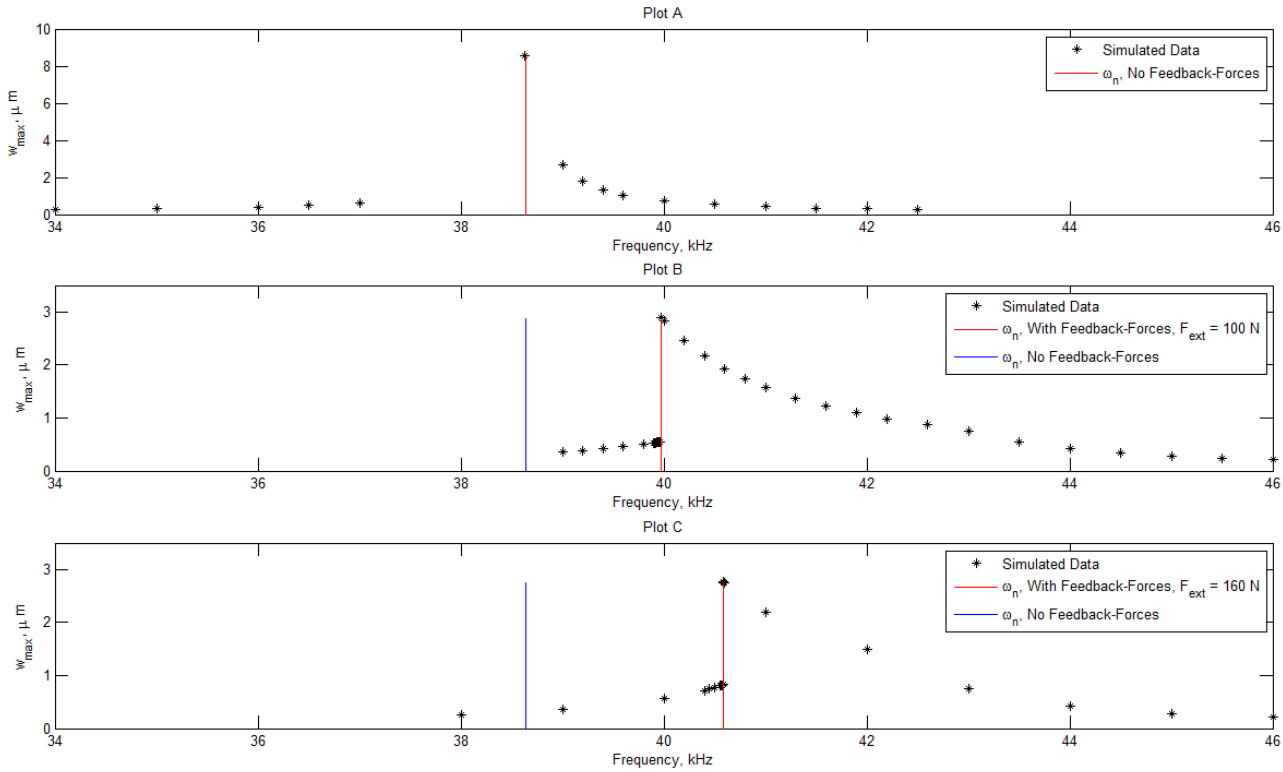

Figure 3.11. Plot A: Free stator response to piezo-excitation. Plot B: Stator response to piezo-excitation and feedback forces, External Pressing Force, F_{ext} = 100 N. Plot C: Stator response to piezo-excitation and feedback forces, External Pressing Force, F_{ext} = 160 N.

As previously mentioned, the steady state traveling wave amplitude is the single most important value calculated in an USM model, as it has the greatest influence on a motors speed and load carrying ability. With this in mind, the most striking difference between Plot A and Plots B-C is the difference in steady state traveling wave amplitudes. The free stator excited at its natural frequency has a steady state wave amplitude of approximately three times larger than coupled stators excited at their individual natural frequencies. In addition, the wave amplitude rolls off at a much greater rate for the free stator beyond its natural frequency than the wave amplitudes of the coupled stators. This leads to another interesting fact: as the external force pushing the stator and rotor together is increased, the natural frequency of the motor will also increase. The natural frequency of Plot A can be determined by linear vibration theory prior to simulation as

$$\omega_n = \sqrt{\frac{k_{s1}}{m_{eff}}} = \sqrt{\frac{k_{s2}}{m_{eff}}} \tag{35}$$

where k_{s1}, k_{s2}, and m_{eff} are the coefficients of the stator system equations (22) and (23). There is no closed form solution for the natural frequency of the stator/rotor combination, so it can only be found through trial and error simulations.

It is clear that a simulation based on the system of Figure 3.10 will not be representative of the fully coupled system of Figure 3.9, as the traveling wave amplitude and system natural frequency are very different from the motor simulation accounting for feedback forces. However, simple signal conditioning would allow the free stator response to mimic a correct response. But how does one continue the debugging process for the vertical and angular rotor systems? These subsystems are not only coupled with the stator and with each other but also with themselves. The solution to this question comes with the understanding that the debugging of an ultrasonic motor model cannot be accomplished by debugging each individual subsystem as a solitary unit. Instead, a two-subsystem-combination must first be debugged and validated, and then the third system can be added, debugged and validated. The tool necessary to accomplish this task, the reduced dynamic model for a USM, is discussed in Chapter 4 .

3.4 CDM: Outputs

To present the outputs of the full Simulink model in a logical fashion, plots of importance from the stator, rotor (vertical) and rotor (angular) subsystems are discussed individually followed by a statement about each outputs significance to the overall system. These simulation results are for an unloaded USM. However, a speed versus frequency plot is also presented to summarize the operational envelop of the model under the effect of resistive loading.

The first of the model outputs are the stator modal displacements taken from the stator subsystem. One phase of these modal displacements is shown in Figure 3.12. The second Phase is not shown, as the overall trend is the same as that in Figure 3.12 and only a highly zoomed frame would show the ninety degrees phase difference between the two signals.

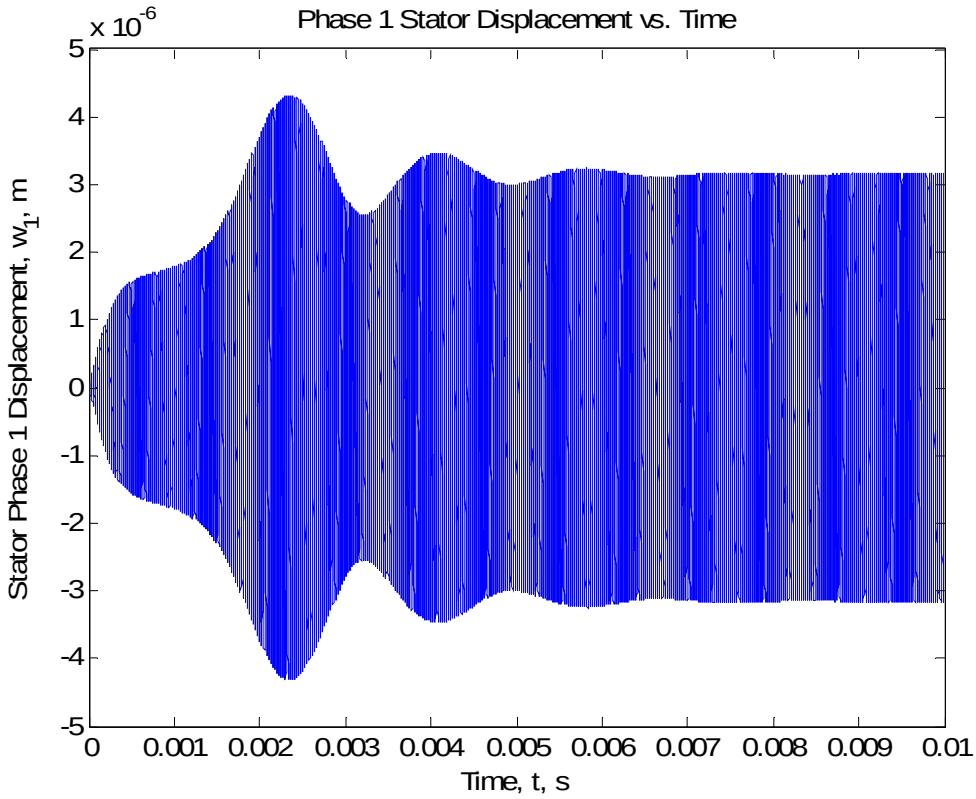

Figure 3.12. Modal displacements for Phase 1 of the stator.

The displacements output by the stator subsystem are significant for two reasons. First, they are used to calculate the amplitude of the traveling wave as in equation (24). Second, the modal displacements of each phase are used at each time step to determine the correct modal feedback forces caused by the interaction between the stator and rotor subsystems.

The traveling wave amplitude output of the model is shown in Figure 3.13. The traveling wave amplitude plays a critical role in the mechanics of a USM, as it is used to determine the contact length of the traveling wave, the feedback forces, and the torque output of the motor.

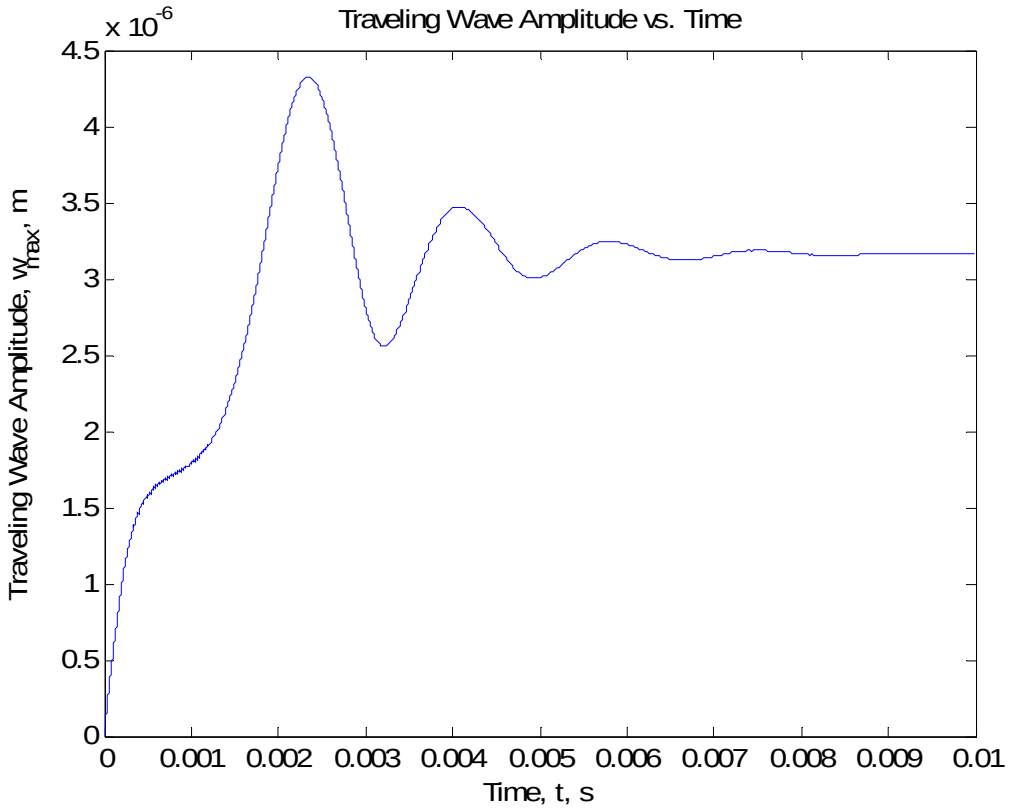

Figure 3.13. Traveling wave amplitude of the stator vs. Time.

The values plotted in Figure 3.13 must be correct in order to simulate the vertical rotor system. In the vertical system, accurate monitoring of the rotor height above the stator is undertaken thereby allowing the half-contact length of traveling wave within the rotor contact material to be determined. A plot showing the height of the rotor over the stator as the traveling wave pushes into it over time is shown in Figure 3.14. There is a critical traveling wave amplitude, $(w_{max})_{min}$, that must be reached before the stator normal force matches and then overcomes the external pressing force. In the time where the wave amplitude is less than the critical value, the force created by the stator wave crest in the rotor's contact area is less than F_{ext}, and the rotor remains pressed into the stator with a height of zero. As seen in Figure 3.14, the time in which the traveling wave amplitude is less than $(w_{max})_{min}$ is less than half of a millisecond.

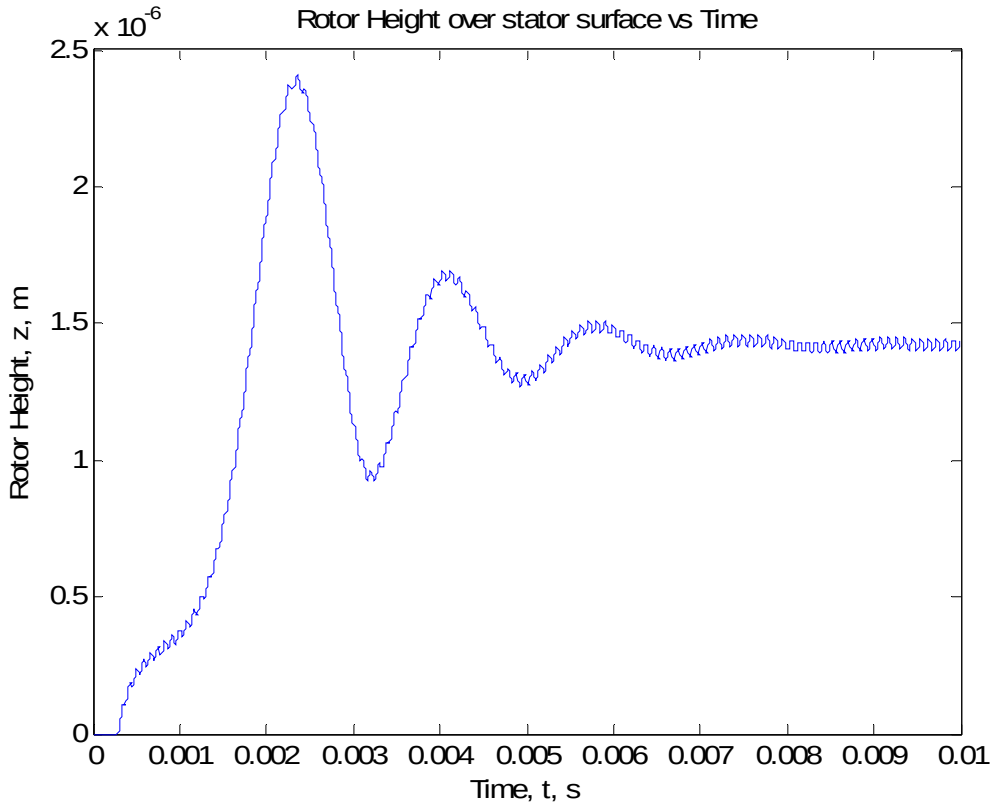

Figure 3.14. Rotor height above the stator vs. Time

During the development of the steady state traveling wave, the stator surface pushes into the rotor contact material, and based on a linear-spring contact theory, the half-contact length will adjust such that the normal force created by the traveling wave is equal and opposite to the external force pushing the rotor into the stator. The plot of half-contact length versus time is shown in Figure 3.15.

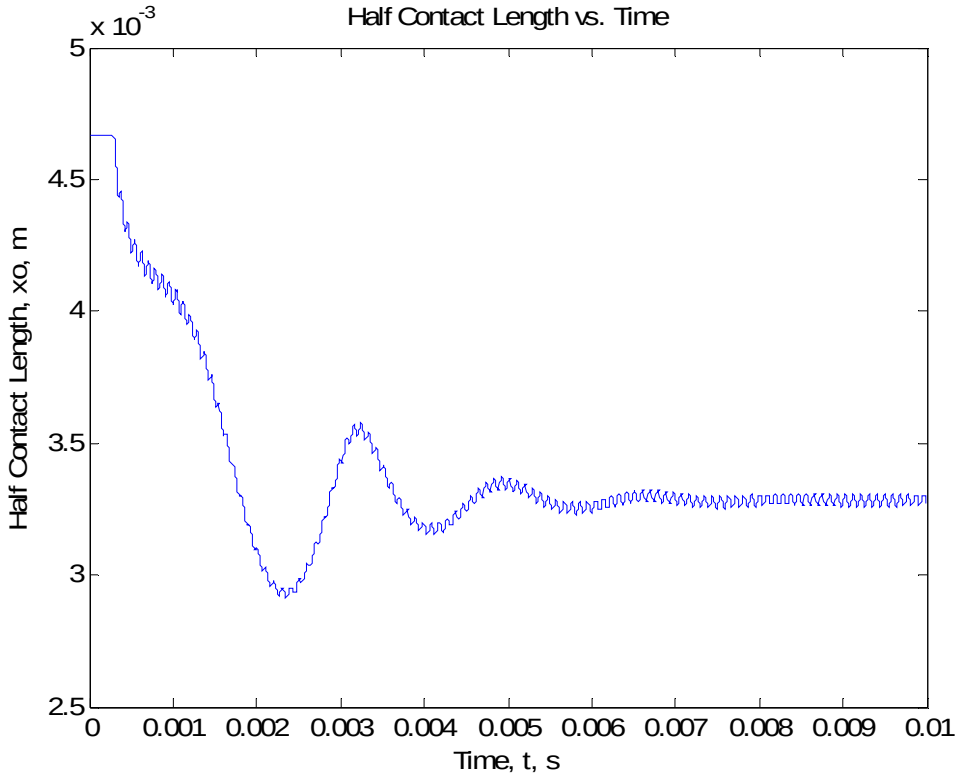

Figure 3.15. Half-Contact Length of the Traveling Wave vs. Time

The period of time where w_{max} is less than $(w_{max})_{min}$ can be observed in the figure above. In order for the simulation to run properly, the half-contact length is given the initial value of $\lambda/4$ which it retains until w_{max} is greater than $(w_{max})_{min}$, at which point the rotor is pushed vertically away from the stator surface, and a new contact length can be calculated by equation (4). The calculation of $(w_{max})_{min}$ is discussed further in Chapter 4 .

The half-contact length is the critical output from the vertical rotor system and is used in the rotor (angular) system to determine the torque that drives the rotor into motion. Once in motion, the horizontal velocity of the rotor, determined by solving equations (10) and (34), is compared to the horizontal component of the stator's surface point velocities to find the stick-point of each wave crest. The stick-point is used along with the half-contact length to calculate the motor torque acting on the rotor. It is given the initial value of $\lambda/4$ which means that at motor startup, only a driving zone exists at the stator/rotor interface. In the transient period of operation, the

stick-point length may be larger than the contact length. If so, it takes on the half-contact length value at that time step as dictated by equation (21).

Over the course of the simulation, the stick-point length adjusts based on the velocity of the rotor to steady state value such that driving and braking regions of the contact zone are equal and opposite in magnitude. A plot of the stick-point as it varies with time is shown in Figure 3.16. Figure 3.15 and Figure 3.16 and are overlaid to show that that in steady state the stick-point is less than or equal to the half-contact length.

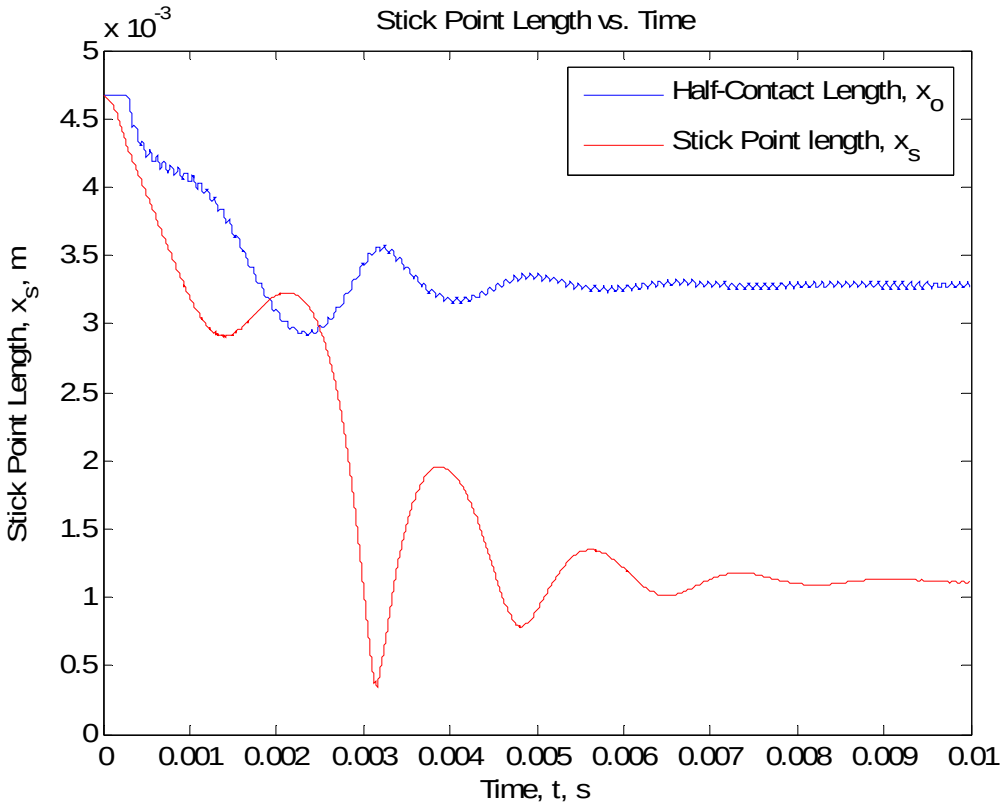

Figure 3.16. Stick-point Length of the Traveling Wave vs. Time

The motor output torque, a function of the traveling wave amplitude shown in Figure 3.13 and the half-contact length and stick-points shown in Figure 3.16, is shown in Figure 3.17.

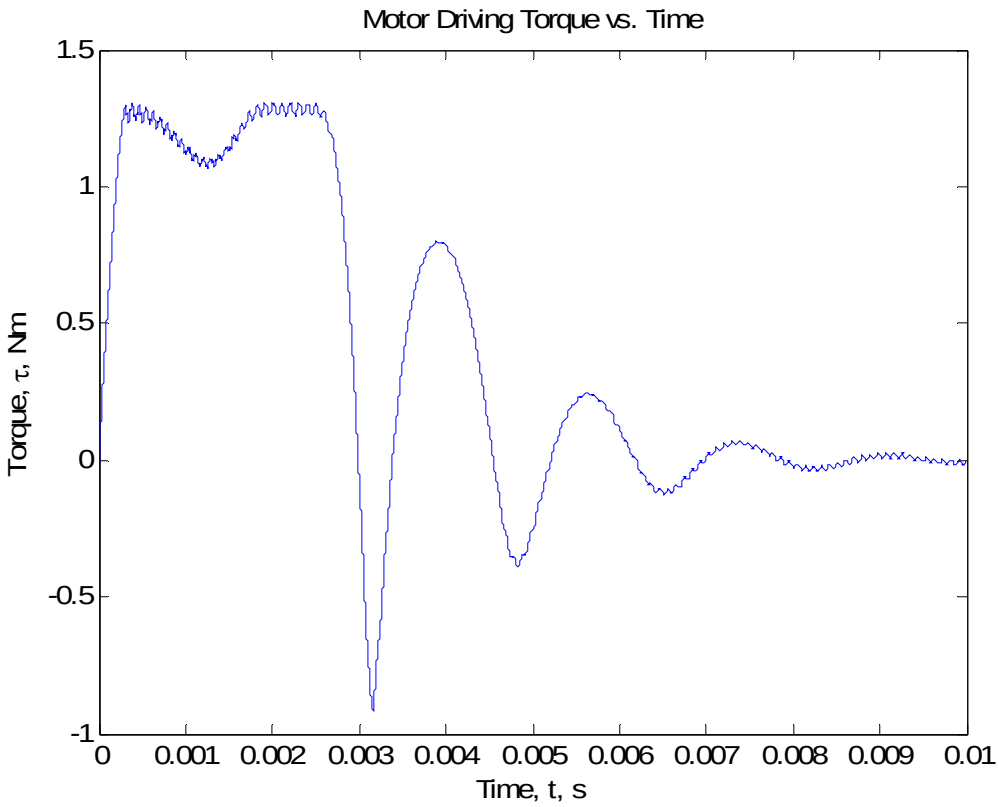

Figure 3.17. Motor Output Torque vs. Time

As previously discussed, when describing the role of the stick-point and half-contact length to the torque generation, in steady state, the motor torque output matches the load placed on it. In this case, the motor is operating under a no load condition, and as such, the motor drive torque tends to zero in steady state.

A unique property of the USM can be seen in plot of Torque versus time. In the time period [0.002 s, 0.00275 s], the torque remains constant at 1.28 Nm, the maximum rated torque of the motor. The reason behind becomes clear after observing Figure 3.16 again. During the same time period, the stick-point length is longer than the half-contact length. Therefore, the entire traveling wave crest within the rotors contact material is driving the rotor forward, the stick-point is given the value of the half-contact length per equation (21) and the motor torque output remains constant at $(M_{USM})_{max}$ for that time period.

The final value monitored in the simulation is the rotor speed, plotted against time in Figure 3.18, which varies with respect to the motor load and the motor drive frequency. The property of quick motor response is clear, as the motor reaches a steady state velocity in approximately seven milliseconds.

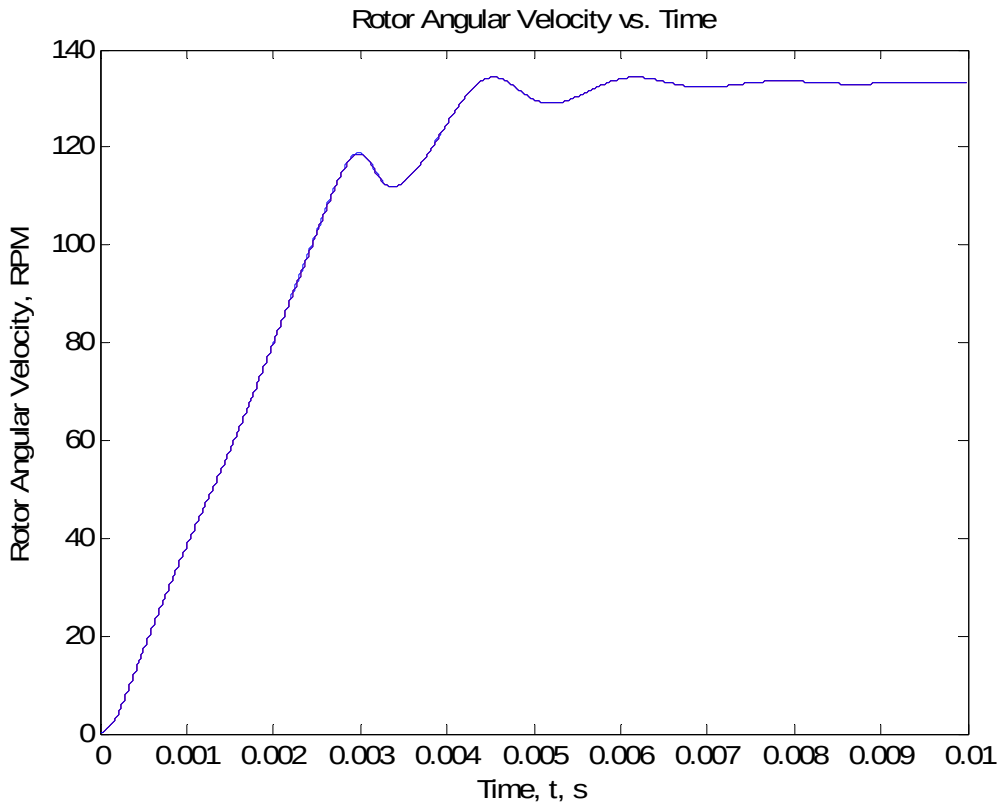

Figure 3.18. Motor Angular Velocity vs. Time

While helpful to understand the motor mechanics during the transient period of operation, Figure 3.12 through Figure 3.18 do not provide the torque dependent speed versus frequency information needed to define the operational envelope of the motor. Such a visual can be assembled by simulating and collecting the steady state motor speed data over the frequency and torque range where the model is valid. The speed-frequency curves for resistive loading are shown in Figure 3.19.

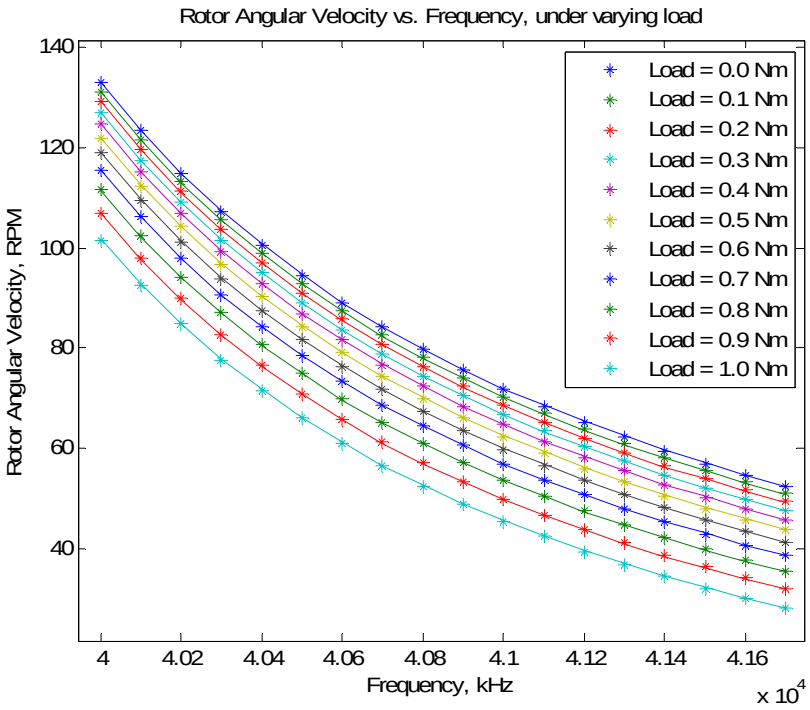

Figure 3.19. Operating envelope of the USM model under varying frequency and torque load, resistive loading.

The performance envelope shown in Figure 3.19 does not describe the entire operational range of the USM. While the Simulink model functions well under the effect of resistive motor loads, it cannot simulate additive loads; a severe limitation of the model, as only a motor under additive loading can provide feedback forces typical of feel-systems. Therefore, a new model that is capable of simulating both types of motor loads is needed.

3.5 CDM: Conclusions

A functioning complex dynamic model of the traveling wave rotary ultrasonic motor was assembled referencing available literature. Through simulation, the operational envelope of the model was determined for resistive loads, and the inability of the model to operate under the influence of additive loads was discovered. A model that is incapable of simulating additive loads is essentially useless for analyzing force-feel scenarios, so a new more robust model of reduced complexity has been developed. The reduced dynamic model is the subject of Chapter 4.

4 Contribution 1: Reduced Dynamic Model (RDM)

This chapter presents a new approach to modeling ultrasonic motors by using simple curve-fitting techniques as substitutes for dynamic systems in the Simulink environment. The complex contact mechanics of the ultrasonic motor are well documented by [7] leading to a generalized form of the motor speed-torque equation for several contact theories. However, the analysis of the formulas derived within it are not representative of an actual motor in that the traveling wave amplitudes and contact lengths are pre-set rather than solved for using a dynamic model of USM stator coupled with a rotor. Many *complete* models detailing USM subsystem equations of motion and subsystem-coupling such as those presented in [11] and [12] have been validated, but these models remain exceedingly complex in order to model the motors transient and steady state operational areas; difficulty in implementing such models in Simulink the byproduct. The newly proposed curve-fitting method simplifies the complete USM models by approximating, with high accuracy, the relationships between traveling wave amplitude, rotor external force, wave contact length, contact stick-points, and the load carrying capability of the motor such that the fundamental equations derived in [7] are satisfied. In addition to predicting steady state motor behavior and aiding in the assembly of more complex dynamic models, the new technique provides an efficient means to check "what-if" scenarios accompanying motor parameter manipulation.

4.1 RDM: Development

The basis for the RDM lies first in understanding each subsystem and how its outputs are required for the rest of the model to function. A summary of the subsystems and their key outputs and their couplings is provided in Table 4.1.

Table 4.1. Model subsystems and their outputs needed for a functioning model

Subsystem	Output	Coupled with	Coupled Variable
Stator	Traveling Wave Amplitude, w_{max}	Rotor (Vertical, Angular)	Wave Contact Length, x_o
Rotor (Vertical)	Wave Contact Length, x_o	Stator, Self	Traveling Wave Amplitude, w_{max} Wave Contact Length, x_o
Rotor (Angular)	Wave Stick-point, x_s, Rotor speed	Stator, Rotor (Vertical), Self	Traveling Wave Amplitude, wmax Wave Contact Length, x_o Wave Stick-point, x_s

As shown in Table 4.1, the lower a systems placement in the subsystem column, the greater the number of systems coupled to it, the greater the number of coupled input variables needed for it to function and the greater the complexity of modeling it. The RDM is based on the assumption that the stator is the only dynamic system is needed to model the USM and that functions approximating the half-contact length and stick-points can replace the rotor subsystems. The process of assembling the RDM is accomplished by first fully understanding the transient and steady states of equations (33) and (34), and then forcing equations (16) and (17) to be satisfied at all times during the simulation instead of only when the traveling wave amplitude has reached steady state.

4.2 Dynamics of the Stator-Rotor Combination

Before deriving the RDM, the dynamics of what is occurring at the stator-rotor (vertical) interface during transient and steady motor operation must be well understood. The system from which the rotor (vertical) equation of motion was derived is shown in Figure 4.1. The rotor height when the motor is off is called z_o and is equal to zero. When the motor is in steady state operation, the normal force created by the traveling wave pressing into the rotor, F_N, is equal to the external pressing force, F_{ext}, and the rotor height is typically greater than zero. Only when the half-contact length is equal to $\lambda/4$ can the steady state rotor height can be equal to zero.

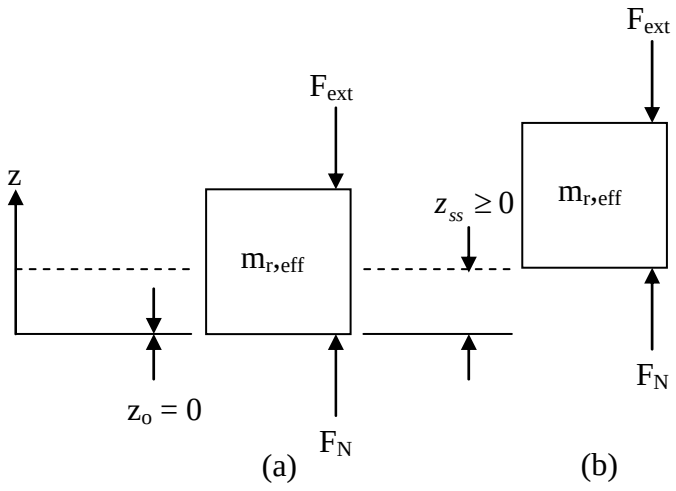

Figure 4.1. Rotor (vertical) system: (a) Motor off or in steady state with $x_o = \lambda / 4$
(b) Motor in steady state operation.

When the motor is turned on, the traveling wave will fluctuate through an exponentially decaying sinusoidal transient period, as is common with underdamped, sinusoidally forced second order systems, finally reaching steady state amplitude. The progression of wave amplitudes through the transient and into steady state is illustrated in Figure 3.13.

As the traveling wave amplitude fluctuates, so will the normal force created by the traveling wave pressing into the rotor contact material. In doing so, the rotor will accelerate in the direction of the net force acting on it

$$F_{net} = F_N - F_{ext}. \tag{36}$$

At steady state, the half-contact length will be such that when plugged into equation (2) along with the traveling wave amplitude

$$F_N = F_{ext}. \tag{37}$$

The stator rotor interface of one traveling wave crest is shown in Figure 4.2. *P(x)* represents the linear spring pressure distribution caused by the traveling wave pressing into the rotor. The

distribution occurs over the total stator contact length from $-x_o$ to x_o, and an integral taken of $P(x)$ over this range results in F_N.

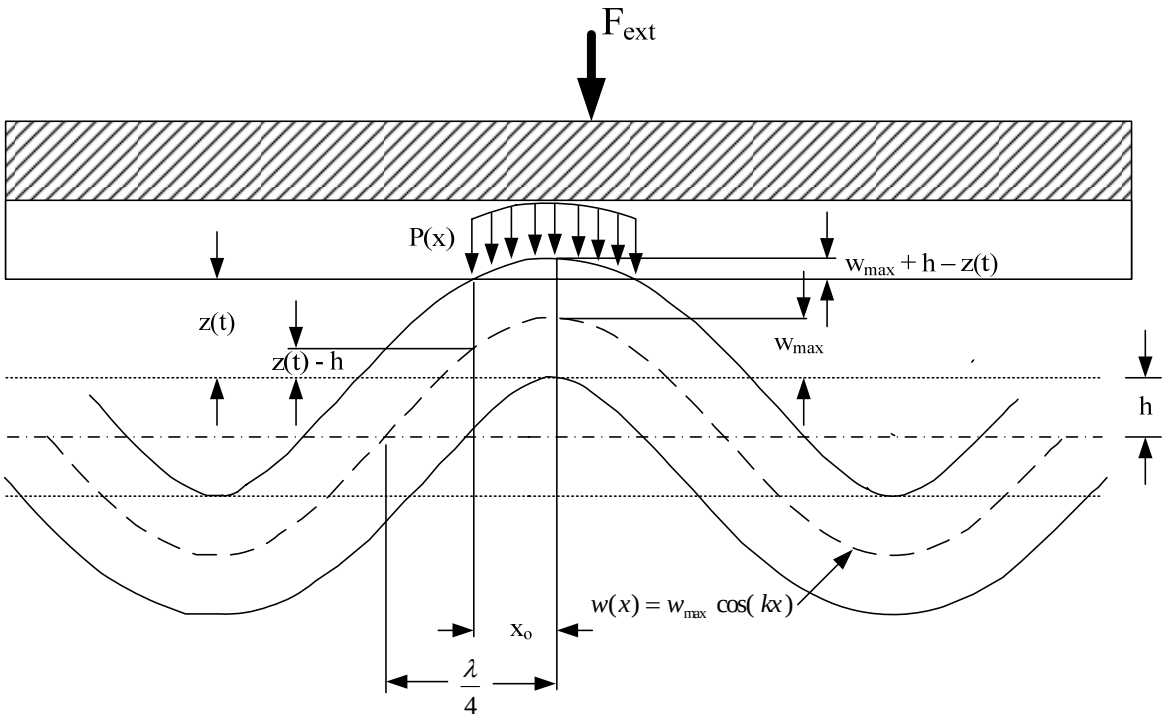

Figure 4.2. Plot of developing traveling wave amplitude with respect to time.

When a model is functioning properly, the rotors height above the stator, determined by simulation of equation (33), is analyzed after each time step to determine the half-contact length of the traveling wave within the rotor. The half-contact length is used to calculate a new normal force, F_N, by (2), which is used in the proceeding time step to determine the next F_{net}, the new rotor height and the new half-contact length; the sole purpose of the rotor (vertical). Therefore, if x_o can be found through some other correlation to the system, the vertical system can be neglected.

4.3 RDM: Pseudo-x_o

As established in the previous section, it is known that during steady state, equation (37) is satisfied meaning

$$F_{ext} = \frac{2nc_N w_{\max}}{k}\left(\sin(kx_{o,S.S.}) - kx_{o,S.S.}\cos(kx_{o,S.S.})\right). \tag{38}$$

where $x_{o,S.S.}$ is the half-contact length needed to satisfy equation (37) when the traveling wave amplitude has reached steady state. If a function can be found such that

$$x_{o,S.S.} = f(w_{\max}) \tag{39}$$

for all time in the simulation, that function can be substituted for the vertical system of the rotor. By replacing it, equation (39) will provide the half-contact lengths for all traveling wave amplitudes, both transient and steady state. To begin finding the function, equation (36) is expanded such that

$$F_{net} = \frac{2nc_N w_{\max}}{k}\left(\sin(kx_{o,S.S.}) - kx_{o,S.S.}\cos(kx_{o,S.S.})\right) - F_{ext}. \tag{40}$$

Next, an F_{net} matrix is produced by evaluating equation (40) over two vectors

$$x_{o,S.S.} = [\left(0.0001 * \frac{\lambda}{4}\right) : \frac{\lambda}{4}] \tag{41}$$

and

$$w_{\max,S.S.} = [(w_{\max,S.S.})_{\min} : (w_{\max,S.S.})_{\max}] \tag{42}$$

where $(w_{\max,S.S.})_{\max}$ is arbitrary but on the order of the expected maximum traveling wave amplitude, and $(w_{\max,S.S.})_{\min}$ is substituted for w_{max} and solved for in equation (40) with $x_{o,S.S.}$ replaced with $\lambda/4$ such that

$$(w_{\max,S.S.})_{\min} = \frac{F_{ext}k}{2nc_N\left(\sin(k\frac{\lambda}{4}) - k\frac{\lambda}{4}\cos(k\frac{\lambda}{4})\right)}. \tag{43}$$

The first and last value in vector (41) and the first value in vector (42) are chosen specifically to satisfy the linear spring contact theory derived in [7]. By that theory, the maximum full-contact length where the derived equations are applicable is $\lambda/2$, meaning the largest half-contact length must be $\lambda/4$. The first value in (41) should be a small percentage of the maximum so a full range of half-contact lengths can be observed, but it cannot equal zero or the contact theory changes from linear spring to point contact. A contact length of zero corresponds with the stator touching the rotor at a point instead of over a length. While the maximum value in vector (42) can be arbitrary, the minimum value cannot be less than that calculated with equation (43) or the contact mechanics will fail.

The F_{net} matrix can then be plotted, as shown in Figure 4.3. As the legend shows, each line represents an evaluation of equation (40) where the half-contact length remains constant over a vector of amplitudes. For ease of viewing, seven half-contact lengths within vector (41) were used.

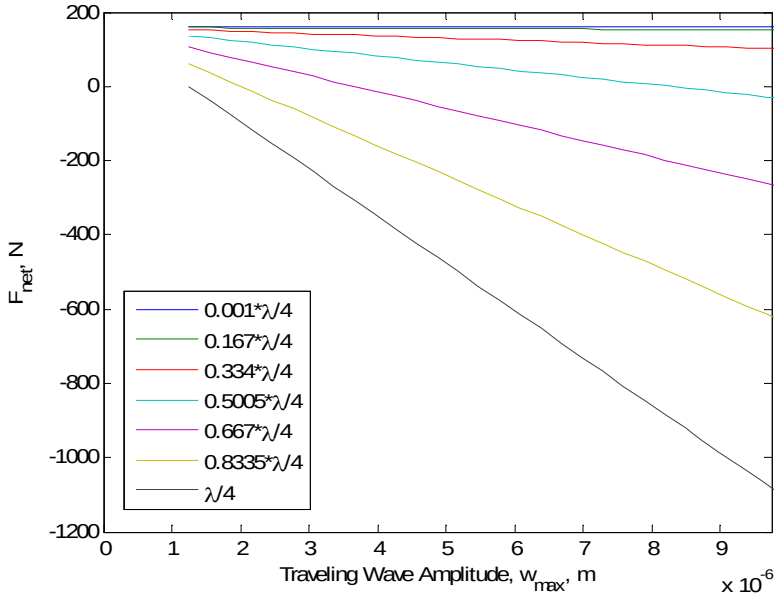

Figure 4.3. F_{net} versus Traveling Wave amplitude for various half-contact lengths.

In the development of equation (39), the points of interest in Figure 4.3 are the zero crossings, and as they satisfy equation (38), both the amplitude and the steady state half-contact length at that point are recorded. These data pairs can be plotted against one another along with a best-fit line, as in Figure 4.4. When the data is plotted on a log-log scale, it is nearly linear allowing for a highly accurate fit-line to be determined.

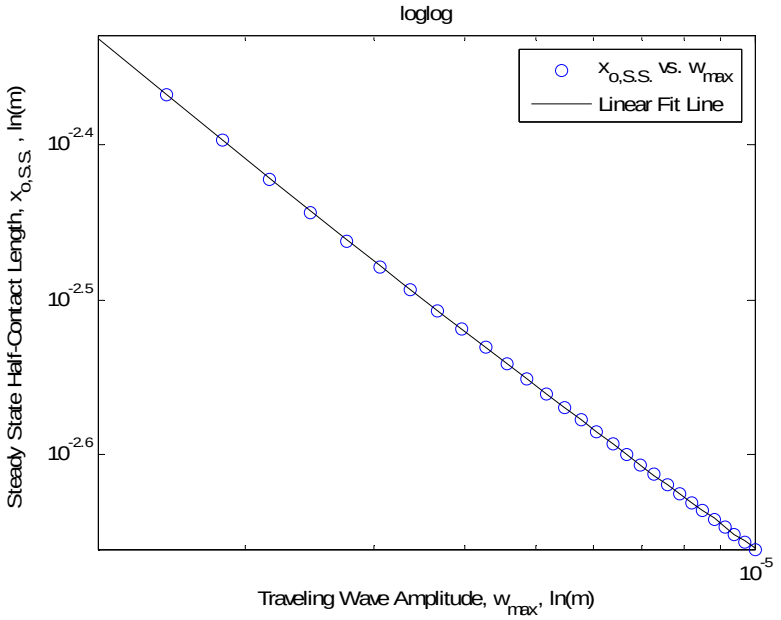

Figure 4.4. $x_{o,S.S.}$ versus w_{max} collected from Figure 6.

Converting both the points taken from Figure 4.3 and the best-fit data of Figure 4.4 back into linear coordinates and plotting them allows for a better visualization of how the steady state half-contact length changes with increasing wave amplitude; in a nearly perfect exponential decay beginning at $(w_{\max,S.S.})_{\min}$ where $x_{o,S.S.}$ is equal to $\lambda/4$.

The MATLAB *polyfit* function was used to generate the best-fit lines of Figure 4.4 and Figure 4.5. Using the fit coefficients, an accurate function that satisfies equation (39) for all traveling wave amplitudes greater than $(w_{\max,S.S.})_{\min}$ can be assembled. The new function can be used as a replacement for the rotor (vertical) subsystem. Equation (39) now becomes

$$x_{o,S.S.} = f(w_{\max} \geq (w_{\max,S.S.})_{\min}) = w_{\max}^{m} e^{b}. \tag{44}$$

where the coefficients m and b are the fit coefficients determined in MATLAB. The code used to determine the coefficients of equation (44) and plot Figure 4.3 through Figure 4.5 is presented in Appendix B.

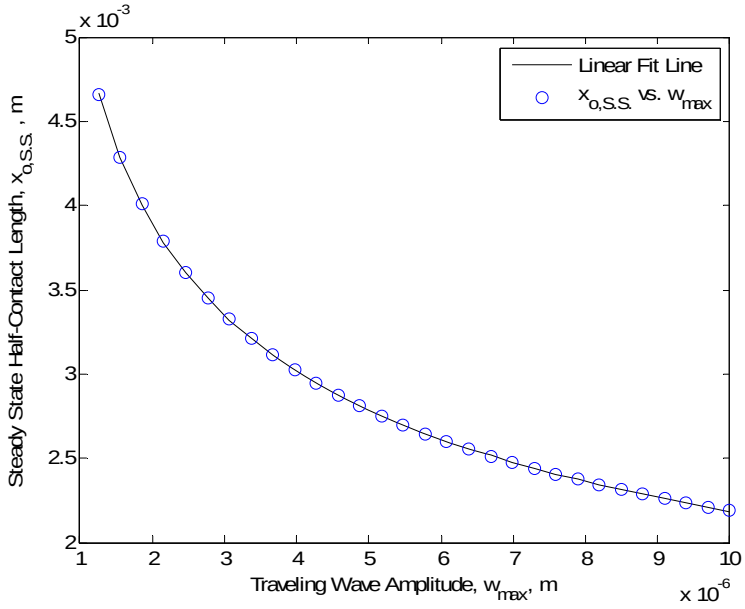

Figure 4.5. Linear plot of $x_{o,S.S.}$ versus w_{max} showing exponential decay.

4.4 RDM: Pseudo-x_s

In the previous section, the equation needed to replace the rotor (vertical) subsystem in the RDM was derived. Instead of solving for the output of a dynamic system and extracting the half-contact length from it, the pseudo-x_o function determines the would-be steady state value of the half-contact length, $x_{o,S.S.}$, such that equation (38) is satisfied for all traveling wave values greater than $(w_{max})_{min}$. The dynamic system is then replaced with a simple exponential function.

A similar approach is used to "fake" the stick-point values of a motor in operation. In steady state, equation (17) must be satisfied; a process carried out in the rotor's angular system of the CDM. The assumption for deriving the pseudo-x_s equation is similar to that needed to find equation (44) in the previous section; that a function can be found that approximates the steady state stick-point, $x_{s,S.S.}$, such that equation (17) is satisfied for all w_{max}, x_o, and M_{load} during the simulation and not solely when the traveling wave amplitude has reached steady state.

The relationship between the steady state traveling wave amplitude and the stick-point necessary to satisfy equation (17) is needed. While it is also a function of the steady state half-contact length, the method of calculating those values as a function of the traveling wave amplitude was already developed in the previous section. Therefore, for any traveling wave amplitude examined, equation (44) can be used to find the half-contact length. Reusing the amplitude values and the steady state half-contact lengths used to generate Figure 4.4, a loop is run in which every steady state amplitude/contact length pair is input into (17) along with a stick-point vector extending from zero to $x_{o,S.S.}(i)$ to plot the motor torque curve it produces. The first loop through is represented in equation form as

$$M_{USM} = \frac{2n\mu c_N w_{\max,S.S.}(i) R_o}{k}\left(2\phi([0:x_{o,S.S.}(i)) - \phi(x_{o,S.S.}(i))\right). \tag{45}$$

The resulting motor torque with respect to the traveling wave amplitude and stick-points is plotted for each loop as shown in Figure 4.6. Each curve is produced using a different steady state traveling wave amplitude, $w_{\max,S.S.}(i)$, and its corresponding half-contact length, $x_{o,S.S.}(i)$, as calculated using equation (44). The curve on the far right represents the largest wave amplitude examined and the curve on the far left represents $(w_{\max,S.S.})_{\min}$. If the external load acting on the motor is known along with the steady state traveling wave amplitude of the stator, the stick-point needed to satisfy equation (17) can be determined from the figure.

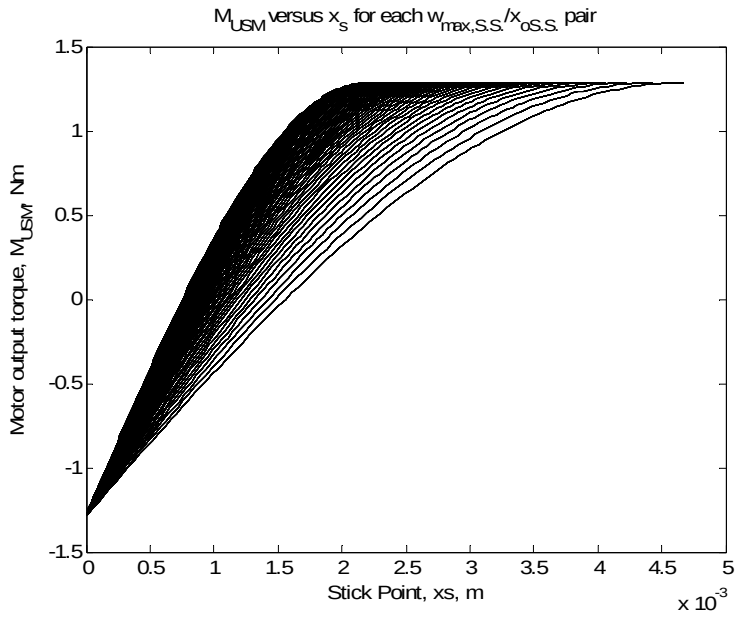

Figure 4.6. Motor output torque versus stick-point for steady state w_{max}/x_o combinations.

The negative maximum torque of Figure 4.6 corresponds to a stick-point length of zero, when only a braking zone exists. Such a case occurs if a torque is placed on the motor in the direction of rotation; an additive torque. The additive torque effectively adds to the driving area of the wave contact, and to reach driving/braking force equilibrium, the stick-point shifts upwards on the wave profile toward the crest. In doing so, the driving zone shrinks and the braking zone increases.

The positive maximum of Figure 4.6 occurs when the stick-point length is equal to the half-contact length as noted in section 3.1. In this scenario, the motor is under the affect of a torque resisting motor rotation, which effectively increases the braking zone. Therefore, the stick-points shift down the wave profile toward the half-contact length. In doing so, the braking zone shrinks, and the driving zone increases. At the positive maximum, only a driving region exists.

The cases of increasing the driving or braking zones depending on the direction of motor load are discussed further in Chapter 5 , as they determine the force-feel capabilities of the motor. In either case, the motor torque opposes the load torque, and the following relationship holds

$$(M_{USM})_{\min} = -(M_{USM})_{\max} \tag{46}$$

where $(M_{USM})_{max}$ is defined by equation (19).

Each curve of Figure 4.6 represents the output torque range of the motor under the influence of a steady state traveling wave amplitude and half-contact length pair that satisfies the contact mechanics reported in [7]. By analyzing each curve individually, the stick-points that produce any motor torque between $M_{USM,min}$ and $M_{USM,max}$ can be identified. In other words, for any motor load or traveling wave amplitude, the steady state stick-point that satisfies the requirement that the net driving and braking forces at the stator/rotor interface must cancel, can be found, or

$$x_{s,S.S.} = f(w_{\max}, M_{load}). \tag{47}$$

With the stick-point value known, the steady state motor speed can be extracted, and the rotor's angular system output can be verified.

The first step in finding equation (47) is to find $x_{s,S.S.}$ for every $w_{max,S.S.}/x_{o,S.S.}$ combination. To do so, two for-loops are used. The outer loop steps through the motor output torque vector of length j. The inner loop increments through the $w_{max,S.S.}/x_{o,S.S.}$ pairs of length i, and for each increment solves for $x_{s,S.S.}$ in the equation

$$M_{USM}(j) - \frac{2n\mu c_N w_{\max,S.S.}(i) R_o}{k}\left(2\phi(x_s) - \phi(x_{o,S.S.}(i))\right) = 0. \tag{48}$$

A matrix of steady state stick-points is then assembled in which each row represents the steady state stick-points for a specific motor torque, and each column presents the steady state stick-points for a specific wave amplitude/half-contact length combination, or

$$\begin{array}{c} \\ [M_{USM}^{(1)} \\ M_{USM}^{(2)} \\ \dots \\ M_{USM}^{(j)}] \end{array} \begin{array}{c} \begin{array}{cccc} [& w_{\max}^{(1)} & w_{\max}^{(2)} \cdots & w_{\max}^{(i)} \quad] \end{array} \\ \begin{bmatrix} x_s(w_{\max}^{(1)}, M_{USM}^{(1)}) & x_s(w_{\max}^{(2)}, M_{USM}^{(1)}) & \cdots & x_s(w_{\max}^{(i)}, M_{USM}^{(1)}) \\ x_s(w_{\max}^{(1)}, M_{USM}^{(2)}) & \ddots & & \vdots \\ \vdots & & & \\ x_s(w_{\max}^{(1)}, M_{USM}^{(j)}) & \cdots & & x_s(w_{\max}^{(i)}, M_{USM}^{(j)}) \end{bmatrix} \end{array}. \tag{49}$$

Similar to Figure 4.4, every row of steady state stick-points in matrix (49) is plotted against the vector of traveling wave amplitudes in Figure 4.7. Fourteen torque values spaced between 99% of the entire torque range of the motor are used; representative of the motors steady state output torque under both additive and resistive loading, the dotted and solid lines, respectively. Using the true maximum output of the motor caused errors in the program, so 99% of max was used instead. Each curve is representative of one motor load.

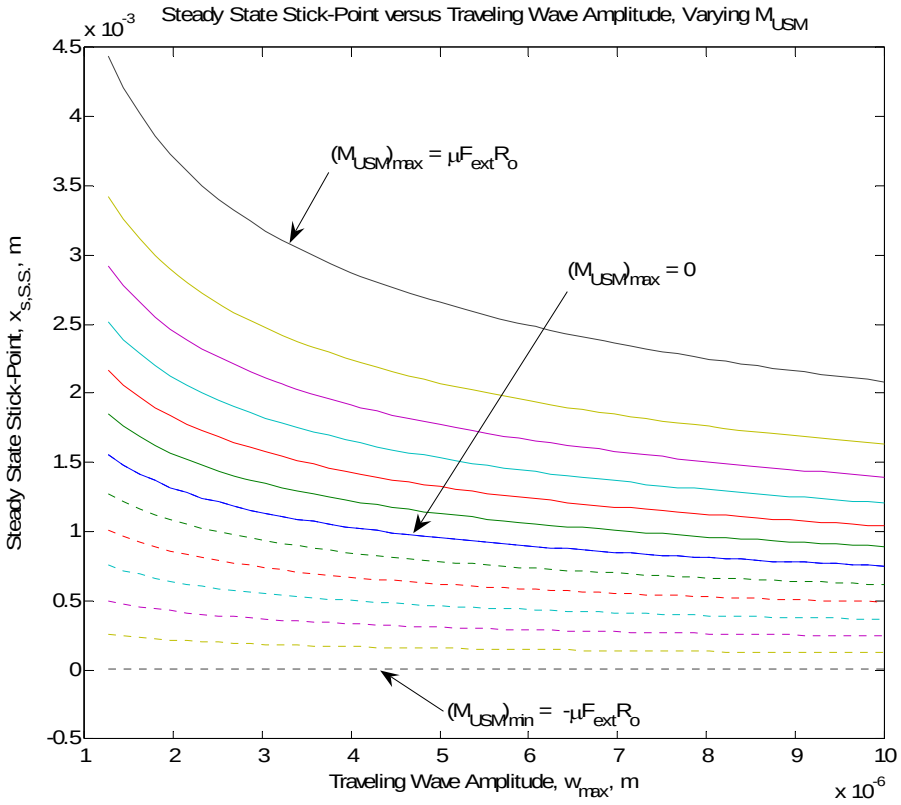

Figure 4.7. Steady State Stick-Points versus Traveling Wave Amplitudes under Varying motor loads.

The upper and lower curves of Figure 4.7 are of the greatest interest, as they approach the motors operational boundary curves. All steady state stick-points must fall on or between these boundary curves in order for the motor to operate, regardless of traveling wave amplitude. The boundary curves also help to illustrate the motion of the stick-points with respect to motor loading. The stick-points move down the wave crest toward the half-contact length point when a resistive load is placed on the motor thereby increasing the motor's driving area. When carrying

the maximum load $(M_{USM})_{max}$, the stick-points align themselves with the contact length. Therefore, the upper curve in Figure 4.7 is nearly the same curve as that shown in Figure 4.5. If the maximum motor torque was used to produce the upper boundary curve, it would match Figure 4.5. Conversely, the stick-points move up the wave crest when an additive load is placed on the motor thereby increasing the motor's braking area. Under a maximum additive load resulting in $(M_{USM})_{min}$, the stick-points are aligned with the traveling wave crest, and their length is zero regardless of traveling wave amplitude; as illustrated by the lower boundary curve of Figure 4.7.

The data of Figure 4.7 when plotted in log-log scale is nearly linear, but a third order curve-fit increases the accuracy of the following technique. A fit curve can be found for every data set of Figure 4.7 such that

$$x_{s,S.S.} = e^{\left(a_3 \ln^3(w_{\max}) + a_2 \ln^2(w_{\max}) + a_1 \ln^1(w_{\max}) + a_0\right)} \tag{50}$$

where a_3-a_0 are the fit-coefficients that vary with the load placed on the motor, such that

$$a_3 = e\left(M_{load}\right) \tag{51}$$

$$a_2 = f\left(M_{load}\right) \tag{52}$$

$$a_1 = g\left(M_{load}\right) \tag{53}$$

$$a_0 = h\left(M_{load}\right). \tag{54}$$

By finding fit-functions *e*-*h*, all space defined by the boundary curves of Figure 4.7 can be described as a function of motor load and traveling wave amplitude. When finding fit-curves to describe equations (51)-(54), it is best to find one set for resistive and one for additive loading, as the full the fit-coefficient versus motor load curves are very difficult to match over the full range of motor outputs torques and accuracy is lost. The process is detailed only for resistive loads placed on the motor from this point forward. The fit-coefficient versus motor load and their fit curves are presented in Figure 4.8 through Figure 4.11.

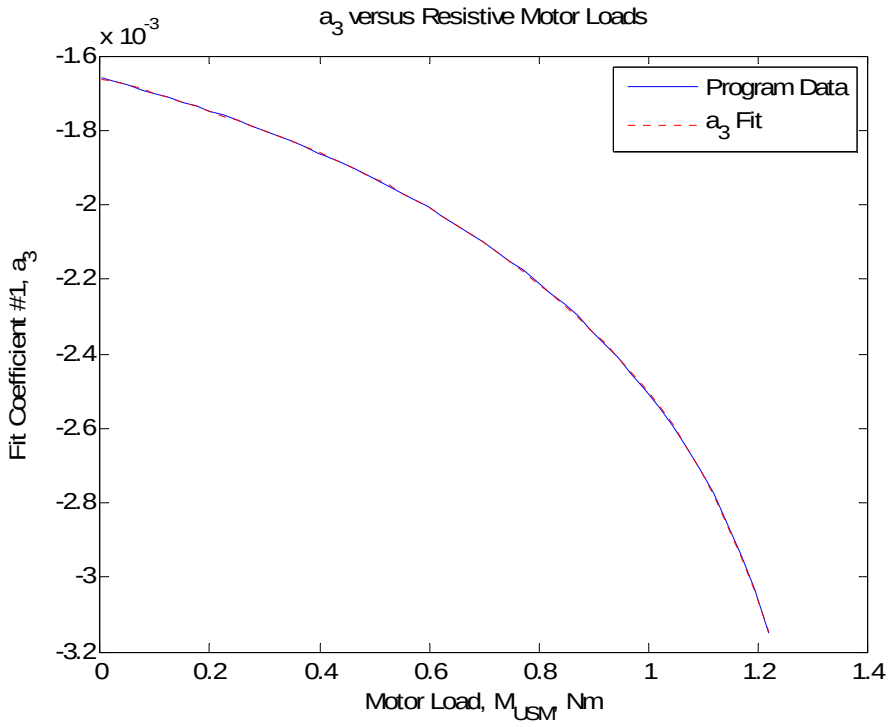

Figure 4.8. a_3 versus resistive motor loads

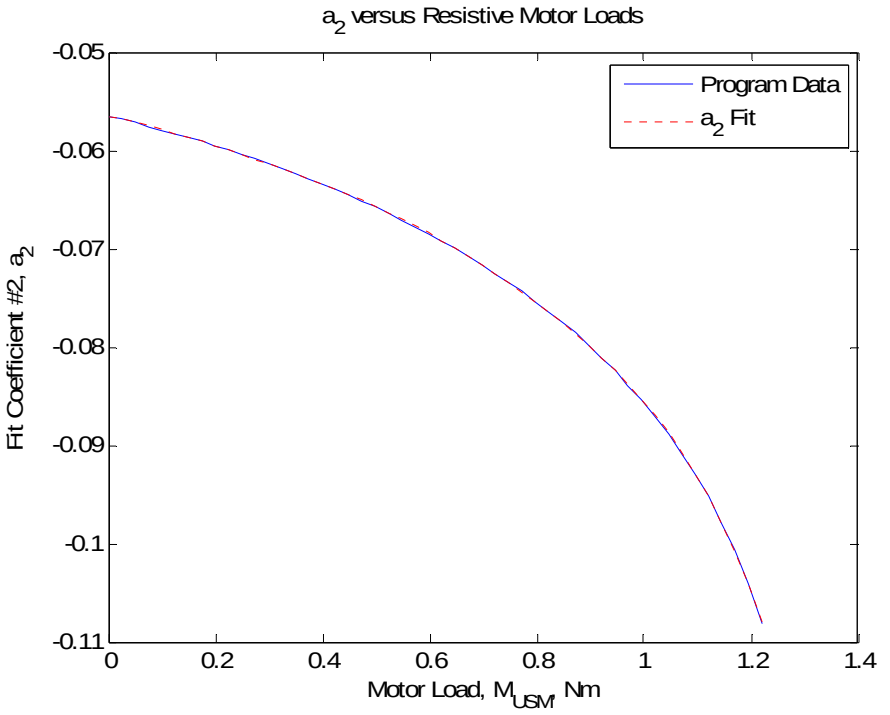

Figure 4.9. a_2 versus resistive motor loads

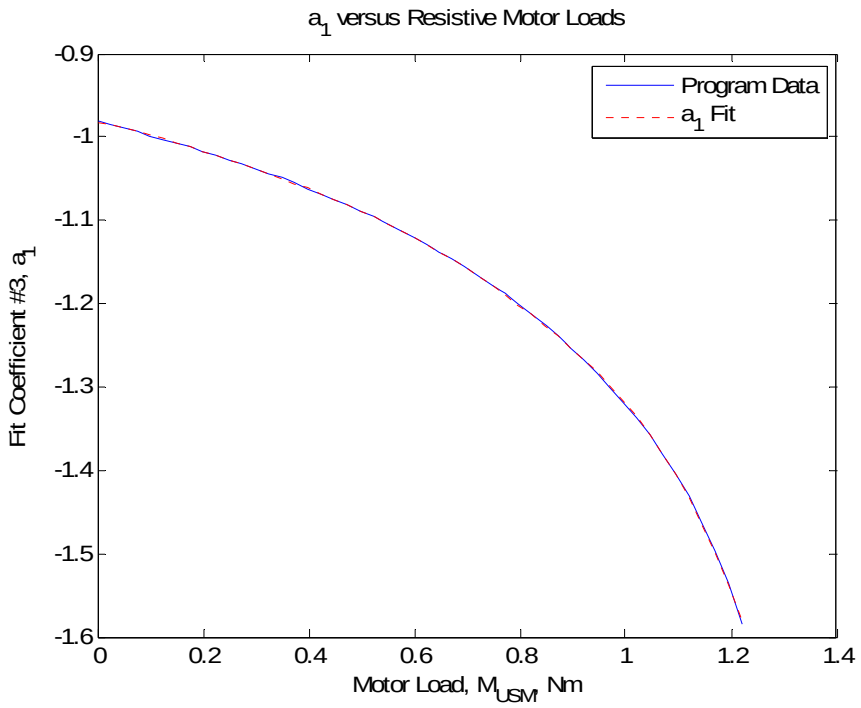

Figure 4.10. a_1 versus resistive motor loads

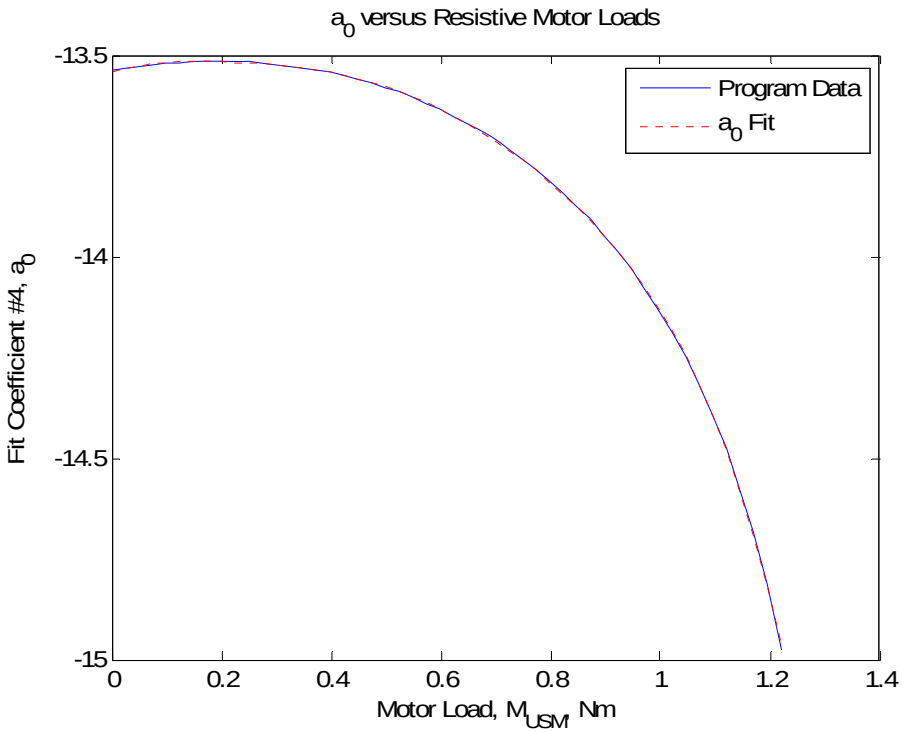

Figure 4.11. a_0 versus resistive motor loads.

With fit-line equations for coefficients a_3-a_0 found, equation (50) can be assembled and used to predict any steady state stick-point value within the operating region of Figure 4.7. Shown in Figure 4.12 are the stick-point curves produced with this method covering 95% of the resistive and additive load range of the motor. The upper and lower 5% of the torque range freezes the program.

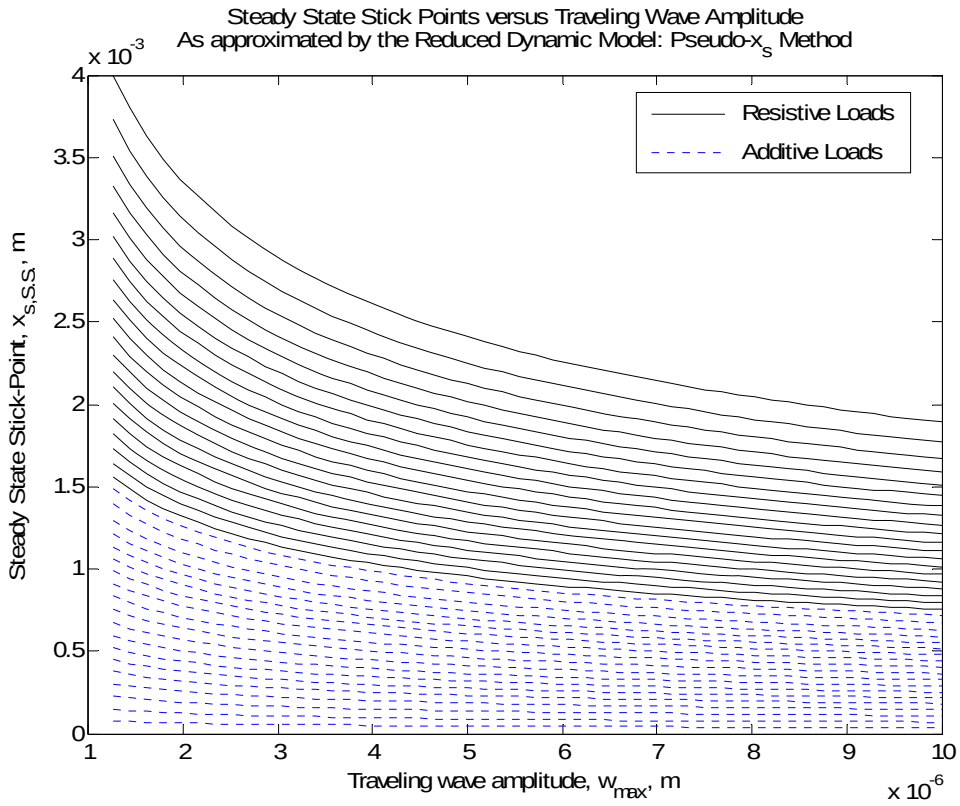

Figure 4.12. Results of the reduced dynamic model: Pseudo-x_s method over 95% of the motors torque range.

Equations (50)-(54) are used to find the steady state stick-point for all loads and traveling wave amplitudes in the motors range during simulation. From the stick-point values, the motor speed can be extracted from equation (11) by solving for $\dot{\theta}$ so that

$$\dot{\theta} = \frac{1}{R_o} v_{h,\max} \cos\left(k x_s\right) \tag{55}$$

where $v_{h,max}$ is defined in equation (9).

4.5 RDM: In Simulink

In the reduced dynamic model, the equations of motion describing the stator subsystem remain intact and an ordinary differential equation solver such as *ODE45* is needed for their solution. However, the rotors vertical and angular dynamic systems, originally used to monitor the half-contact length and stick-points, have been replaced by fit formulas that approximate the same values. The main assumption used in the development of the RDM is that the steady state feedback forces calculated using pseudo-x_o and pseudo-x_s are close enough to the CDM feedback forces that the natural frequency of the model will not shift and the two speed outputs will converge in steady state.

An in-depth breakdown of the complex dynamic model has been given in Appendix A followed by the same breakdown of the reduced dynamic model. The angular and vertical rotor block diagrams of the CDM are replaced by the simplified block diagrams shown in Figure 4.13 and Figure 4.14.

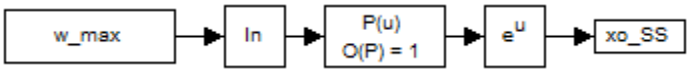

Figure 4.13. Simulink diagram of the math function used to calculate the $x_{o,S.S.}$ in the reduced dynamic model.

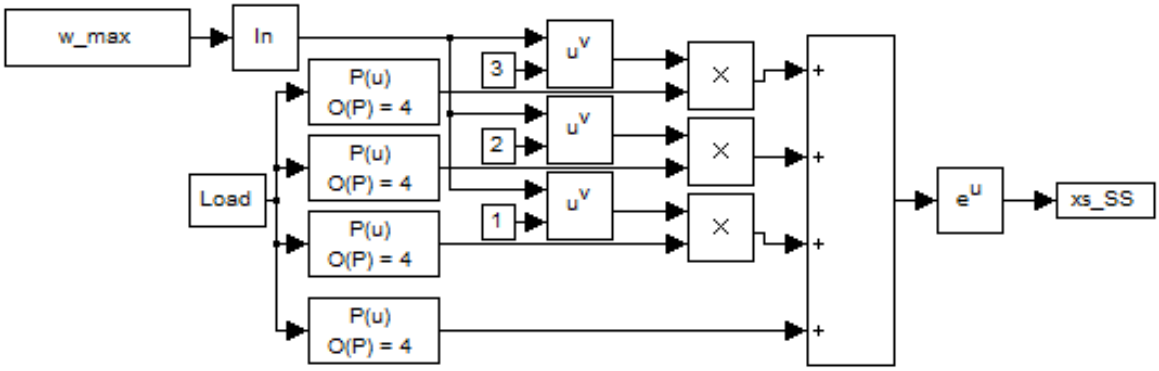

Figure 4.14. Simulink diagram of the math function used to calculate the $x_{s,S.S.}$ in the reduced dynamic model.

4.6 RDM: Validation

To verify that the reduced and complex dynamic models converge in steady state, the outputs of the systems that the reduced model replaces are compared for both. The first output to be validated is the half-contact length. In the complete dynamic model, the rotor height above the undeformed stator surface is monitored, and the half-contact length is extracted. In the reduced model, an equation relating the half-contact length to the traveling wave amplitude was determined. The half-contact length determined by both models is shown in Figure 4.15 to be nearly identical.

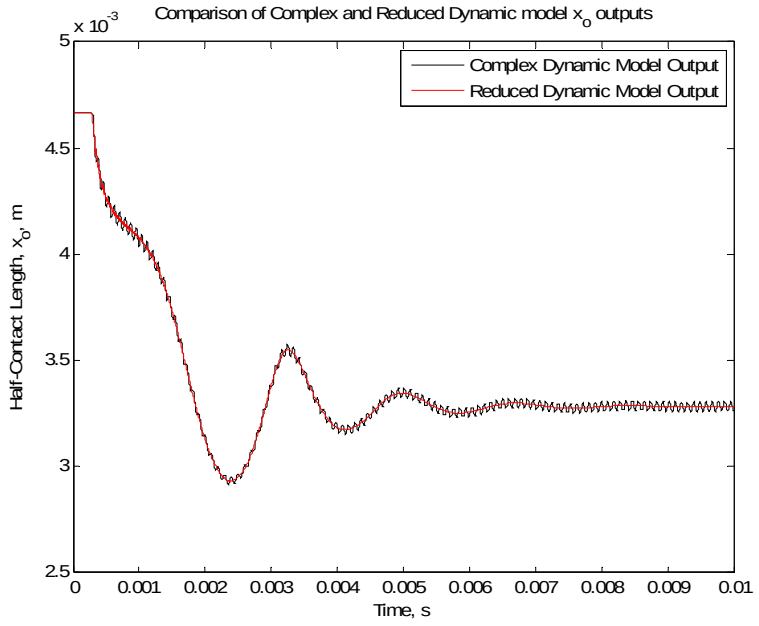

Figure 4.15. Validation of half-contact lengths for complex and reduced dynamic models.

In the complex dynamic model, the height of the rotor is determined by solving an ordinary differential equation. In the reduced dynamic model, the height of the rotor above the stator is calculated by solving equation (33) for *z(t)* and plugging in the $x_{o,S.S.}$ values determined by equation (44). The rotor height as determined by both cases is shown in Figure 4.16. As with the half-contact length, a near perfect agreement between the rotor heights is shown for both models.

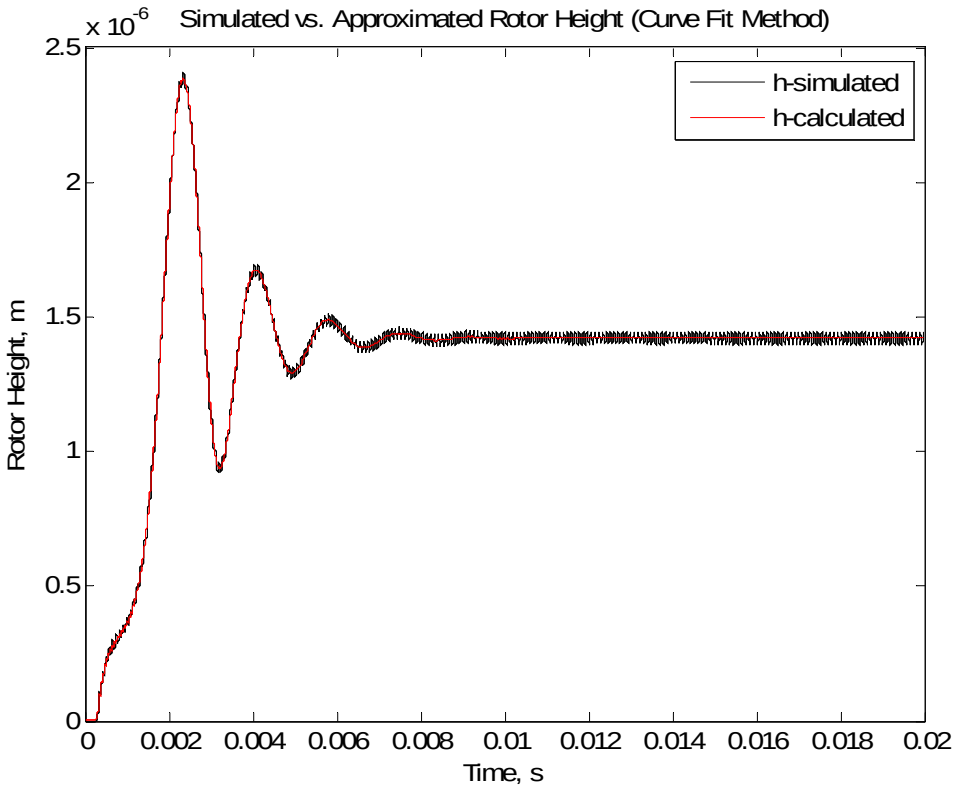

Figure 4.16. Validation of rotor heights for complex and reduced dynamic models.

In the complex dynamic model, the stick-points are determined by comparing the speed of the rotor to the horizontal velocity components of the stator surface points. In the reduced dynamic model, the stick-points are calculated by a fit-formula that determined the stick-point that satisfies the steady state criteria of the contact mechanics for any motor load in the motor's range and any traveling wave amplitude greater than $(w_{\max,S.S.})_{\min}$. Shown in Figure 4.17 are the stick-point curves resulting from three loading cases to show the convergence between the CDM and RDM. Convergence between the stick-points of the two models ensures convergence of the rotor speed.

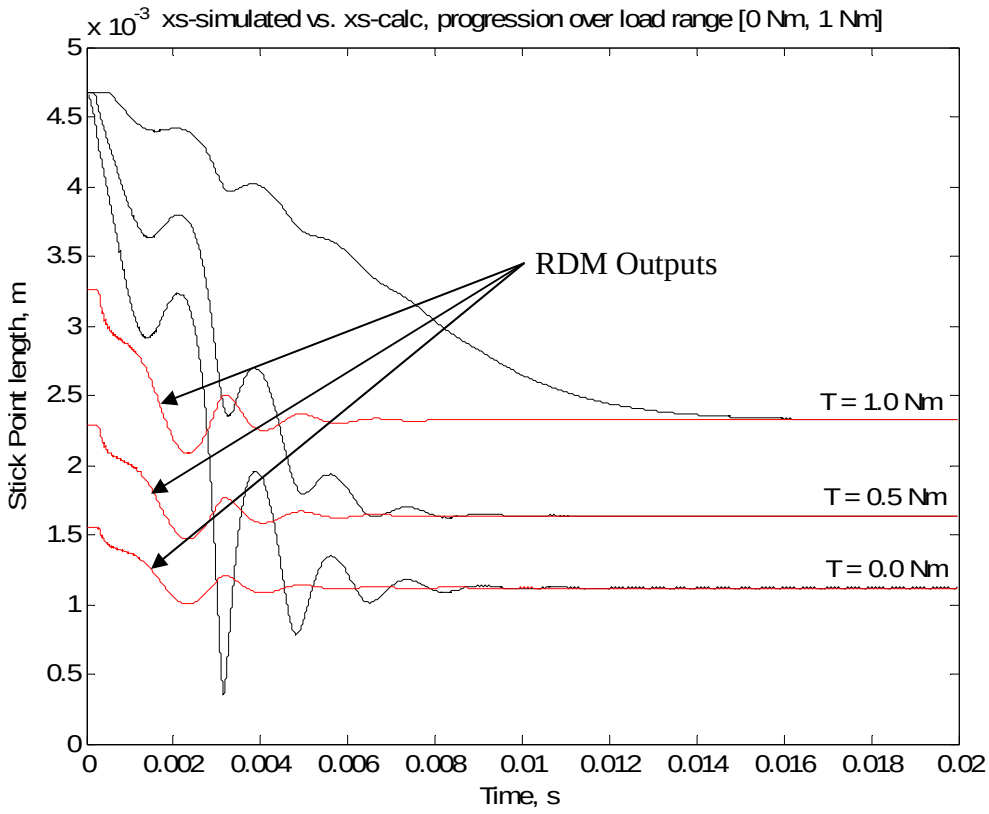

Figure 4.17. Validation of rotor stick-points for complex and reduced dynamic models.

The convergence between the models on a final steady state stick-point value is clear, and the settling time to the steady state value varies depending on the motor load. This can be explained by the fact that the traveling wave amplitude reaches steady state within one millisecond of simulation time regardless of the load. If the traveling wave is at steady state, the stick-point value determined with the reduced model is also at steady state. In the dynamic model, however, the output forces of the motor's contact zones are counteracted by the external load working to decelerate the rotor, thereby delaying the rotors settling time.

The final plot included in this section is not representative of a reduced dynamic model validation. Instead, the speed versus frequency curves for various additive motor loads are given. While the complex model is only capable of simulating resistive loads, the reduced model can simulate additive and resistive loads, further increasing its value when qualifying the USM for feel-systems. The response of the USM to additive loading is presented in Figure 4.18.

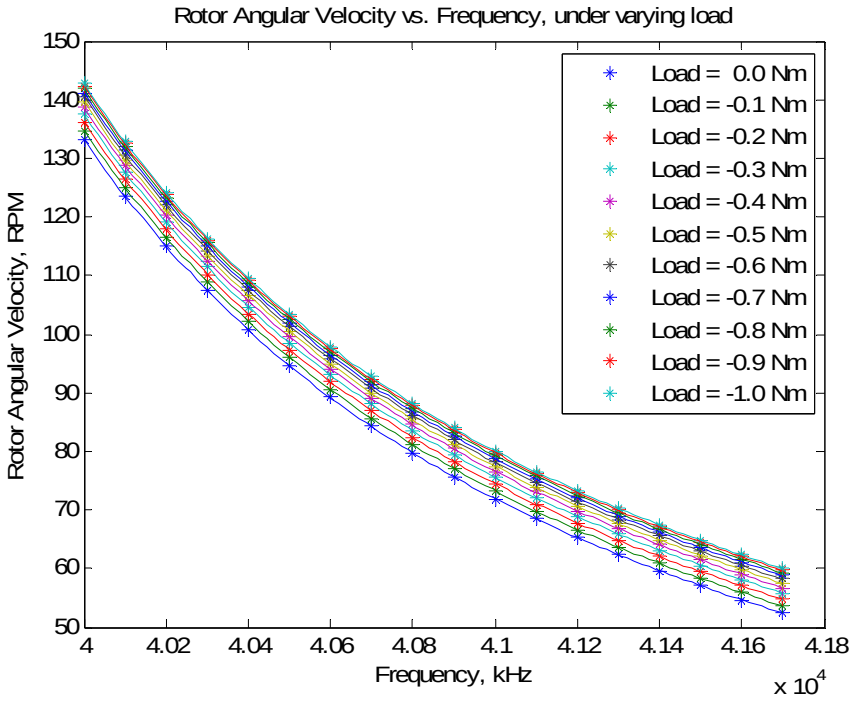

Figure 4.18. Operating envelope of the USM model under varying frequency and torque load, additive loading.

4.7 RDM: Conclusions

A reduced dynamic model has been derived such that steady state motor outputs can be approximated without the angular and vertical rotor subsystems typical of a complex dynamic model. The reduced model was validated against the complex model showing convergence in steady state. Both models are useful tools for observing the response of the motor model under various loading scenarios. The simulations prove useful in understanding the relationship between motor excitation frequency, output torque, load torque and speed.

In the next chapter, the models are used to analyze the USM as the primary actuator in force-feel applications. Several output scenarios essential to providing a robust feel system are explored. The outputs of each scenario are examined, and conclusions about the motors functionality for each case are drawn.

5 Contribution 2: Force-Feel Capabilities of USMs

The subsystems comprising the ultrasonic motor were discussed in Chapter 3 , and using their equations of motion and the contact mechanics formulae, a complete dynamic model was assembled. In Chapter 4 , a model of reduced complexity was developed and then validated against the complex model to show agreement in steady state. In this chapter, the dynamic models are used to determine USM functionality when used as the sole actuator in a force-feel system.

As explained in Chapters 3 and 4, a USM's torque output is bounded as a function of the external force pressing the rotor into the stator. Furthermore, the transient motor torque between $(M_{USM})_{max}$ and $(M_{USM})_{min}$ cannot be controlled externally. Instead, the transient and steady state motor torque, whether net driving or braking, is either adjusting to match or matches the load placed on the motor. Resistive motor loads are counteracted by an increased driving motor torque, and additive motor loads are counteracted by increased braking torques. In either case, the steady state torque balance results in a constant rotor speed; the motor output that *is* controllable. For the ideal traveling wave motor models of this thesis, the piezoelectric excitation frequency is the control variable of choice.

To have an actuator acting as a torque-source in a feel-system whose transient torque output cannot be controlled is clearly not desirable. However, under special loading scenarios, the USM can still be considered capable of the task, so further exploration is justified. In the following section, the fundamental differences between the typical force-feel actuator, the brushless direct current motor (BDC), and the proposed actuator, the USM, are discussed. Next, a discussion of how the dynamic USM models are used to analyze force-feel scenarios is given. Finally, the capability of the USM to serve as the actuator in a feel system is explored for four scenarios; these are constant-force feel and linear-spring feel under resistive and additive loading. A summary of findings is included in the conclusions section.

5.1 BDCs versus USMs in Force-Feel

The fundamental difference between a feel-system using DC motors and one using USMs is the direction the motors must spin to provide a reaction force. DC motors are magnetically driven and capable of producing a constant motor torque, proportional to input current, despite the direction of output shaft rotation. However, for the purposes of feel systems, the motor always *opposes* an operator's input, a direction hereafter referred to as *negative rotation*. The net force at the operator input device (OID) contact surface, is

$$F_{net} = F_{operator} - F_{feel} \tag{56}$$

where the feel force, F_{feel} always opposes the pilot input force and is calculated

$$F_{feel} = \frac{M_{BDC}(i(\alpha))}{L} \tag{57}$$

where L is moment arm of the OID and M_{BDC} is the motor torque controlled by input α. For various required feedback forces, the motor torque is varied by α such that

$$F_{feel} \leq F_{operator}. \tag{58}$$

unless the actuator is returning the input device to a neutral position after the operator relaxes the force input.

Converse to the operation of a DC motor in feel systems, USMs must rotate *in the direction of* the OID rotation instead of opposing it, a direction hereafter referred to as *positive rotation*. The reason for this lies in the contact mechanics between the vibrating stator and the driven rotor. Under a no load scenario, the motor rotates at its maximum angular velocity in a direction determined by a positive or negative phase difference between the signals exciting the piezoelectrics. If a resistive load is imposed, the motor remains spinning in a direction opposing the load, but the angular velocity decreases on account of the driving zone increasing and the stick-point moving down the wave crest where the stator horizontal velocity components are of

lower magnitudes. Under a load of $(M_{load})_{max}$, the motor reaches its minimum speed, where the stick-point takes on the same value as the half-contact length, and for all loads greater than $(M_{load})_{max}$ slipping between the rotor and stator surfaces will occur. At which point, the force felt by a pilots hand from feedback forces is

$$F_{feel} = \frac{(M_{USM})_{STATIC}}{L} = \frac{(M_{USM})_{\max}}{L} = \frac{\mu F_{ext} R_o}{L}. \tag{59}$$

Stated simply, if the USM is used like a DC motor to oppose the input motion of an OID, the only feel-force possible is that of equation (59), unless the forces applied to the OID are restorative. Therefore, in a feel-system where the feedback forces must be variable, it is not feasible to run the USM in the same manner as the DC motor. Instead, the USM rotates in the positive direction. The operator input effectively adds to the driving zone of the motor, and in response, the stick-point moves up the wave crest, increasing the braking zone and rotor speed. The additional braking zone acts against the OID, and the force the operator inputs is reflected through at the OID interface with the value

$$F_{feel} = \frac{-(M_{load})_{additive}}{L} \tag{60}$$

where the negative sign reflects the fact that the feel-force is being exerted in the direction opposite to the forward spin of the motor. A more detailed analysis of how to use positive motor rotation to accomplish force-feel is presented in the following sections.

5.2 Using the Simulink Models for Analysis

It has been well documented that the speed output of USMs is a nonlinear function of the piezoelectric excitation frequency and the load acting on the motor. Additionally, an actual working motor's performance will degrade due to stator natural frequency shifts caused by frictional heating. Over time, friction wear between the rotor and stator will also have negative effects on the motor's performance.

Fortunately, for the analysis of this thesis, only the ideal motor is considered, one in which natural frequency shifts and frictional wear are not included. The USM dynamic models output the same speed-torque and speed-frequency characteristics regardless of simulation length or of how many simulations are run. This is advantageous for using the models to predict the motors performance in force-feel scenarios because it allows curve fitting of the speed-frequency-torque curves of Figure 3.19 and Figure 4.18 such that the steady state speed of the motor can accurately be predicted, pre-simulation, as a function of the motor load and excitation frequency.

The method used to fit the curves of Figure 3.19 and Figure 4.18 is identical to the process used to find a pseudo-x_s formula in 4.4. It was recognized that an accurate fit of the speed-frequency data could be represented in the form

$$RPM(M_{load,i},\ f) = a_{3,i}^{3} f^{3} + a_{2,i}^{2} f^{2} + a_{1,i} f + a_{0,i} \tag{61}$$

where the fit coefficients are functions of the motor load such that

$$\begin{aligned} a_{3,i} &= b_3^3 M_{load,i}{}^3 + b_2^2 M_{load,i}{}^2 + b_1 M_{load,i} + b_0 \\ a_{2,i} &= c_3^3 M_{load,i}{}^3 + c_2^2 M_{load,i}{}^2 + c_1 M_{load,i} + c_0 \\ a_{1,i} &= d_3^3 M_{load,i}{}^3 + d_2^2 M_{load,i}{}^2 + d_1 M_{load,i} + d_0 \\ a_{0,i} &= e_3^3 M_{load,i}{}^3 + e_2^2 M_{load}, i^2 + e_1 M_{load,i} + e_0 \end{aligned} \tag{62}$$

The fit coefficients of equation (62) are given in Table 5.1 and Table 5.2 for resistive and additive loading, respectively. In the tables, maximum resistive loads are positive valued and the maximum additive loads are negative valued, as the sign cancels when put into the summing block of the Simulink simulation file.

Table 5.1. Fit-coefficients for equation (62) to predict speed-frequency curves under resistive loading

Fit-coefficients, resistive loading, T = [0, 1]Nm				
	b_3	b_2	b_1	b_0
a3	-1212	45193	-561646	2326661
	c_3	c_2	c_1	c_0
a2	1082	-40335	501384	-2077507
	d_3	d_2	d_1	d_0
a1	-369	13766	-171098	708897
	e_3	e_2	e_1	e_0
a0	-1991	74541	-930413	3871182

Table 5.2. Fit-coefficients for equation (62) to predict speed-frequency curves under additive loading

Fit-coefficients, additive loading, T = [0, -1]Nm				
	b_3	b_2	b_1	b_0
a3	-12.40	461.08	-5717	23633
	c_3	c_2	c_1	c_0
a2	-47.53	1770.23	-21978	90961
	d_3	d_2	d_1	d_0
a1	-69.17	2578.67	-32046	132758
	e_3	e_2	e_1	e_0
a0	-2001.22	74933.98	-935298	3891422

Equation (61) can be solved by setting certain variables as constants while solving for the others. For example, if a constant load/speed combination is desired, $M_{load,i}$ and $RPM(M_{load,i}, f)$ are set as constants, and the frequency needed to satisfy the equation is solved for. Then, the program is run at that excitation frequency under the given load, and the original desired speed is checked against the programs steady state speed. Individual force-feel scenarios are covered in the following sections. It warrants mention that the output speeds of the motor model in the following examples are too fast for any force-feel system without some sort of reduction gear. Also, the motor models are only operational within a small frequency range where high motor speeds are typical, so the following sections serve only as proof-of-concepts.

5.3 Case 1: Constant-Force Feel

Two cases of constant-force feel exist for a USM. The first case is the result of resistive motor loading and the other to additive loads. Both cases are the subject of their own sections below. The two sections outline how the constant force-feel scenarios are achieved referencing the contact mechanics of the USM. As the model outputs for the constant-force feel are just variations of the simulation outputs of Chapter 3 no simulation results are shown. However, model outputs are shown for the case of linear-spring feel, discussed later, as it a more complicated extension of the constant-force feel example with an interesting series of steady state plots to be analyzed.

5.3.1 Constant-Force feel, Resistive Motor Loading

Net driving torque is exerted by a motor experiencing resistive loading, and the driving torque provides the constant feel-force. The torque induces forces at the OID interface, equal and opposite to the input force and in the direction of motor spin. Such a feel-scenario would be used to overcome small operator inputs and return the OID to its neutral position after a maneuver.

If the input torque is less than the maximum output torque of the motor, the motor will match the torque and rotate against it. The speed at which the motor returns the OID to its neutral position can be controlled by the input frequency. For example, referencing Figure 3.19, if a torque of one Nm is input to the OID, the motor will rotate against it. By Figure 3.19, the steady state motor speed ranges from just over 101 RPM to 28 RPM, when carrying the one Nm load. A frequency can then be found by solving equations (61) and (62) with M_{load} and RPM input as constants, set such that the desired return speed is met and the operator experiences a restorative feel-force of

$$F_{feel} = \frac{1Nm}{L} \tag{63}$$

where L is the length of the moment arm connected to the motor. The motor can be programmed to stop when the neutral position has been reached.

5.3.2 Constant-Force feel, Additive Motor Loading

Net braking torque is exerted by a motor experiencing constant additive loading, and the braking torque provides the constant feel-force. The torque induces forces at the OID interface, equal and opposite to the input force and opposing direction of motor spin. Such a feel-scenario would be used to reflect operator input forces giving the operator a feel for the OID in response to their system inputs.

An introduction to a motor's response to additive loading was given in section 5.1. The operator forces the OID forward, in the direction of motor rotation thereby accelerating it. In response, the braking zone of the contact area increases, and a back-force is felt at the OID interface. Again, the back-torque, felt as a force at the OID interface by the operator, is equal and opposite to the input torque, but unlike the resistive loading scenario, the back-torque is in the direction opposite of motor spin. The motor speed can be adjusted by altering the piezoelectric driving frequency. For example, referencing Figure 3.19, if a torque of one Nm is input to the OID as an additive value, the simulated motor will accelerate. In steady state, the braking area will have increased to resist the additive load. By Figure 3.19 the motor speed ranges from 60 RPM to 143 RPM. A frequency can then be found by solving equations (61) and (62) with the M_{load} and RPM input as constants, such that the desired forward motor speed is met and the operator experiences a resistive feel-force of

$$\frac{1\,Nm}{L}. \tag{64}$$

5.4 Case 2: Linear Spring Force

The goal of this section is to develop the method that allows a USM to produce a linear force gradient with respect to the rotor displacement angle while maintaining constant speed. The main assumption made is that the input torque supplied by the operator linearly increases with

motor displacement angle. Under this assumption, a frequency sequence may be solved for out of equations (61) and (62) such that when input to the dynamic model the linear spring forces are reflected at the OID interface while the motor speed remains constant. Two cases are presented: In the first, restorative torques are provided by the motor in a linear spring fashion, and in the second, additive torques are supplied to the motor and they too are reflected to provide the linear spring feel. For ease of explanation, the scenarios are presented referencing a force-feel system attached to a single degree of freedom control stick.

5.4.1 Linear Spring Force-Feel, Resistive Loads

In a flight scenario, it may be desired that the force on the pilots hand be proportional to the stick displacement such that

$$F_{pilot} = k\theta \tag{65}$$

where in the case of a torsional spring, k is a linear spring constant, and the resulting Force versus Stick-Angle curve is linear. In such a scenario, the force the pilot feels is only a function of the angular displacement. In a feel system using a BDC motor, a position control algorithm can be used to monitor the stick position and increase or decrease the force output as necessary.

In the case of the traveling wave motor, equation (65) does not involve a linear spring constant. Instead, the force reflected to a pilot's hand is equal and opposite to the input force. Equation (65) becomes

$$F_{pilot} = \frac{-M_{load}}{L} \tag{66}$$

where L is the length of the control stick. The relationship between speed, torque and frequency can be seen in the curves of Figure 3.19 and Figure 4.18. By observation of Figure 3.19, it is clear that there are areas where a constant rotor speed can be maintained with the correct manipulation of the excitation frequency even with a resistive load torque that is increasing

linearly with respect to stick angle. Examples of these areas are highlighted in Figure 5.1 using horizontal lines.

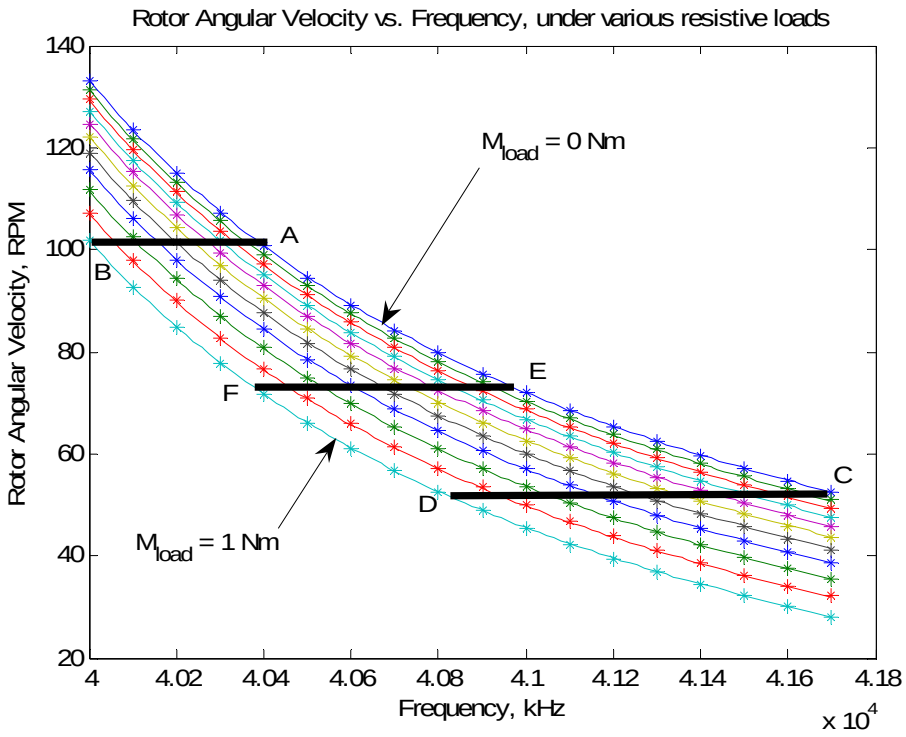

Figure 5.1. Simulation results, Rotor Angular Velocity vs. Frequency, resistive loads.

The lines segments of Figure 5.1 also define the operational envelope where the full range of motor output torques can be reflected while maintaining the constant rotor speed. A motor run at a speed above segment A-B, while still able to operate at a constant speed, will be limited by in its maximum torque capability. This is clear by the fact that a horizontal line drawn above the segment will not contact the speed curve where the motor load is equal to one Nm. A motor run at a speed below segment C-D can still maintain a constant speed, but in this case, the minimum torque output is greater than zero. This is clear by the fact that a horizontal line drawn below the segment will not intersect the speed curve where the motor load is equal to zero. Segment E-F represents a motor speed where the full range of motor torques between zero and $(M_{USM})_{\max}$ can be used. In short, the operational envelope for the motor, where the full range of output torques is possible while maintaining a constant speed, lays between the segments A-B and C-D.

To achieve a linear torque output of the motor at a constant speed, the desired motor speed must be chosen. Next, a set of frequencies must be solved for from equations (61) and (62) such that the constant motor speed is maintained despite increased resistive loading at all time points during the sweep of the stick. One problem remains: the time at which to excite the motor at those particular frequencies remains unknown.

To begin solving this problem, two new variables are introduced, $\theta_{\max}$ and t_{sweep}, representing the maximum angular displacement of the control stick and the time allotted to sweep this displacement, respectively. Combining these two variables, the required motor speed can be calculated as

$$\dot{\theta}_{req} = \frac{\theta_{\max}}{t_{sweep}}. \tag{67}$$

At this speed, the angular displacement of the motor at any point in time is

$$\theta(t) = \dot{\theta}_{req} * t. \tag{68}$$

A linear relationship between torque and angular displacement is written

$$\tau = k\theta(t) \tag{69}$$

where

$$k = \frac{\tau_{\max} - \tau_{\min}}{\theta_{\max}} \tag{70}$$

and equations (67) and (68) can be substituted for $\theta(t)$ and $\dot{\theta}(t)$ such that equation (69) becomes

$$\tau = \left(\frac{\tau_{\max} - \tau_{\min}}{t_{sweep}} \right) t \tag{71}$$

which represents the relationship between the resistive motor loads over the time that the control stick maneuver must take place. By inserting a time vector extending from zero to t_{sweep} into (71), the vector of torque values to load the model with can be found. Next, each torque component can be substituted into equations (61) and (62) along with $\dot{\theta}_{req}$ and the frequency required to maintain $\dot{\theta}_{req}$ at each torque can be solved for. The frequency vector can then be plotted against the original time vector and a fit-curve determined. The equation of that fit-curve, a function of only time, approximates the frequency needed to drive the motor at $\dot{\theta}_{req}$ at any instant in time having determined the exact torque that will be acting on the motor at that time.

As an example, the process above was carried out for

$$t_{sweep} = 5\text{s}$$
$$\dot{\theta}_{req} = 77.13\ RPM$$
$$\tau_{\min} = 0\ \text{Nm}$$
$$\tau_{\max} = 1\ \text{Nm}$$

where t_{sweep} was chosen at random, and $\dot{\theta}_{req}$ was selected for its midpoint location in the motors operating range. Entering the above variables into equation (61) and solving for the needed excitation frequencies, it was found that the excitation frequency range extends from 40.312 kHz at zero load to 40.865 kHz with a load of one Nm to maintain the 77.13 RPM rotor speed. The frequency versus time vector needed to maintain a constant motor speed is shown in Figure 5.2.

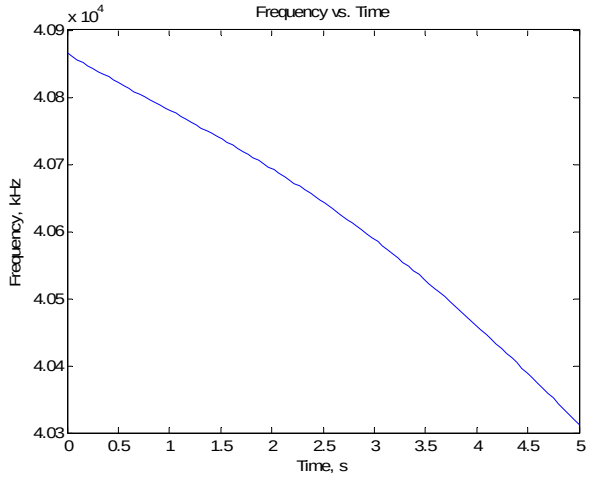

Figure 5.2. Frequency versus time data needed to maintain constant rotor speed with increasing resistive load.

5.4.2 Linear Spring Force-feel, Resistive Loads, Simulation results

With the information of Figure 5.2, a function describing the frequency with respect to time was determined, and with this function, a series of simulations was run to show that a USM is capable of reflecting a linearly increasing force input while maintaining its rotational speed under the correct frequency manipulation.

The plot of motor output torque versus time is represented in Figure 5.3. Positive motor output torque means that the torque and the motor displacement are in the same direction.

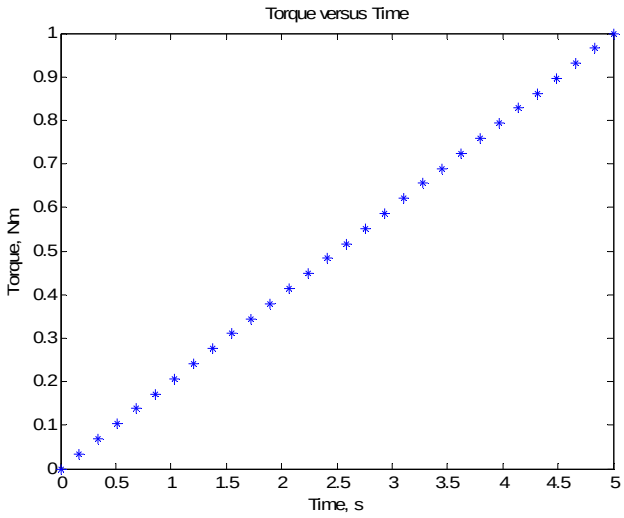

Figure 5.3. Output torque of the USM experiencing linearly increasing resistive loading versus time.

Shown in Figure 5.4 is the speed versus torque data recorded from the simulations. Under varying loads, the speed was kept to within 0.2 RPM of the desired 77.13 RPM by carefully selecting the motor excitation frequencies.

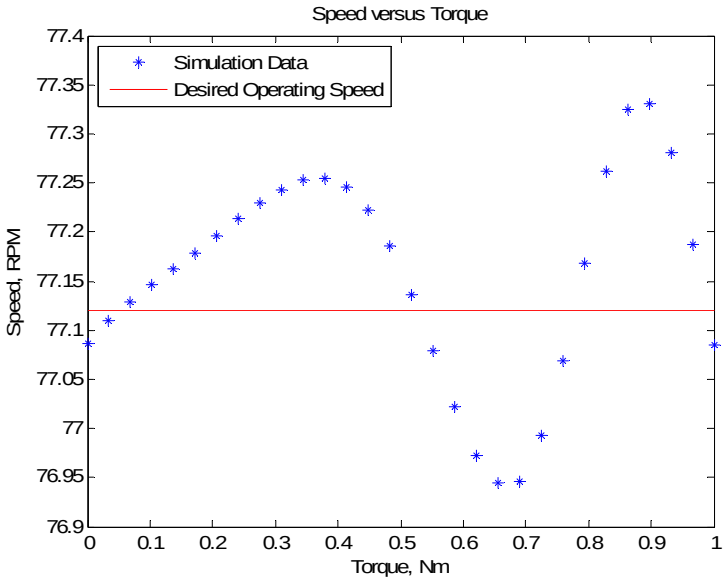

Figure 5.4. Motor speed versus load torque, resistive loading.

The most important plot resulting from the simulations is the torque versus angle plot shown in Figure 5.5. As theorized, a linear relationship between a rotors angular displacement and the motors output torque is possible if the motor is excited with the correct frequencies during the simulation assuming that a resistive load, linearly increasing with the displaced rotor angle, is placed on the motor.

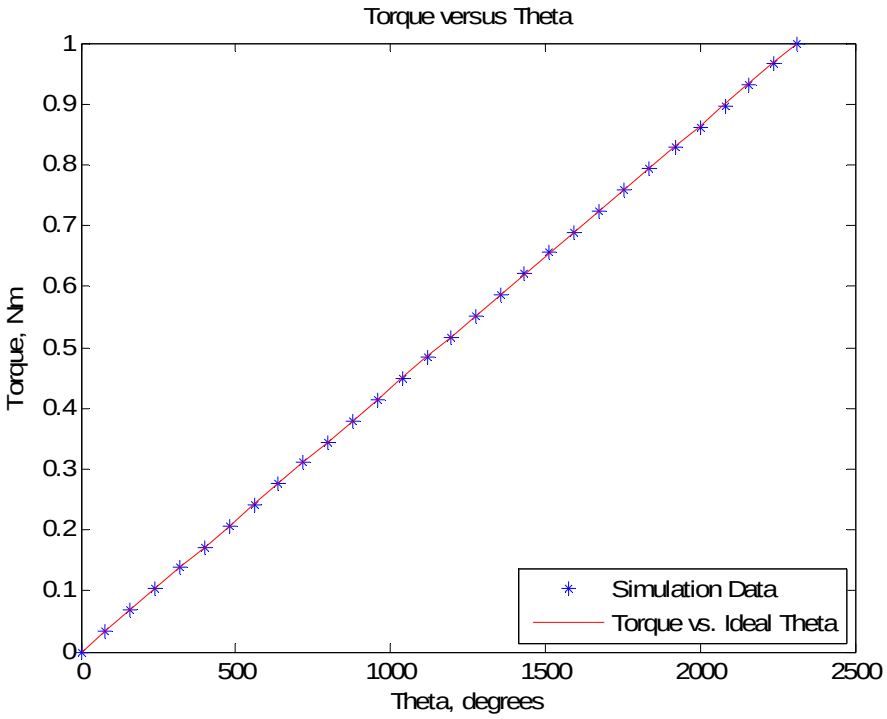

Figure 5.5. Torque versus motor angle, resistive loading.

5.4.3 Linear Spring Force-feel, Additive Loads

Linear spring force-feel for additive loads is based on the same principle as the previous section with one exception: the motor loading is additive instead of resistive. The difference between the two is best described by considering a pilot input to an aircraft control stick. In the previous section, the resistive pilot's inputs to the control stick were overcome by the motor, allowing the motor to return the stick to a neutral position. An assigned frequency sweep was sought in order to excite the motor so it would rotate against the load with a constant angular velocity and return the control stick to a neutral position. Now, a new frequency sweep is sought such that a motor can rotate with constant angular velocity in the direction of the load while reflecting an equal and opposite force back to the pilot. The assumption that the pilot input force is increasing linearly with rotor displacement angle is still used.

The speed versus frequency curve for the motor experiencing additive loading is shown in Figure 4.18 and is recreated in Figure 5.6 to show the constant speed full torque operating range of the motor. The plots of Figure 5.1 and Figure 5.6 share a common curve, zero load, but whereas the zero load represents the upper speed-frequency curve in Figure 5.1, it represents the lower curve in Figure 5.6. This is explained by the type of loading the motor experiences. Under resistive loads at a given frequency, a higher load slows the motor. Under additive loads at a given frequency, the increased load forces the rotor to a higher speed.

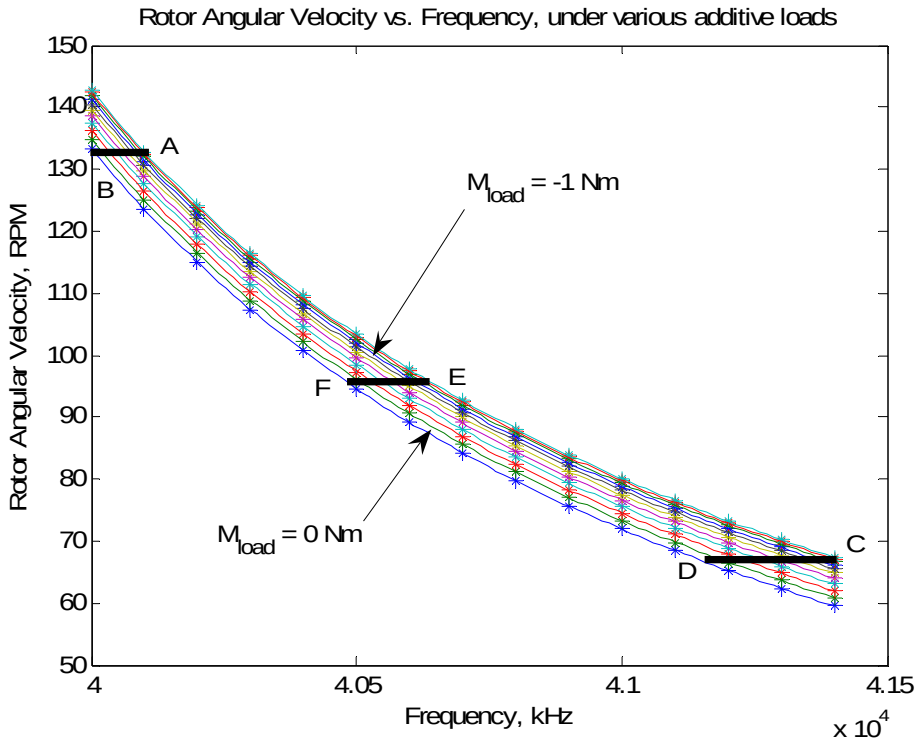

Figure 5.6. Simulation results, Rotor Angular Velocity vs. Frequency, additive loads

The process of determining the frequency versus time function needed to maintain motor speed under the increasing load follows that of the section 5.4.1. First, equations (61) and (62) are recalculated to fit the additive motor loading speed-frequency data. By Figure 5.6, the speed range of the motor where the full range of feedback torques resulting from additive loads is possible is 67 – 133 RPM, so the speed requirement is set to in the middle of this range. The sweep time, motor speed requirements and torque range explored in the simulation are

$$t_{sweep} = 5\text{s}$$
$$\dot{\theta}_{req} = 96\,RPM$$
$$\tau_{\min} = 0\ \text{Nm}$$
$$\tau_{\max} = -1\ \text{Nm}$$

The excitation frequency range extends from 40.467 kHz at zero load to 40.623 kHz with a load of -1 Nm to maintain the 96 RPM rotor speed. The frequency versus time curve extracted is shown in Figure 5.7

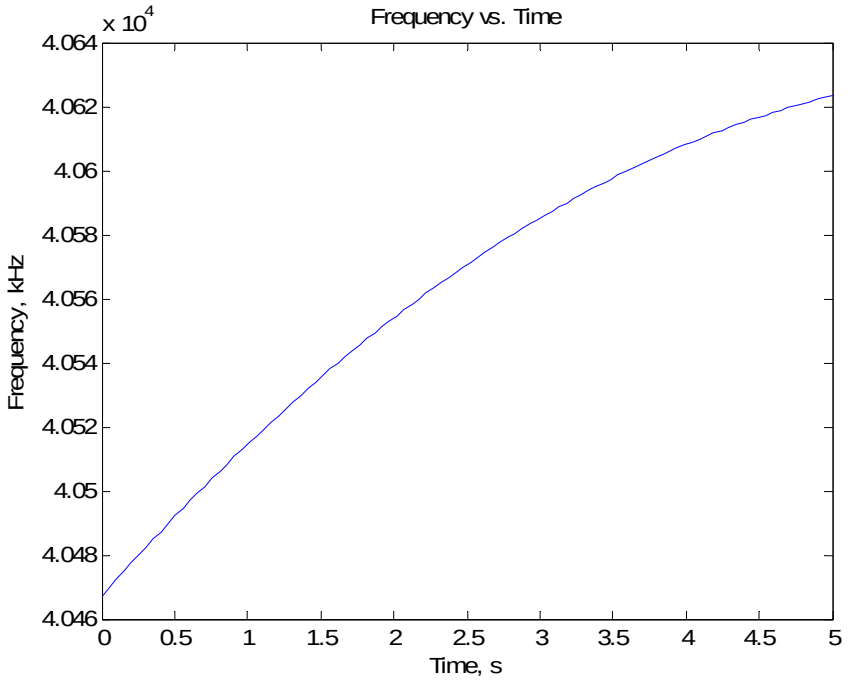

Figure 5.7. Frequency versus time data needed to maintain constant rotor speed with increasing additive load.

The difference in trend between Figure 5.2 and Figure 5.7 is immediately clear; the positive or negative slope of the curve depending on the desired operation. In order to maintain constant speed under the increasing resistive loads, the frequency must be swept from high to low. At a set frequency, a motor decelerates under increased resistive loading. The deceleration is counteracted by reducing the motor excitation frequency towards the natural frequency, which under a constant load increases motor speed. For a motor under additive loading, the frequency must sweep from low to high frequencies. At a set frequency, a motor accelerates under additive

loading. The acceleration is counteracted by increasing the motor excitation frequency away from the natural frequency, which under a constant load would decrease the motor speed

5.4.4 Linear Spring Force-feel, Additive Loads, Simulation results

The simulations that produced Figure 5.3 to Figure 5.5 were repeated using the new operating requirements of section 5.4.3. The plot of motor output torque versus time is represented in Figure 5.8. Negative motor output torque means that the net motor torque and the motor displacement are in opposite directions.

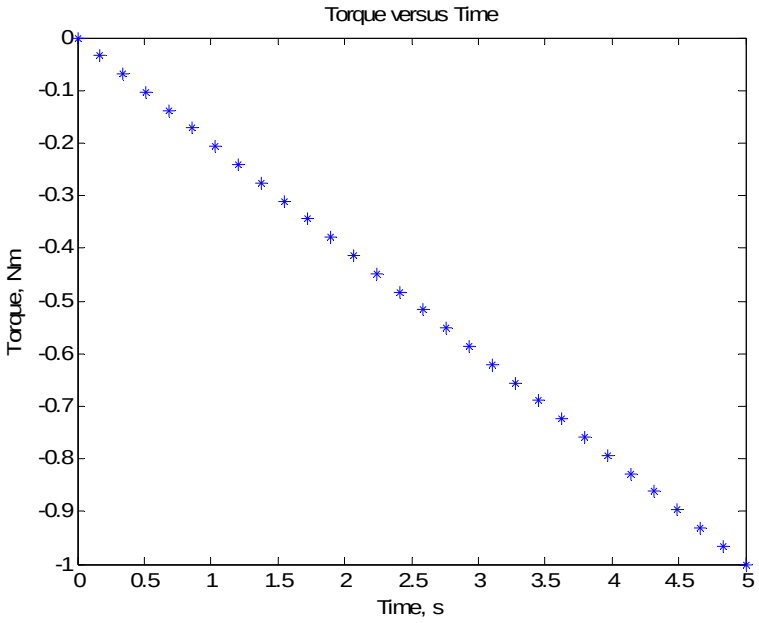

Figure 5.8. Output torque of the USM experiencing increasing additive loading versus time.

Shown in Figure 5.9 is the speed versus additive load torque data recorded from the simulations. Under varying loads, the speed was kept to within 0.2 RPM of the desired 96.5 RPM by carefully selecting the motor excitation frequencies. The negative torque values in the figure correspond to the way in which the loads must be input in the model at the summer block in order to represent additive loads.

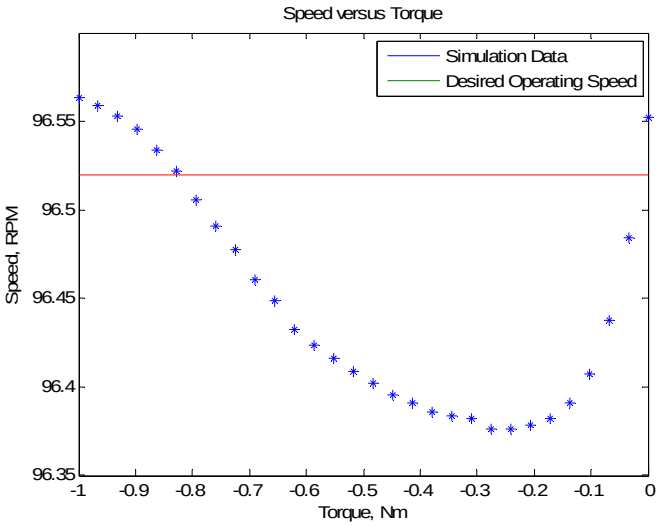

Figure 5.9. Motor speed versus load torque, additive loading.

The most important plot resulting from the simulations is the torque versus angle plot shown in Figure 5.10. As theorized, constant velocity linear spring feel is possible if the additive load on the motor is controlled and the correct frequency sweep being supplied to the motor is determined.

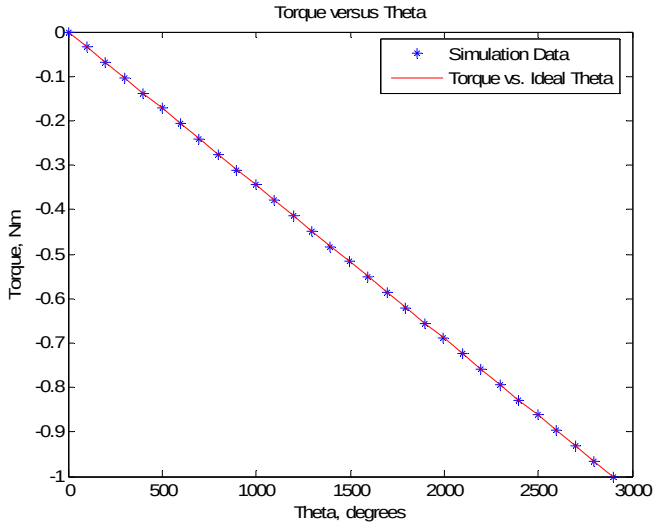

Figure 5.10. Torque versus motor angle, additive loading.

5.5 Conclusions

In sections 5.4.1 through 5.4.4, the constant force feedback and linear spring force feedback capabilities of the motor were explored for both additive and resistive motor loads. It was shown that under the correct loading assumptions, the USM is capable of producing both types of feedback. Unfortunately, real world force-feel systems are not often, if ever, subjected to ideal loading scenarios. Additionally, the underlying purpose of the feel-system is to output forces through an OID that are proportional to what is happening at the control surface, not what is happening at the OID/operator interface. An aircraft pilot needs to feel resistance of the control stick based on the dynamics of the aircraft control surfaces. The automobile driver needs to feel resistance to turning a steering wheel proportional to vehicle speed and tire/ground dynamics. The surgeon operating through a tele-robotic unit must be able to feel resistive forces in his joystick that are proportional to the tissue forces acting on the robotic manipulators. The feel forces *should not be* 1:1 reflections of the OID input forces as the case would be for feel systems using USMs as actuators. Therefore, USMs should be dismissed from the pool of actuators being considered for use in updated feel-systems or any system where transient torque control is essential to its function.

6 Conclusions and Future Work

A summary of the research covered by this thesis is provided in this chapter. After reviewing the modeling efforts that led to the assembly and validation of the reduced dynamic model, the benefits of the reduced model are discussed. Next, the methods used to qualify the ultrasonic motor for use in a feel-system are revisited. Suggestions for future work relating to ultrasonic motors in feel-systems conclude the chapter.

6.1 Summary

The force-feel systems accompanying by-wire control systems are an ever-evolving technology. As such, the electromechanical actuators needed to provide the forces and displacements of the feel-system must be improved to meet new design and performance criteria, or they must be replaced with actuators that can. Ultrasonic motors have been proposed as a feel-system actuator upgrade from the industry standard, brushless DC motors. The high torque density, high torque output at low speeds, and high programmability of the motors make them viable means to reduce the size, weight and complexity of current systems. Several publications document both the construction of active control stick prototypes using USMs actuators and the testing of new motor torque control laws, integral to any feel-system. The basis for the control laws, however, was the assumption that a motor's output torque is a function of the motor speed, just as the motor's speed is a function of the output torque. Simply put, if the speed of a motor can be controlled, its torque can be controlled. Though the results of the torque control law were promising, no references to the contact mechanics that dictate the motors operation were made, and the concept of torque control in feel-systems was left as plausible but unproven. The goal of this thesis was to provide a comprehensive analysis of the mechanics dictating an ultrasonic motors movement to determine the feasibility of developing a torque control law that would allow USMs to be used in force-feel systems.

In order to qualify the USM for use in feel systems, a math model was assembled by referencing available literature. Once assembled, the model was used to predict the steady state motor

response under various loads and external excitation frequencies, and various outputs of the model subsystems were explored. Recognizing the difference in how USMs and DC motors must be actuated to provide feel-forces, a severe limitation of the motor model became clear; the model could only handle resistive motor loading, those that opposed the rotor motion. Observing the USMs steady state outputs as a function of additive loads was impossible. As a solution, the reduced dynamic model was formulated.

The reduced dynamic model of Chapter 4 uses fit formulas in place of the two dynamic rotor systems covered in Chapter 3 . The half-contact length is no longer treated as a function of the rotor height, nor the stick-point as a function of the rotor speed and stator surface point velocities. Instead, the two values are treated as functions of the traveling wave height. The half-contact length formula determines the x_o that satisfies the steady state vertical force balance on the rotor for all traveling wave heights greater than a cutoff value. The stick-point formula determines x_s such that the steady state braking/driving zone equilibrium requirement is satisfied for all traveling wave heights greater than the same cutoff and under the motor load used for that simulation. The rotor speed is then extracted from stick-point value.

The reduced dynamic model was validated against the complex model to show agreement between the steady state stick-point lengths for resistive loads. It was then applied to predict the motor's response to additive loading; a regime not previously explored in USM research. Additionally, the reduced model proves to be a useful tool, allowing the piece-by-piece assembly of the complex model, a task previously not possible due to the complex coupling of the three motor subsystems.

Upon completion of the complex and reduced dynamic models, it became clear that torque control of the USM was not possible, as the transient torque output by the motor is solely a function of the external load, whether resistive or additive. In other words, the assumption allowing the torque control laws suggested in previous research, that a motors output torque is proportional to the motor speed, is incorrect. The point is proven by observation of the speed-frequency curves under varied loading where it is clear that a motor rotating at a constant velocity can in fact drive a range of loads depending on the frequency with which it is excited.

Despite the inability to control a USMs transient output torque with an external signal, several cases of how a USM might be used to provide feedback forces, assuming an externally controlled load acting on the motor, are covered in Chapter 5 . First, the fundamental difference between USMs and DC motors and the way they must be used in feel-systems was presented. Next, a brief tutorial on how to use a USM model to simulate force-feel scenarios was given. Finally, constant force and linear spring force feedback scenarios are presented for both resistive and additive external motor loads.

6.2 Future Research

The benefits of using the USM over the DC motor for certain applications remain. USMs are capable of carrying high torques at low speeds whereas DC motors often need reduction gears to increase torque output while reducing speed. Unfortunately, the highest torque commercially available USMs can carry only a fraction of the load even small DC motors are capable of, so gearing must be employed anyway. Therefore, the first priority of future research involving USMs should be to increase their torque carrying capability. Another focus of future research should be on increasing the lifespan of USMs. Based on the USMs frictional operating principle, the contact surface of the rotor wears rapidly from long periods of continuous motor operation. The surface wear decreases the torque range of the motor, causes natural frequency shifts and ultimately leads to increased project costs based on a higher frequency of motor repairs.

USMs remain excellent controllable positioning devices. Future research might explore their application as the electromechanical actuators used to displace the control surfaces of machines requiring force feel systems. The motors could also be applied as the actuators needed in an autopilot system, displacing the angle of an automobile steering wheel when fed external cues. A simple application of the USM would be within a cruise control system requiring the coiling or uncoiling of a cable to adjust a throttle.

The contents of this thesis have shown that the transient output torque of ultrasonic motors cannot be controlled externally, and thus they should not be considered for application as the sole torque actuators in force-feel systems. If, however, the aim of a future project is to incorporate

the USM into a feel system, the goal of the research should be to expand upon the concept presented in [6] by developing a system that couples the motor with another active component. As demonstrated, the USM can serve as a velocity source and a means to restore the input device to neutral positions after maneuvers. The active component, such as a magnetic clutch or a brake can be used to vary the reactions forces felt by the operator. The research would then need to focus on the development of the relevant torque control laws.

References

1. Schenker, P., et al., *A Composite Manipulator Utilizing Rotary Piezoelectric Motors: New Robotic Technologies For Mars in-situ Planetary Science,* in *Smart Structures and Integrated Systems*. 1999: San Diego, CA, USA.
2. Burdea, G.C., *Haptic Feedback for Virtual Reality*. 1999, Rutgers - The State University of New Jersey: Piscataway.
3. Burdea, G.C., *Force and Touch Feedback for Virtual Reality*. 1996: Wiley-Interscience. 360.
4. Maas, J., T. Schulte, and N. Frohleke, *Model-based control for ultrasonic motors.* Mechatronics, IEEE/ASME Transactions on, 2000. 5(2): p. 165-180.
5. Giraud, F., B. Semail, and J.T. Audren, *Analysis and phase control of a piezoelectric traveling-wave ultrasonic motor for haptic stick application.* Industry Applications, IEEE Transactions on, 2004. 40(6): p. 1541-1549.
6. Chapuis, D., et al. *A Haptic Knob with a Hybrid Ultrasonic Motor and Powder Clutch Actuator*. in *EuroHaptics Conference, 2007 and Symposium on Haptic Interfaces for Virtual Environment and Teleoperator Systems. World Haptics 2007. Second Joint*. 2007.
7. Flynn, A.M., *Piezoelectric ultrasonic micromotors*. 1995. p. 209.
8. Ming, H. and C. Weishan. *Analysis and Design of a Ring-type Traveling Wave Ultrasonic Motor*. in *Mechatronics and Automation, Proceedings of the 2006 IEEE International Conference on*. 2006.
9. Maeno, T., T. Tsukimoto, and A. Miyake, *Finite-element analysis of the rotor/stator contact in a ring-type ultrasonic motor.* Ultrasonics, Ferroelectrics and Frequency Control, IEEE Transactions on, 1992. 39(6): p. 668-674.
10. Frangi, A., et al., *Finite element modelling of a rotating piezoelectric ultrasonic motor.* Ultrasonics, 2005. 43(9): p. 747-755.
11. Ghouti, N.E., *Hybrid Modeling of a Traveling Wave Piezoelectric Motor,* in *Department of Control Engineering*. 2000, Aalborg University: Aalborg. p. 190.
12. Hagood, N.W.I. and A.J. McFarland, *Modeling of a piezoelectric rotary ultrasonic motor.* Ultrasonics, Ferroelectrics and Frequency Control, IEEE Transactions on, 1995. 42(2): p. 210-224.
13. Maas, J., et al. *Simulation model for ultrasonic motors powered by resonant converters.* in *Industry Applications Conference, 1995. Thirtieth IAS Annual Meeting, IAS '95., Conference Record of the 1995 IEEE.* 1995.

Appendix A

Simulink Block Diagrams for CDM and RDM

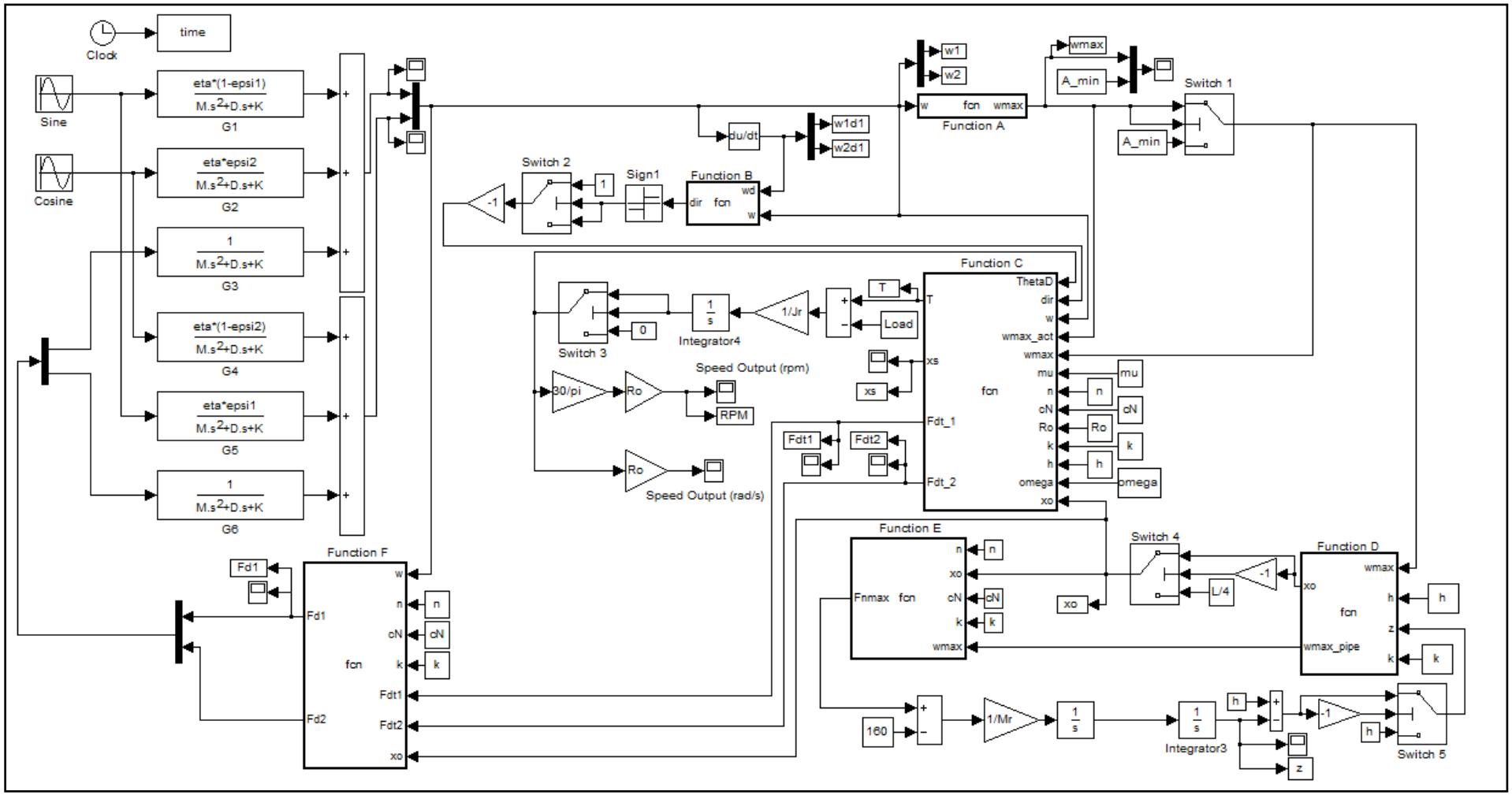

A. 1. MATLAB Simulink block diagram for Complex Dynamic Model of Ultrasonic Motor

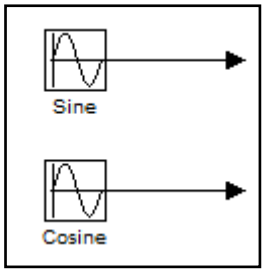

A. 2. Electrical Supply to USM Model

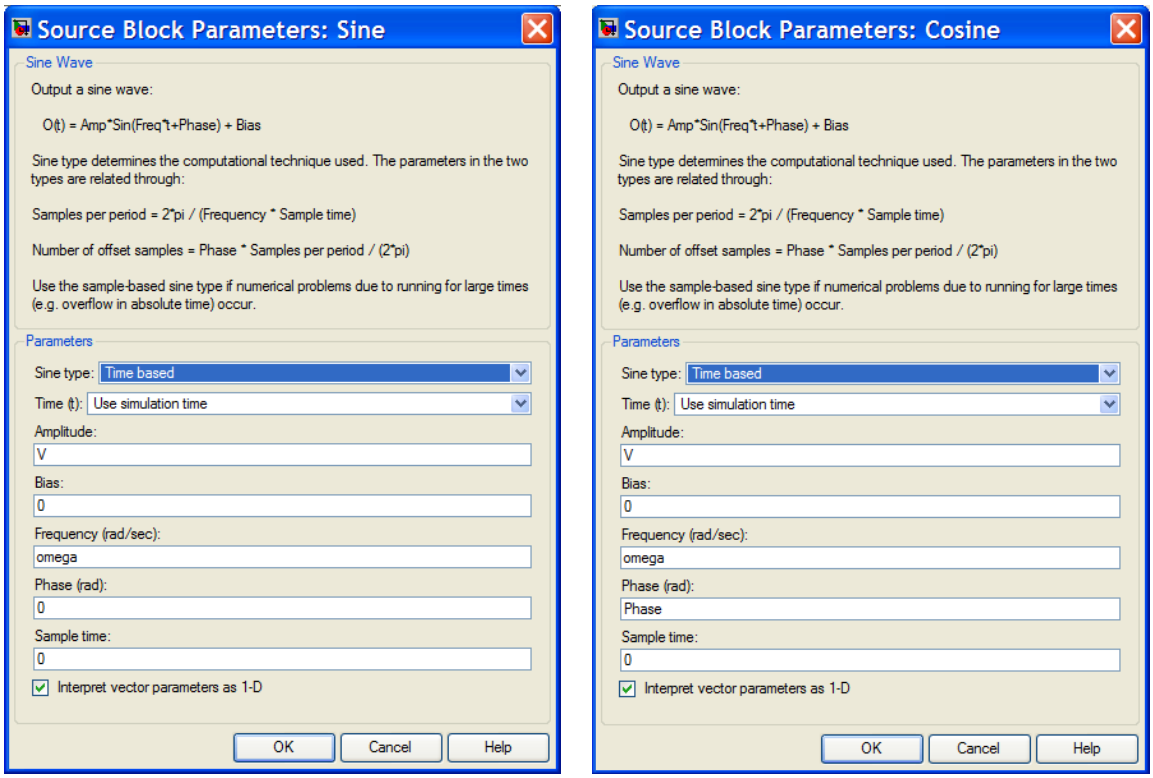

A. 3. Parameter boxes for electrical sources. The constants are set in the workspace.

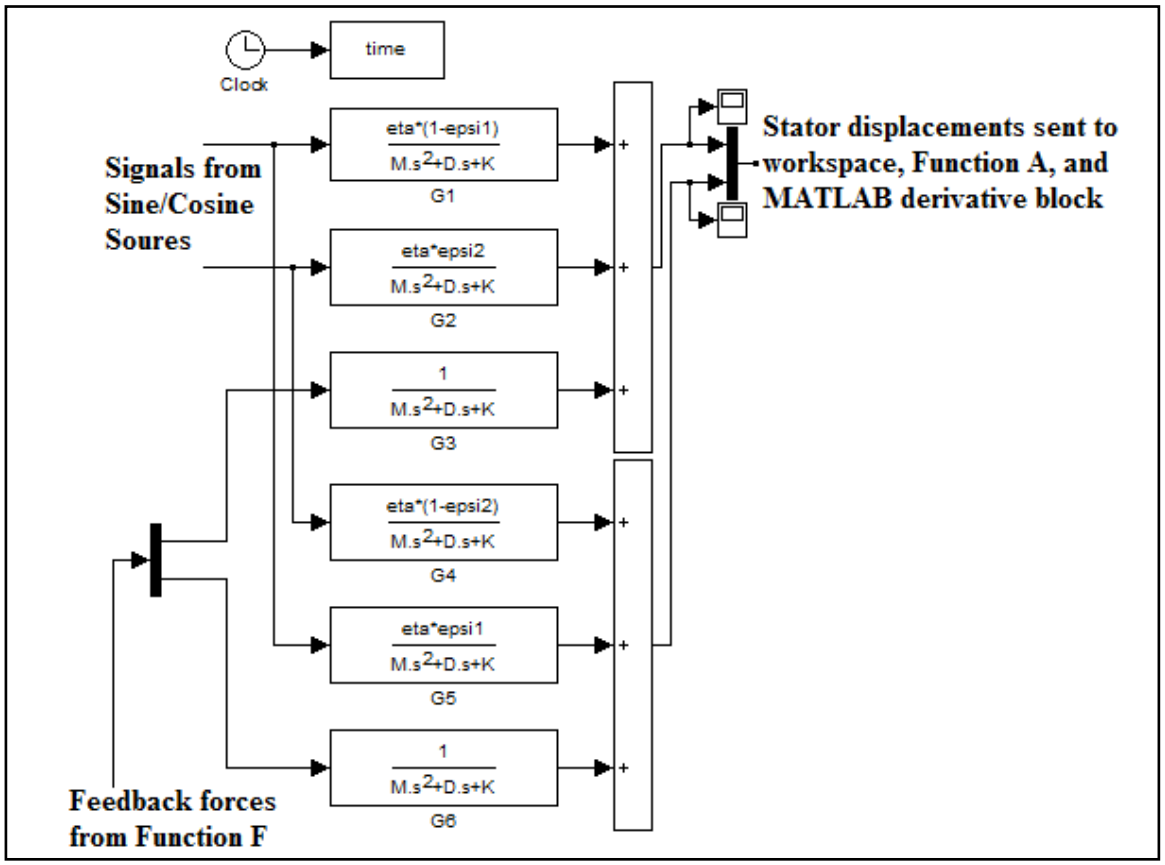

A. 4. Stator System. Blocks G1-G6 are MATLAB Transfer Functions

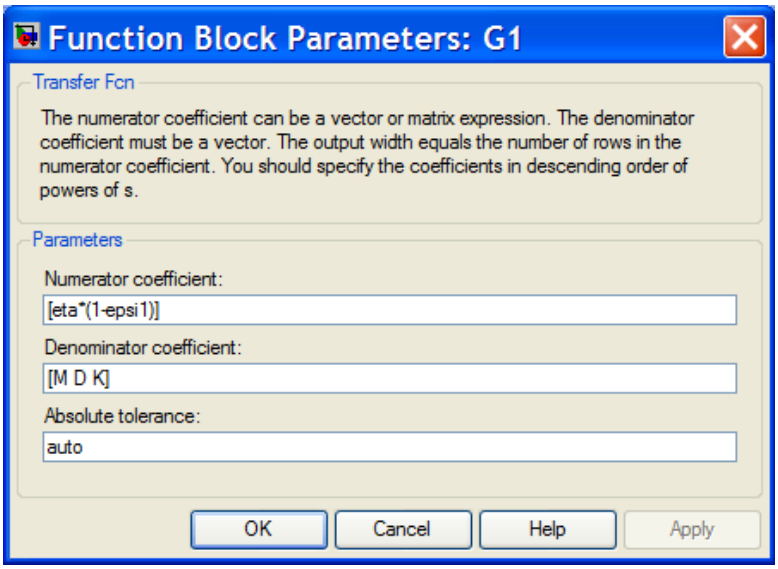

A. 5. G1 Transfer Function block of stator system, for example

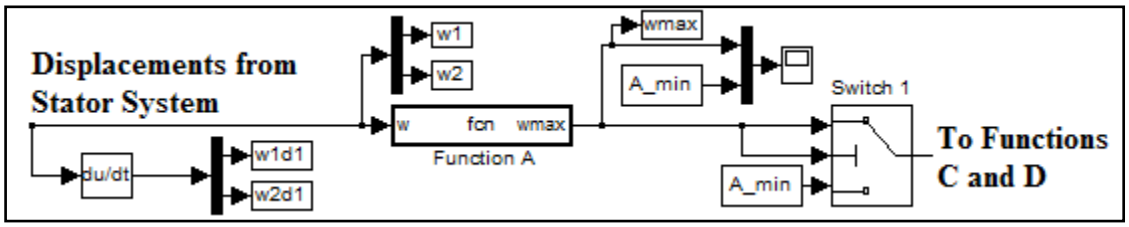

A. 6. Branch function: (1) differentiate the stator displacements for rotor direction calculation, (2) calculate traveling wave amplitude, w_{max} (Function A), (3) compare w_{max} to A_min in switch 1 and pass the decision to Functions C and D.

.

Code written within Function A.

```
function wmax = fcn(w)

% This block supports an embeddable subset of the MATLAB
language.
% See the help menu for details.
wmax = (w(1)^2 + w(2)^2)^(1/2);
```

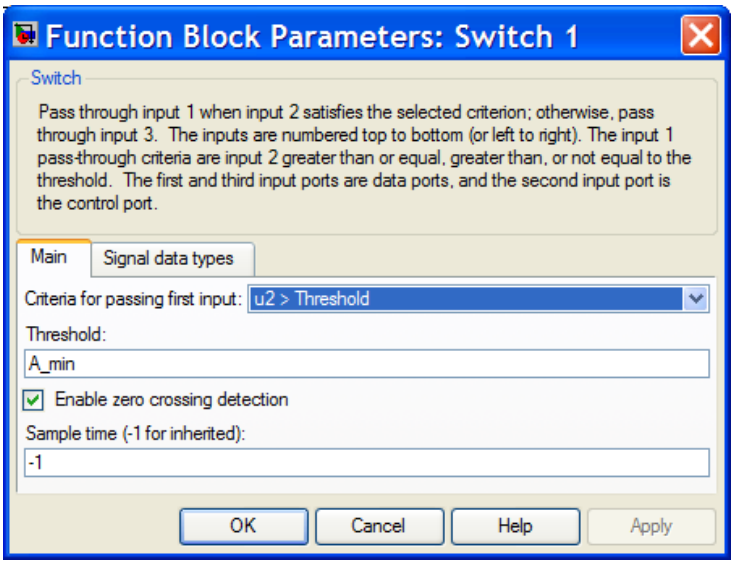

A. 7. Parameter box for Switch 1. Traveling wave amplitude, w_{max}, passes through the switch if w_{max} > A_min, otherwise A_min is passed through.

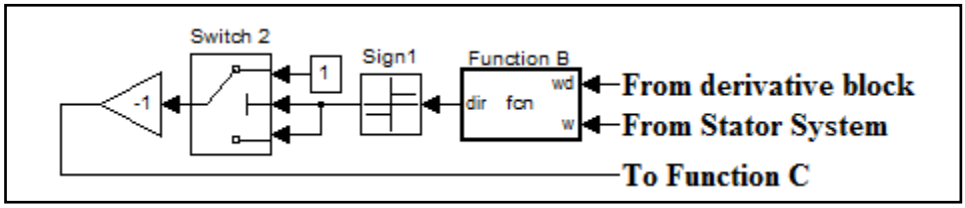

A. 8. Loop determines the direction of the rotor by analyzing stator surface point displacements and velocities.

Code written within Function B

```
function dir  = fcn(wd, w)
% This block supports an embeddable subset of the MATLAB
%language.
% See the help menu for details.

dir = wd(1)*w(2)-wd(2)*w(1);
```

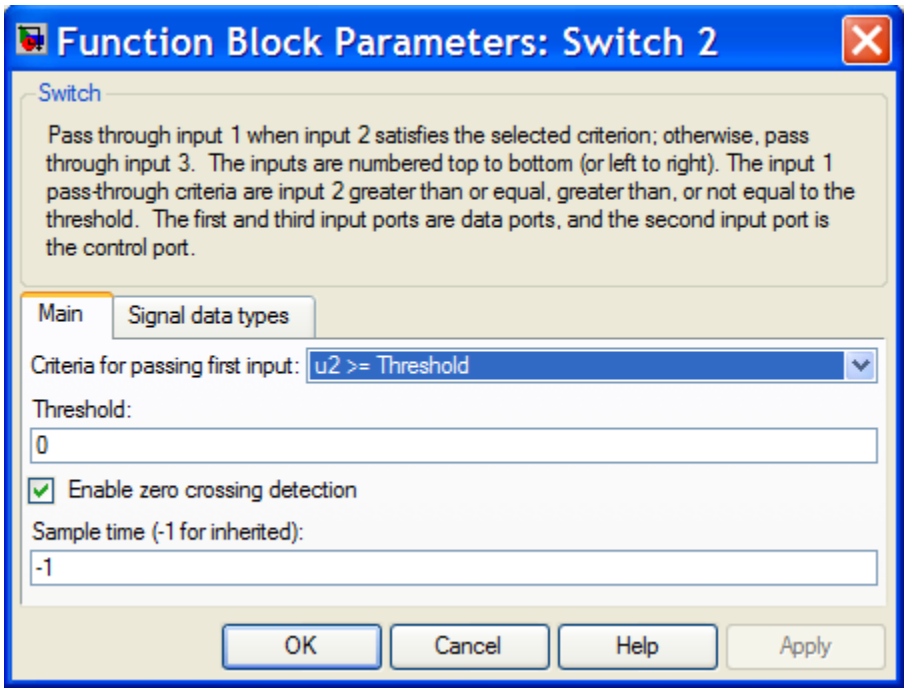

A. 9. Parameter box for Switch 2. Switch outputs "1" when the input is "1" or "0" and passes through "-1" when the input is "-1".

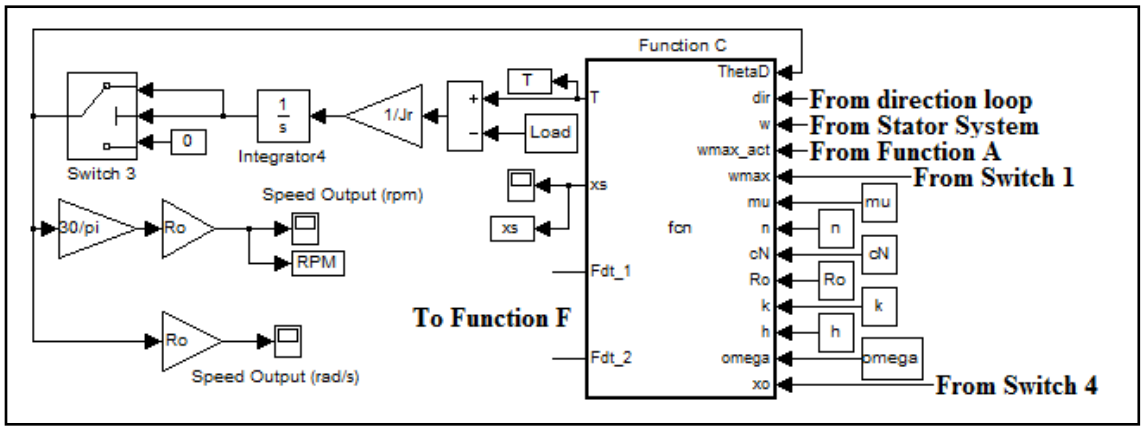

A. 10. Rotor (horizontal) system. The speed of the rotor as a function of the net torque acting on its surface ($T_{drive} - T_{load}$) is approximated here.

Code written within Function C

```
function [T, xs, Fdt_1, Fdt_2]  = fcn(ThetaD, dir, w, wmax_act,
wmax, mu, n, cN, Ro, k, h, omega, xo)

% This block supports an embeddable subset of the MATLAB
% language.
% See the help menu for details.

     %Stick-point Calculation
     xs = 1/k*acos(Ro^2*ThetaD/(k*h*wmax*omega));

     %Indefinite Integral Calculation
     phi_xo = sin(k*xo) - k*xo*cos(k*xo);
     phi_xs = sin(k*xs) - k*xs*cos(k*xo);

     if xs>=xo
          %The hold contact zone is driving the rotor into
     motion
          T = 2*n*mu*cN*wmax_act*Ro/k*(phi_xo);
     else
          %The contact region is split here into T_drive and
     T_brake
          T = 2*n*mu*cN*wmax_act*Ro/k*(2*phi_xs - phi_xo);
     end
```

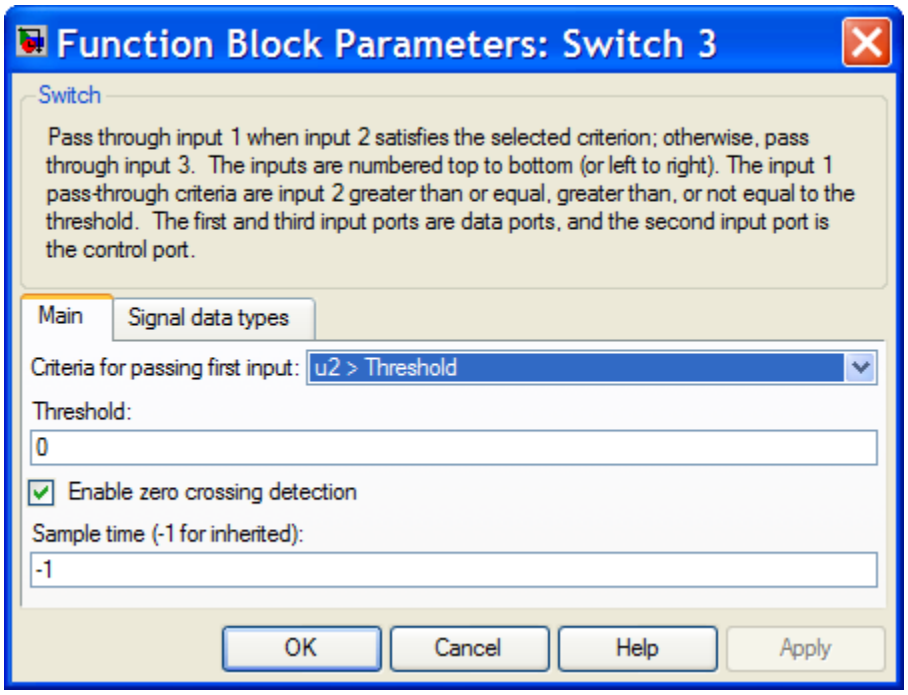

A. 11. Parameter box for Switch 3. Outputs "0" if the input is not greater than "0"

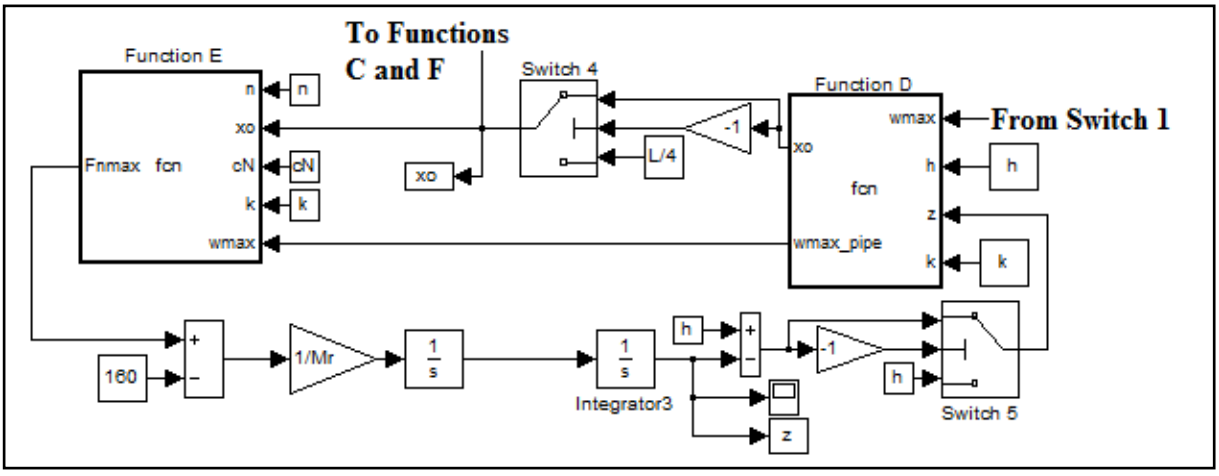

A. 12. Rotor (vertical) system. Based on the amplitude of the traveling wave, w_{max}, the reaction force between the stator and the rotor is calculated to determine the displacement height of the rotor above the stator in the vertical plane. The half contact length, x_o, is calculated from that height.

Code written within Function D. Using the height calculated in the Rotor (vertical) loop, the contact length, x_o, is determined

```
function [xo, wmax_pipe]  = fcn(wmax, h, z, k)
% This block supports an embeddable subset of the MATLAB language.
% See the help menu for details.

%Calculating the contact area
xo = 1/k*acos((h-z)/wmax);

%wmax_pipe passes wmax through the function to avoid
%crossing wires,m further complicating the simulink diagram

wmax_pipe = wmax*1;
```

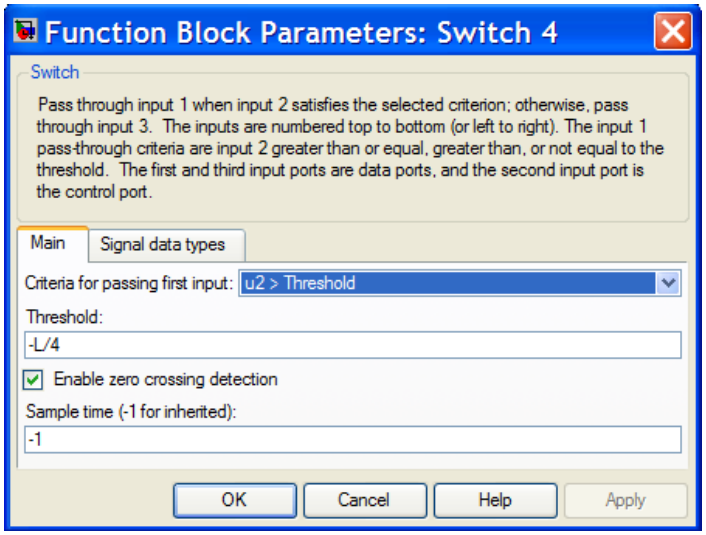

A. 13. Parameter box for Switch 4. The switch ensures that the maximum contact length passed through the switch does not exceed $\lambda/4$.

Code written within Function E to determine the contact force between the rotor and the stator caused by the traveling wave pressing into the rotor

```
function Fnmax = fcn(n, xo, cN, k, wmax)
% This block supports an embeddable subset of the MATLAB language.
% See the help menu for details.

%Calculating the contact force between the rotor and the stator
Fnmax = 2*n*cN*(wmax)/k*(sin(k*xo) - k*xo*cos(k*xo));
```

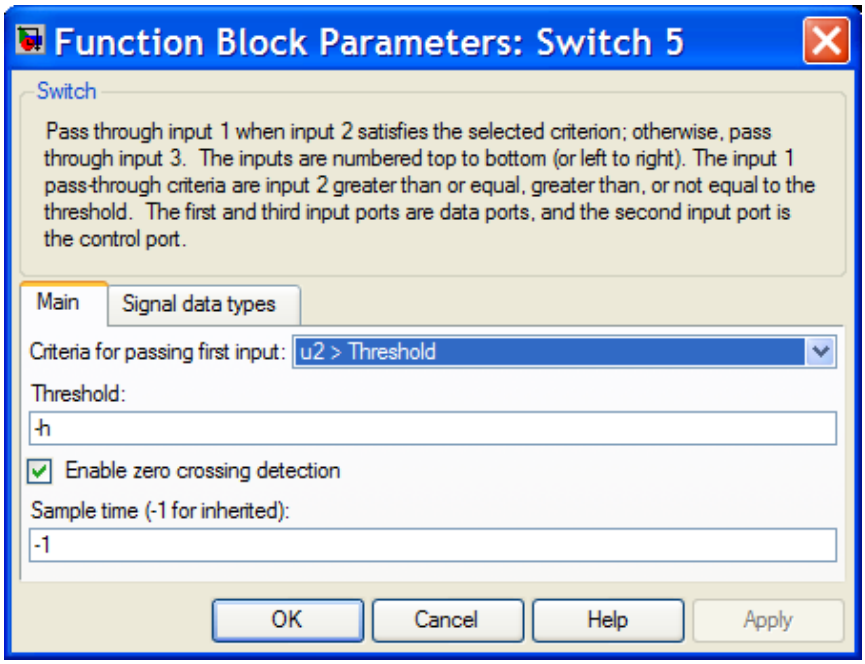

A. 14. Parameter box for Switch 5.

Code written within Function F. Calculates the feedback forces, a result of the interaction between the rotor and stator, that are fed to the stator.

```
function [Fd1, Fd2] = fcn(w, n, cN, k, Fdt1, Fdt2, xo)
% This block supports an embeddable subset of the MATLAB language.
% See the help menu for details.

Fn1 = -n*cN/k*w(1)*(k*xo - sin(2*k*xo)/2)*0.765;
Fn2 = -n*cN/k*w(2)*(k*xo - sin(2*k*xo)/2)*0.765;

Fd1 = Fn1 + Fdt1; %Fdt1/Fdt2 have no effect on simulation outputs
Fd2 = Fn2 + Fdt2; %and can be given values of “0” if so desired
```

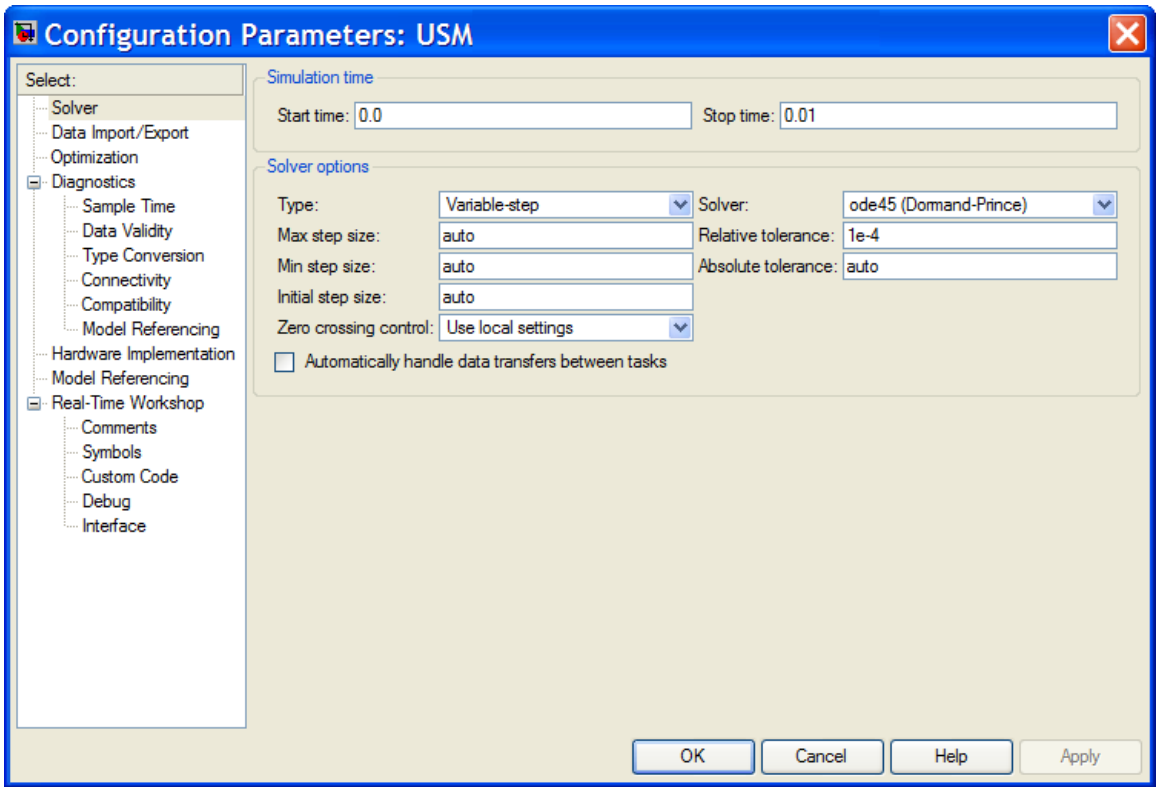

A. 15. MATLAB Simulink USM Simulation Configuration Parameters box

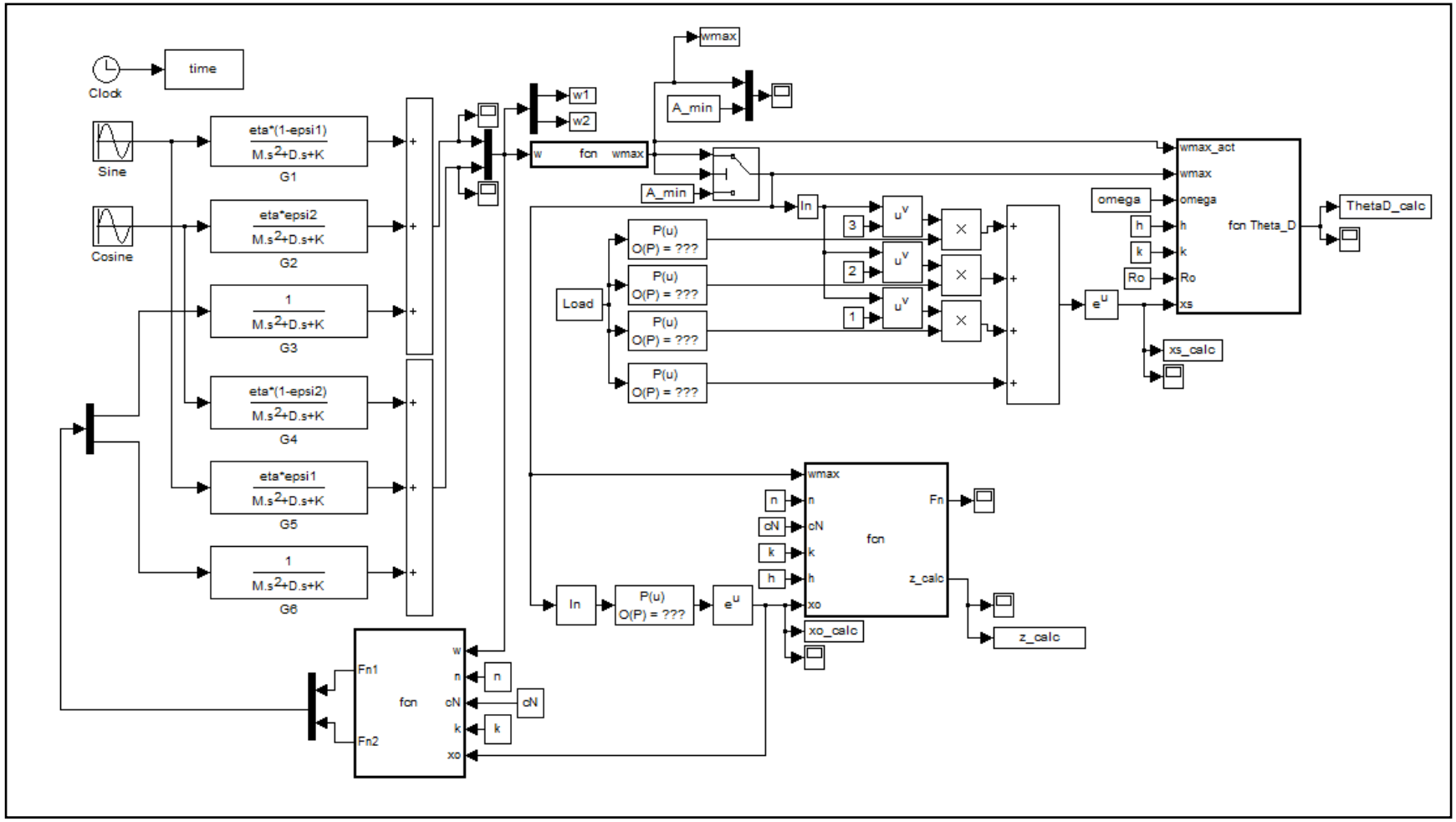

A. 16. Reduced Dynamic Model Simulink block diagram

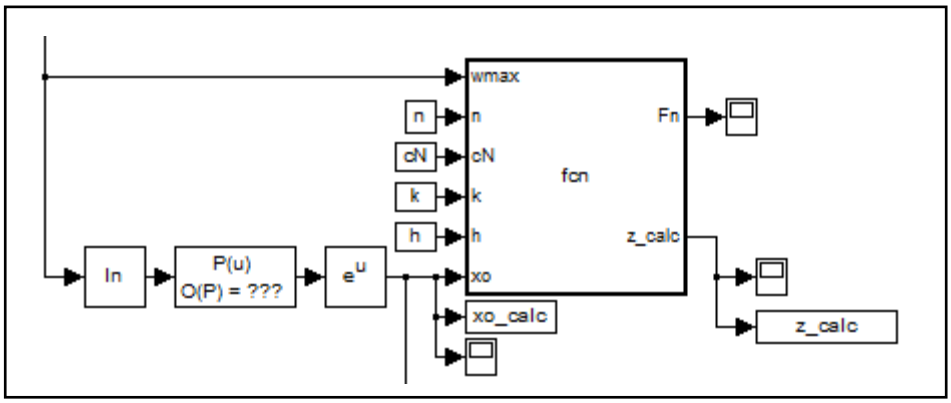

A. 17. Pseudo-x_o function feeding into RDM function calculating rotor height

Code inside RDM function used to calculate rotor height (z_calc)

```
function [Fn, z_calc] = fcn(wmax, n, cN, k, h, xo)
% This block supports an embeddable subset of the MATLAB language.
% See the help menu for details.

Fn = 2*n*cN*(wmax)/k*(sin(k*xo) - k*xo*cos(k*xo));
%z_calc = wmax*cos(xo*k);
z_calc = wmax*cos(k*xo);
```

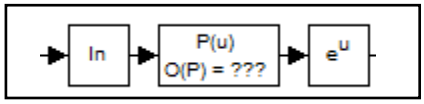

A. 18. RDM pseudo-x_o function producing (x_o_calc)

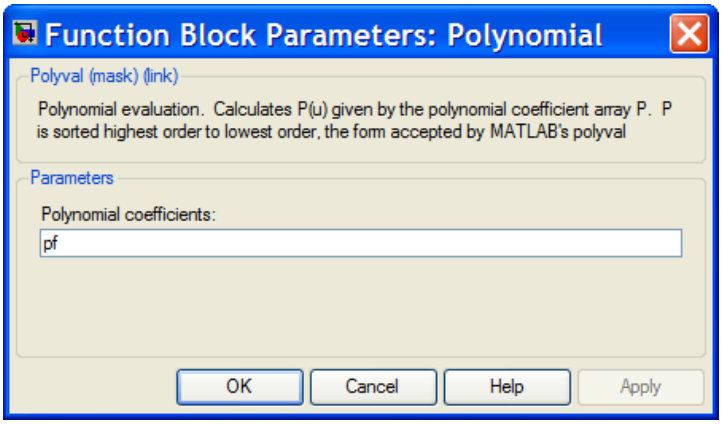

A. 19. Inside P(u) block of pseudo-x_o function.
"pf" is generated in the second .m-file of Appendix B.

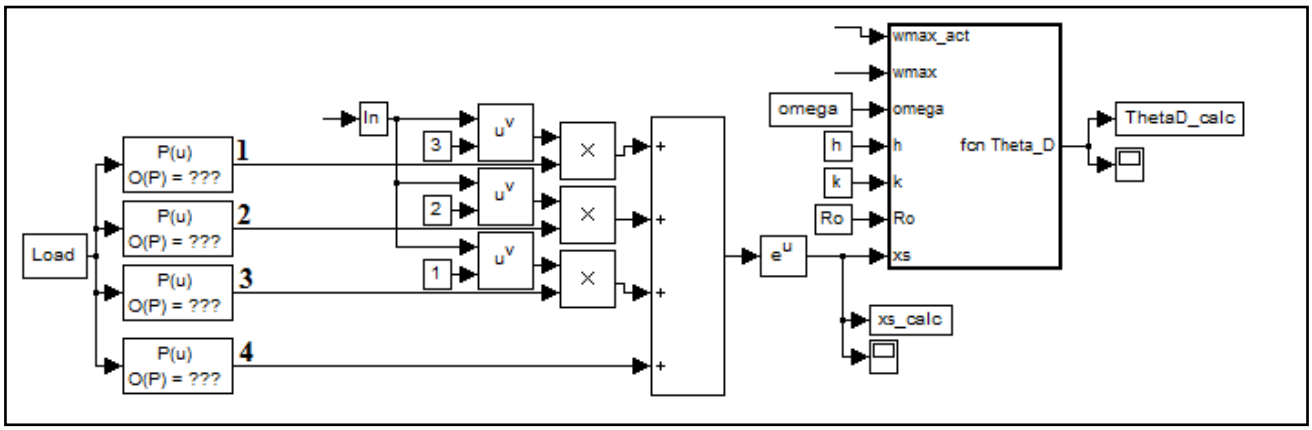

A. 20. Pseudo-x_s function feeding into RDM function calculating rotor speed

Code inside RDM function used to calculate rotor speed (ThetaD_calc)

```
function Theta_D = fcn(wmax_act, wmax, omega, h, k, Ro, xs)
% This block supports an embeddable subset of the MATLAB language.
% See the help menu for details.

 Theta_D = k*omega*h*wmax_act/Ro*cos(k*xs)*30/pi;
```

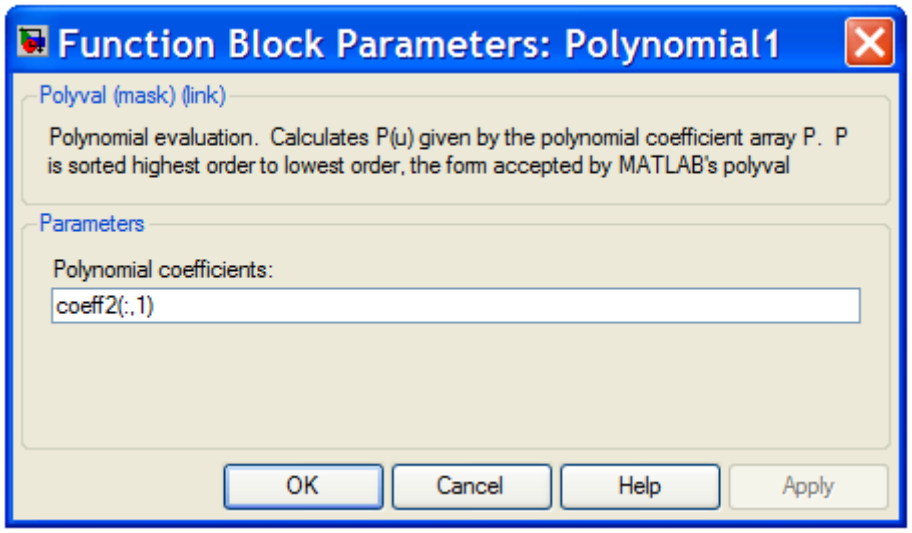

A. 21. Inside P(u) block of first pseudo-x_s function. coeff2() is generated in the second .m-file of Appendix B. P(u) blocks 2, 3, and 4 need “coeff2(:,2)”, “coeff2(:,3)”, and “coeff2(:,4)” placed inside the Polynomial coefficients text field, respectively.

Appendix B

.m-file #1: Code defines all constants for the Complex Dynamic Model in the workspace. This code must be run prior to starting the CDM simulation.

```
close all, clear all
%Properties of electrical system forcing function
    eta   =  0.2263;        %(N/V) – Force/Voltage coupling factor
    V     =  130;           %(V)
    omega =  40.000e3*2*pi; %(rad/s)
    Phase = pi/2;           %(rad)

%Properties of stator:
    %Equation of motion Constants and property calculations
        M    = 10.1e-3;              %(kg)
        D    = 15.4;                 %(Ns/m)
        K    = 5.9524e8;             %(N/m)
        wn0   = (K./M).^(1/2);           %natural frequency of system prior
                                     to feedback forces (rad/s)
    %Stator Dimensions
        Ro    = 26.75e-3;             %Effective radius of contact (m)
        b      = 4.41e-3;                 %Width of traveling wave in radial
                                      direction, (m)
        n     = 9;                     %Number of wave peaks
        h     = 1.5e-3;                %half thickness of stator, (m)
        L     = 2*pi*Ro/n;             %Wave Length (m)
        k     = 2*pi/L;                %Wave Number (1/m)
        epsi1 = 0;                    %Coupling factor (Simulated IDEAL... i.e.
                                      %epsi = 0)
        epsi2 = epsi1;

%Properties of rotor:
    %Vertical System
    Mr = 30e-3;             %(kg)
    %Rotary System
    Jr    = 7.2e-6;         %(kg*m^2)
    %Load
    Load = 0;

%Contact Mechanics
    Kr     = 5.4e11;        %N/m^3
    cN     = Kr*b;          %(N/m^2)
    mu     = 0.3;           %friction coefficient
    Fext   = 160;           %Stator/Rotor external pressing force, (N)
    xo_max = L/4;           %Max xo by contact mechanics, (m)

%A_min calculation: Minimum wave height that satisfies the force balance
between the rotor and the stator in the vertical (perpendicular to the stator
surface) direction

    A_min = Fext/(2*n*cN/k*  (sin(k*xo_max) - k*xo_max*cos(k*xo_max)));
```

.m-file #2: Code defines all constants for the Reduced Dynamic Model in the workspace. This code must be run prior to starting the RDM simulation.

```
close all, clear all, format long
%Properties of forcing function
    eta   =  0.2263;     %N/V - Modal Coupling factor of the stator
    V     =  130;        %Vrms
    omega =  40e3*2*pi;  %Rad/s [40.586e3 using calculated xo
    Phase = pi/2;                  %[40.589e3 for simulated xo

%Properties of stator:
    %Equation of motion Constants and property calculations
        M    = 10.1e-3;              %kg
        D    = 15.4;                 %Ns/m
        K    = 5.9524e8;              %N/m (Before added stiffness term
                                      %from feedback)
        wn0  = (K./M).^(1/2);        %natural frequency of system prior to
                                      %feedback forces rad/s
        Rr   = 0.7;                  %Traveling wave constant, (not using
                                      %temporarily)
    %Stator Dimensions
        Ro    = 26.75e-3;             %Effective radius of contact (m)
        b     = 4.41e-3;              %Width of traveling wave in radial
                                      %direction, (m), (Epsilon in Ghouti)
        n     = 9;                    %Number of wave peaks
        h     = 1.5e-3;               %half thickness of stator, (m)
        L     = 2*pi*Ro/n;
        k     = 2*pi/L;
        epsi1 = 0;                    %Coupling factor
        epsi2 = epsi1;

%Properties of rotor:
    %Vertical System
    Mr = 30e-3;

    %Rotary System
    Jr    = 7.2e-6;   %kg*m^2
    Load  = 0;        %Nm
%Contact Mechanics
    Kr     = 5.4e11;    %Kr = E/h and "h" is unknown for Ghouti, just use
                        %number provided, (N/m^3)
    cN     = Kr*b;
    mu     = 0.3;
    Fext   = 160;        %External applied force
    xo_max = L/4;

%Find relationship between "xo" and "A" below
    A_min = Fext/(2*n*cN/k*(sin(k*xo_max) - k*xo_max*cos(k*xo_max)));
```

```
%Number of points in amplitude vector, and Amplitude vector creation
    NA    = 50;
    A_max = 10e-6;
    A     = linspace(A_min,A_max,NA);

%finding xo_minimum and "xo"  vector development
    %xo_min = fzero(@(x) Fext - 2.*n.*cN.*max(A).*n./k.*(sin(k.*x) -
k.*x.*cos(k.*x)),0);
    xo_min  = 0.001*xo_max;
    N_xo   = 7;
    xo     = linspace(xo_min, L/4, N_xo);

FLYNN            = zeros(length(A), length(xo));
xo_zero          = zeros(1, length(A));
FLYNN_zero_check = zeros(1, length(A));

%initial guess for fzero() inside loop, reset to each no xo_zero once in loop
    xo_prev = xo_min;
    for i = 1:NA

        FLYNN(i,:)            = Fext - 2.*n.*cN.*A(i)./k.*(sin(k.*xo) -
k.*xo.*cos(k.*xo));
        xo_zero(i)            = fzero(@(xo) Fext - 2*n*cN*A(i)/k*(sin(k*xo) -
k*xo*cos(k*xo)), xo_prev);
        xo_prev               = xo_zero(i);
        FLYNN_zero_Check(i,:) = Fext - 2.*n.*cN.*A(i)./k.*(sin(k.*xo_zero(i))
- k.*xo_zero(i).*cos(k.*xo_zero(i)));

    end

%     %Plotting to make sure that the xo_zero values do in fact set the
%     %GHOUTI Equation to zero
%     plot(A, FLYNN),  title('FLYNN Equation set to zero versus w_m_a_x')
%                      xlabel('Traveling Wave Amplitude, w_m_a_x, m')
%                      ylabel('FLYNN Equation set to zero, \deltaF, N')
%     figure
%     plot(xo_zero, FLYNN_zero_Check), title('Zero Check')
%                                      xlabel('Contact length satisfying
FLYNN equation, xo_z_e_r_o, m')
%                                      ylabel('Value of FLYNN equation,
\deltaF, N')



%-------------------------------------------------------------
%-LOGLOG PLOTTING AND POLYFITTING FOR "xo_zero vs. A" curves-
%-------------------------------------------------------------
%Order of polyfit
    DOF = 3;
%Finds coefficients of order DOP to calculate fit line
%Used in a polynomial block in the Simulation.  Input: pf
    pf = polyfit(log(A), log(xo_zero), DOF);
```

```
%uses pf fit coefficients from above to determine fit line
    xo_zero_fit = polyval(pf, log(A));

%     %Plotting the xo versus wmax data calculated above
%         figure
%
%         loglog(A, xo_zero, 'o'), hold on, loglog(A, exp(xo_zero_fit), 'k')
%             title('xo found by f-zero vs. xo found by fit-coefficients')
%             xlabel('Traveling Wave Amplitude, w_m_a_x, m')
%             ylabel('xo satisfying FLYNN equation, xo-zero, m')
%
%         figure
%
%         plot(A, xo_zero), hold on, plot(A, exp(xo_zero_fit), 'o')
%             title('xo found by f-zero vs. xo found by fit-coefficients')
%             xlabel('Traveling Wave Amplitude, w_m_a_x, m')
%             ylabel('xo satisfying FLYNN equation, xo-zero, m')
%
%         figure
%
%         plot(A, xo_zero-exp(xo_zero_fit), 'k')
%             title('Residuals between fzero and fit-line')
%             xlabel('Traveling Wave Amplitude, w_m_a_x, m')
%             ylabel('Residuals, m')


%The code below determines the FIT for coefficients for xs
%as a function of Tmax and wmax such that the FLYNN torque
%equation is satisfied (i.e. Tdrive = Tbrake).

%Fundamental Equations and variables:
%Phi(x) = sin(kx) - kxcos(kx)
%
%T_r(xs, xo) = 2*mu*cN*wmax*Ro/k*(2*Phi(xs)-Phi(xo))
%
%Tmax = Max driveable torque of the motor based on contact mechanics
%Tload = load vector, all within the +/- Tmax range
%xo_zero = vector of half-contact lengths on interval [0, L/4] found above
%          in determining the xo = f(wmax).
%xs = vector of stick-points lengths on interval [L/4, 0]

T_max = mu*Fext*Ro;

%T_load = [0:-.1:-T_max];
%T_load = linspace(0, -1, 20);
%T_load = [0:-.1:-0.7788*T_max];
%T_load = linspace(0, -0.8*T_max, 8);
T_load = linspace(0, -0.95*T_max, 20);
%T_load = linspace(-0.8*T_max, 0.9*T_max);

NTL = length(T_load)';
```

```
xs_SS = zeros(NTL, NA);

dof1 = 3;
coeff1 = zeros(NTL, dof1 + 1);

guess = 0; %Initial guess for fzero(xs_SS) solver
for j = 1:NTL
    %The following loop runs through 1 time for every amplitude in the
    %Amplitude vector 'A' used in the xo = F(wmax) coding above.
    %A separate phi_xo is found for every xo_zero value determined above.
    %xs: a vector extending from 0 (stick is at wave crest), to xo_zero(i)
    %T: The driving torque of the motor for a given xo_zero and calculated
    %   a vector of xs values as in the range discussed above.
    %xs_SS: Steady state xs value that insures that Tdrive = Tbrake
    %       xs_SS = f(Tload, wmax) and thus the fit coefficients the
    %       'xs_SS vs. A' curve are first determined as functions
    %       themselves of the load torque (Tload).

    for i = 1:NA

        phi_xo = sin(k.*xo_zero(i)) - k.*xo_zero(i).*cos(k.*xo_zero(i));
        xs = linspace(0, xo_zero(i));
        phi_xs = sin(k.*xs) - k.*xs.*cos(k.*xo_zero(i));

        T = 2.*n.*mu.*cN.*A(i).*Ro./k.*(2.*phi_xs - phi_xo);

        %Must be a matrix if taking into account multiple load torques.
        %#Columns = Number of Amplitudes in 'A' vector = 'NA'
        %#Rows = Number of load values in 'Tload' vector = 'NTload'
        xs_SS(j, i) = fzero(@(x) 2*n*mu*cN*A(i)*Ro/k*(2*(sin(k*x) -
k*x*cos(k*xo_zero(i))) - phi_xo) - T_load(j), guess);

        %plots "Torque versus xs_SS", one curve for each amplitude in the 'A'
            plot(xs, T, 'k')
            hold on

        guess = xs_SS(j, i);
    end

    %Determines fit coefficients for xs_SS vs. A for each T_load
    coeff1(j, :) = polyfit(log(A), log(xs_SS(j, :)), dof1);

end
    %labels for the plot in the next for-loop above.
        xlabel('Stick Point, xs, m')
        ylabel('Motor output torque, M_U_S_M, Nm')
        title('M_U_S_M versus x_s for each w_m_a_x_,_S_._S_./x_o_,_S_._S_.
pair')
        figure
    plot(A, xs_SS,'-')
        xlabel('Traveling Wave Amplitude, w_m_a_x, m')
        ylabel('Steady State Stick-Point, x_s_,_S_._S_., m')
```

```
        title('Steady State Stick-Point versus Traveling Wave Amplitude,
Varying M_U_S_M')

%-----------------------------------------------------------------
%Determines fit coefficients FOR fit coefficients saved in 'coeff1'
%-----------------------------------------------------------------
    dof2 = 4;
    coeff2 = zeros(dof2 + 1, dof1 + 1);

%-----------------------------------------------------------------
%Finds equations for the fit coefficients with respect to load torque
%-----------------------------------------------------------------
    for i = 1:dof1 + 1
        coeff2(:,i) = polyfit(T_load', coeff1(:,i), dof2);
    end

% %---------------------------------------------------------------
% %---------------------------------------------------------------
% %     Plots each column of coeff1 versus T_load to check linearity
% %     Also overplots each linearity check with the fit line for each
% %     To check accuracy
%     for i = 1:dof1+1
%         plot(T_load, coeff1(:,i))
%         hold on
%         plot(T_load, polyval(coeff2(:,i), T_load), ':r')
%         figure
%     end
%     close
%-----------------------------------------------------------------
%-----------------------------------------------------------------

%-----------------------------------------------------------------
%-----------------------------------------------------------------
%     Develops a matrix of coefficients
%     Each column is a coefficient used to find a FIT for coeff1
%     Each row is the new column coefficient with respect to T_load
    for i = 1:dof1+1
        coeff3(:,i) = polyval(coeff2(:,i), T_load);
    end
%-----------------------------------------------------------------
%-----------------------------------------------------------------

%-----------------------------------------------------------------
%   Uses coeff3 along with polyval() to setup a "FIT" matrix
%   of xs_SS versus A
    xs_SS_fit = zeros(NTL, NA);
    for i = 1:NTL
        xs_SS_fit(i, :) = polyval(coeff3(i, :), log(A));
    end
%-----------------------------------------------------------------
%-----------------------------------------------------------------
```

```
%Plots xs_SS WRT to wmax as found by fzero()
hold on
figure
plot(A, xs_SS),hold on

%Plots xo_zero WRT to wmax as found by fzero() in first part of program
    %plot(A, xo_zero, 'k')

%Plots "curve-fit method" xs_SS WRT to wmax
    plot(A, exp(xs_SS_fit), ':b')
```